The Dissertation Committee for Jeremiah Edward Mangold certifies that this is the approved version of the following dissertation:

Predicting Ion Adsorption onto the Iron Hydroxide Goethite in Single and Multi-Solute Systems

Committee:

Lynn E. Katz, Supervisor

Howard M. Liljestrand

Gerald E. Speitel

Danny D. Reible

James A. Holcombe

Predicting Ion Adsorption onto the Iron Hydroxide Mineral Goethite in Single and Multi-Solute Systems

by

Jeremiah Edward Mangold, B.S.; M. Environ. E.

Dissertation

Presented to the Faculty of the Graduate School of

The University of Texas at Austin

in Partial Fulfillment

of the Requirements

for the Degree of

Doctor of Philosophy

The University of Texas at Austin

December 2013

Dedication

…to God the Father and my Savior Jesus Christ, who has walked with me every step of the way, and carried me when necessary

…and to my wife and family, whose love, support, and encouragement have been invaluable

Acknowledgments

I would like to acknowledge, first and foremost, God the Father and my Savior Jesus Christ, who have made everything possible and given me the strength to persevere and succeed. I would also like to thank my wife and family for all their love and support.

I am deeply appreciative for my supervisor, Dr. Lynn Katz, for all her help and assistance over the past five years. There were many times I felt overwhelmed or inadequate, and she was always there to give me the pep talk I needed at that point in time. For all their assistance in this process, much appreciation also goes out to the rest of my committee: Dr. Howard Liljestrand, Dr. Gerald Speitel, Dr. Danny Reible, and Dr. James Holcombe. I would also like to thank the entire EWRE department (faculty, staff, and students) for all their help and support during my time at UT, especially: Dr. Desmond Lawler, Dr. Kerry Kinney, Ellison Carter, Lee Blaney, Amanda Van Epps, Chia-Chen Chen, Chang Min Park, Fernando Almada, Celina Dozier, and the rest of the Katz research group.

Finally, I would like to thank the Department of Energy – Basic Energy Sciences for providing the financial support for this research.

Predicting Ion Adsorption onto the Iron Hydroxide Mineral Goethite in Single and Multi-Solute Systems

Jeremiah Edward Mangold, Ph.D.

The University of Texas at Austin, 2013

Supervisor: Lynn E. Katz

Surface complexation models (SCMs) have proven to be a useful tool in predicting ion adsorption at the mineral – water interface. In particular, previous research has shown that the Diffuse Layer Model (DLM), Constant Capacitance Model (CCM), and Triple Layer Model (TLM), are all capable of predicting ion adsorption in relatively simple single solute systems.

To better simulate the environmental conditions experienced by groundwater sources present in the Earth's subsurface, experimental adsorption studies have been conducted for more complex multi-solute systems. Under these conditions, SCMs have not proven to be reliable in consistently predicting ion adsorption behavior for the adsorbates of interest. This inability of these SCMs to predict ion adsorption for more complex, multi-solute systems is thought to stem from the variable site density (N_S) values utilized in these models.

In this research, a methodology was developed for characterizing mineral surface heterogeneity that allows for the different site density values predicted from

crystallography, microscopic imaging, tritium exchange, surface saturation data, and surface charging data to all be explained using a single unified theory. This methodology was applied to a goethite mineral sample used in performing batch adsorption studies in single and bi-solute systems with Cd(II), Pb(II), and Se(IV). The adsorption behavior of these adsorbates onto the goethite sample was successfully predicted using the Charge Distribution Multi-Site Complexation (CD-MUSIC) Model and surface complexes consistent with spectroscopic data and computational molecular modeling simulations.

A second, separate modeling study was performed using CD-MUSIC to predict Hg(II) adsorption onto different goethite samples of varying size and crystal morphology in single and multi-solute systems. In this study, site density values were predicted for the mineral samples studied utilizing a linear relationship observed for goethite between specific surface area and proton reactive site density. The CD-MUSIC model proved successful in predicting Hg(II) adsorption over all conditions studied while employing only surface complexes consistent with molecular scale analyses. In addition, a novel method for quantifying carbonate's presence in experimental systems was developed.

Table of Contents

List of Tables

List of Figures

Chapter 1 : INTRODUCTION

1.1. Background

The manufacturing and energy sectors of society along with current agricultural and waste management practices have all contributed to the environment becoming increasingly burdened with a myriad of pollutants. In areas where the release of heavy metals into the water and sediment phases has caused concentrations of these metals to rise to unsafe levels, a remediation strategy may be employed to restore the contaminated site to its previous condition. To facilitate selection of the optimal cleanup method, fate and transport models are often utilized to ascertain the pollutant's mobility in the environment as well as the extent and severity of contamination; thereby allowing for selection of the remediation strategy best suited for that particular site. Oftentimes, the metal contaminants in question at these remediation sites are observed to adsorb to mineral surfaces. In fate and transport models, contaminant adsorption behavior has often been described using retardation coefficients; however these coefficients are of limited use and accuracy. Hence, a better predictive tool is desired for describing ion adsorption at the mineral – water interface.

Surface complexation models (SCMs) have shown great promise in predicting ion adsorption onto metal oxide and clay minerals. In these models, adsorption reactions are thought to be similar to aqueous complexation reactions where reactive sites present on the mineral surface act as ligands with the adsorbate. A number of different surface complexation models have been developed over the last forty years that can range in

complexity depending on their description of the mineral – water interface and the number of adjustable parameters required.

The application of these SCMs to field scale prediction of metal ion fate and transport has evolved significantly over the last decade; however, the extensibility of these models is still hampered by several fundamental issues including mineral surface characterization, surface precipitation reactions, ternary surface complex formation, and accurately accounting for carbonate's impact on ion adsorption behavior. This research focused on addressing two of these issues: quantification of surface sites on mineral surfaces and incorporation of the effects of carbonate adsorption.

1.2. Problem Statement

1.2.1. Site density

In empirical adsorption models, ion adsorption behavior is typically described using one or more empirical constants and the concentration of the adsorbate in solution. The only knowledge of the adsorbent surface that is required in these instances is the total surface area of the adsorbent in the system. In SCMs however, more information about the mineral surface is needed because adsorption dynamics are dependent on the type of functional group present at the surface of a mineral. In particular, oxide and oxyhydroxides contain hydroxyl functional groups at the mineral surface. The number of surface hydroxyl sites present or reactive per unit surface area on a mineral surface is represented by the surface site density (N_S).

Quantifying the value of Ns for particular minerals has remained a challenge for surface complexation models in part due to differences in reactivity of different functional groups on the surface and in part because different techniques for measuring surface site density often yield different values. Several different techniques such as objective curve fitting, crystallography, tritium exchange, and surface saturation data have been used previously to estimate the N_S parameter for adsorbents of interest. In the case of the iron (hydr)oxide goethite, N_S values determined using the methods listed above have been found to range from 0.5 to 20 sites/nm^2.

In most modeling studies, once a site density value is selected for a given mineral, it is considered valid for all samples of that particular mineral. For example, the site density of 16.4 sites/nm^2, obtained from tritium exchange data for a goethite sample with a specific surface area (SSA) of 54 m^2/g, has been utilized in a number of SCM studies for goethite samples with SSAs ranging from 49 to 95 m^2/g. While this assumption regarding a uniform site density is useful in reducing the number of fitting parameters needed to run a SCM, there is strong evidence suggesting that N_S varies between mineral samples. From crystallography it has been shown that mineral surfaces are composed of different crystal faces possessing unique site types and site densities that vary from one crystal face to another. Microscopic imaging studies have observed the contribution of these crystal faces to differ between mineral samples, especially when comparing samples with differing SSAs. Given this information, it stands to reason that the current modeling practice of using the same site density value for all samples of a given mineral is not realistic.

Although numerous modeling studies have proven successful in predicting single solute adsorption data utilizing different site densities within the range of 0.5 to 20 sites/nm^2, there are a number of problems that have been encountered. In particular, the equilibrium constants determined for surface complexation reactions in one modeling study are not often transferrable to other modeling studies utilizing a different mineral sample or employing a different site density value. This result has poor implications for field scale predictions where constants generated from one site are unlikely to be extensible to other field sites. Furthermore, SCM predictions of ion adsorption in multi-solute systems are often inaccurate; a result that is believed to be due, at least in part, to the site density value(s) employed in the model.

In summary, different techniques have been utilized by researchers estimate Ns for adsorbents of interest. In the case of goethite, the N_S values determined with these methods ranges from 0.5 to 20 sites/nm^2. Researchers often employ a single site density value for all samples of a given mineral or utilize the N_S value predicted from a particular technique to estimate a mineral's site density. Both of these approaches disregard all other N_S values that were predicted from theoretical and experimental studies of goethite. Hence, there is a need for a methodology to be developed that unifies the different site density values predicted and explain their apparent incongruence.

1.2.2. Carbonate in batch adsorption experiments

Experimental adsorption data used for calibrating and testing SCMs typically comes from batch adsorption studies. In these experiments, great care is taken to ensure

a CO_2 free environment for the solid – solution system being researched. However, given carbon dioxide's ubiquity in the environment and the numerous preparation steps involved in conducting these adsorption experiments, carbonate often manages to be present, to some degree, in these solid – solution systems. Authors of experimental adsorption studies have acknowledged the difficulty in creating a truly carbonate free system, and for the most part have refrained from claiming such in their work; instead, opting to state that procedures were employed to *limit* CO_2's presence in the system. Therefore, carbonate's presence in these solid - solution systems is not the result of poor laboratory technique, but rather the reality of batch adsorption experiments in general.

With that being said, there is a need to quantify the amount of carbonate present (i.e., $[CO_3^{2-}]_{TOT}$) in these systems. For iron hydroxide minerals such as goethite, carbonate has been observed to adsorb strongly with the mineral surface; hence, its presence in a solid – solution system is believed to influence the adsorption behavior of the adsorbate being studied. Currently, there is no method available for determining the amount of $[CO_3^{2-}]_{TOT}$ present in these experimental systems. If the concentration of $[CO_3^{2-}]_{TOT}$ was quantified, the adsorption behavior for the adsorbate of interest could be better predicted by SCMs. Furthermore, since carbonate is found in numerous environmental systems, the experimental adsorption data and the SCMs developed using that data would provide researchers with a useful tool for predicting the oxyanion's impact on contaminant migration through the subsurface.

1.3. Objectives

Given mineral surface site density's (N_S) importance in surface complexation modeling and the need to quantify carbonate's concentration ($[CO_3^{2-}]_{TOT}$) in solid – solution systems, the objectives of this work were to:

1. Develop a methodology for appropriately characterizing mineral surface heterogeneity that will allow for the disparate N_S values determined from different estimation techniques to be understood in a single unified theory

2. Evaluate the methodology for characterizing mineral surface heterogeneity developed in objective 1 for a range of single- and bi-solute adsorption data that include both metal cations and oxyanions.

3. Develop a methodology for incorporating the presence of carbon dioxide and carbonate into single-solute and multi-solute metal ion adsorption and oxyanion sorption.

4. Evaluate the methodology developed in objective 3 for metal cation adsorption onto goethite in the presence of carbonate and chloride.

1.4. Dissertation Outline

This dissertation is made up of seven chapters. In the introduction presented in Chapter 1, the reasons and objectives for the research conducted are discussed. Chapter 2 is a literature review of surface complexation theory and some of the more common surface complexation models currently used by researchers. Chapters 3, 4, and 5 address the research objectives of this work. Chapter 6 summarizes the results of this research. Finally an appendix that provides further information on the titration congruency method discussed in Chapter 3.

Chapter 2 : LITERATURE REVIEW

2.1. Surface Complexation Theory

Contaminant mobility in the subsurface is heavily influenced by its reactivity with mineral – water interfaces [1-4]. Previously, adsorption behavior has been predicted through the use of empirical methods such as isotherms or partition coefficients [5]. Prediction of ion adsorption in solid-solution systems by empirical means has proven to be of limited use however because of the dependence on the chemical composition of the aqueous solution [6-9]. Using a theoretical framework to describe the physicochemical processes that occur at the mineral-water interface, surface complexation models (SCMs) provide a viable alternative in predicting ion adsorption onto mineral surfaces and are capable of overcoming the deficiencies associated with empirical approaches.

Surface complexation theory developed from the observation that ion adsorption to mineral surfaces was analogous to the formation of solution-phase complexes [10-12]. Just as a hydroxide ion can complex with a metal ion in solution, it was found that mineral surfaces could behave in a similar manner with one or more surface site(s) acting as a ligand and associating with an aqueous metal ion, thereby binding the metal ion to the mineral surface. In SCMs, adsorption of dissolved chemical species to the mineral surface is described thermodynamically via formation reactions between solutes and surface sites [13]. The free energies associated with these formation reactions have a chemical and electrostatic component to them, both of which are influenced by the surface sites involved [6].

Where the boundaries of the mineral and water phases meet is termed the mineral – water interface. On an atomic level, the formation of this interface causes an imbalance in the surrounding environment which in turn triggers a restructuring of the two phases' molecular constituents in the interfacial region. This structural rearrangement of molecules at the interface brings about a separation of electrical charge that consequently produces, relative to the bulk solution, an electric potential [6, 13].

There are two primary ways in which charge on a mineral surface is developed: structurally and through interactions between surface sites and charged chemical species present in the solution phase [14]. Structural charge (σ_0) stems from isomorphic substitutions in the mineral between ions of varying valence. Charge arising from interactions between surface sites and aqueous ions is divided by Sposito [14] into two categories: net proton charge (σ_H) and net adsorbed ion charge (Δq). Sposito [14] defines net proton charge as the difference between the moles of protons and hydroxide ions complexed to the mineral's surface sites. Therefore protons and hydroxide ions present in the diffuse layer are not considered when determining σ_H. An adsorbent's intrinsic charge (σ_{in}) is defined as the sum of the mineral's structural charge and net proton charge (cf. Equation 2.1) [14].

$$\sigma_{in} \equiv \sigma_0 + \sigma_H \tag{2.1}$$

The net adsorbed ion charge, Δq, as defined in Equation 2.2, is comprised of three subcategories: σ_{IS}, σ_{OS}, and σ_d; which represents the net charge of ions adsorbed as

inner-sphere complexes, outer-sphere complexes, or in the diffuse ion swarm, respectively [14].

$$\Delta q \equiv \sigma_{IS} + \sigma_{OS} + \sigma_d \tag{2.2}$$

The σ_{IS} and σ_{OS} terms can be consolidated into one term called the Stern layer charge (σ_S) which represents the net charge produced from ions complexed with the mineral's surface sites.

$$\sigma_S \equiv \sigma_{IS} + \sigma_{OS} \tag{2.3}$$

The total charge attributed to the adsorbent's surface is termed the net total particle charge, σ_p, expressed typically as a charge density (C/m^2) and is composed of the mineral's intrinsic charge and its stern layer charge (Equation 2.4) [6, 14].

$$\sigma_p \equiv \sigma_{in} + \sigma_S \tag{2.4}$$

In most instances, σ_p is not equal to zero and therefore must be counterbalanced to maintain electroneutrality in the solid – solution system. To offset the particle's charge, counterions from the solution amass near the adsorbent's surface in what is described by Davis and Kent [6] as a "diffuse atmosphere" or by Sposito [14] as a "diffuse ion swarm". Unlike ions bound to the surface as inner-sphere or outer-sphere complexes, the

ions present in the diffuse ion swarm are completely dissociated from the surface and relatively free to engage in diffusive motion [6, 14]. The net charge present in the diffusive ion swarm (σ_d) offsets the net total particle charge (σ_p) thereby providing charge balance to the system (Equation 2.5) [6, 14].

$$\sigma_p + \sigma_d = 0 \tag{2.5}$$

A core tenet in surface complexation theory is the idea that the adsorbed ions which make up σ_H, σ_{IS}, σ_{OS}, and σ_d reside at specific locations within the mineral – water interface. In general, there are three possible regions for ion adsorption to occur: the surface layer, the compact layer, or the diffuse layer. These three layers comprise what is termed the electrical double layer (EDL) [6]. The positioning of adsorbed ions within the EDL results in a separation of charge that in turn creates an electrical potential difference across the mineral – water interface (Figure 2.1).

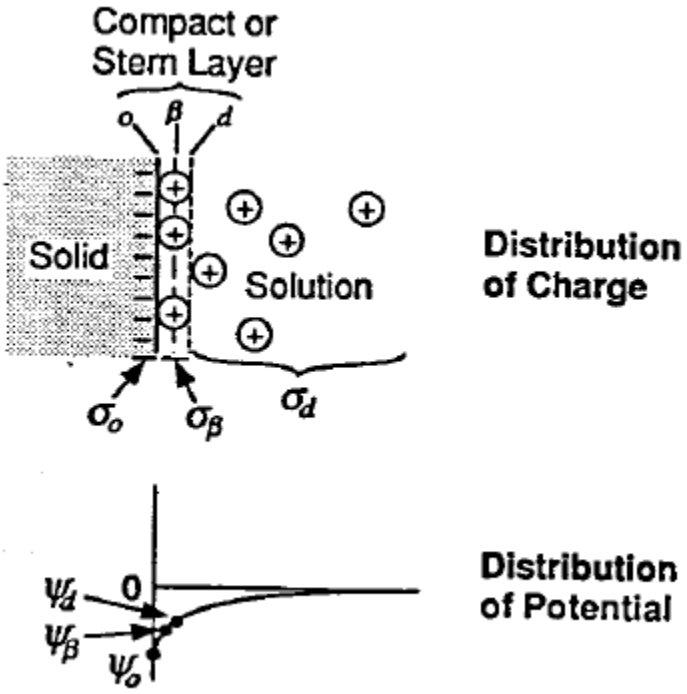

Figure 2.1 Illustration depicting the electrical double layer (EDL) using the Stern-Grahame model. The σ_0 value in the illustration is equivalent to σ_{in} in Equation 2.1, and σ_β is equivalent to σ_S in Equation 2.3. (Taken from James and Park [15]).

In SCMs, the surface and compact layers of the EDL are modeled as electrostatic planes termed the 0- and β-planes, respectively. These electrostatic planes run parallel to the adsorbent's surface with potentials ψ_0 and ψ_β, respectively. This theoretical construct implies that all ions adsorbed in a given layer as well as their charge, reside on the same plane and are the same horizontal distance from the mineral's surface. Therefore, although ions that adsorb in the surface or compact layers can be located on or between electrostatic planes, for modeling purposes, the charge of these adsorbed ions must be placed on either the 0-plane or the β-plane.

The beginning/boundary of the diffuse layer is also modeled as an electrostatic plane, termed the diffuse or d-plane, with potential ψ_d. In this case, the charge of the adsorbed ions present in the diffuse layer (i.e., the diffuse ion swarm) is not placed on the electrostatic d-plane. The electrostatic potential of the d-plane is described using Gouy-Chapman theory (Equation 2.6) [16, 17] that relates the surface charge density (σ_d) of the electrostatic plane to its potential (ψ_d):

$$\sigma_d = (8RT\varepsilon\varepsilon_0 c \times 10^3)^{1/2} \cdot \sinh\left(\frac{Z\psi_d F}{2RT}\right) \quad (2.6)$$

where σ_d is the surface charge density of the electrostatic d-plane in units of C/m^2; R is the universal gas constant (8.314 J/mol·K); T is the temperature in Kelvin; ε is the dielectric constant for water and is dimensionless; ε_0 is the permittivity of free space (8.854 x 10^{-12} C/V·m); c is electrolyte concentration in units of mol/L; F is Faraday's constant (96,485 C/mol); ψ_d is the electrical potential (J/C) of the d-plane; and Z is valence of the symmetrical electrolyte. At 25^{o}C, Equation 2.6 can be simplified and yield Equation 2.7

$$\sigma_d = -0.1174 \cdot (I)^{1/2} \cdot sinh\left(\frac{Z\psi_d F}{2RT}\right) \quad (2.7)$$

where I is the ionic strength of the aqueous solution (mol/L), and all other variables are as defined previously.

2.2. Thermodynamics of Adsorption Reactions

As mentioned above, in surface complexation theory the free energy of an adsorption/desorption reaction is comprised of two components, electrostatic and chemical. While the electrostatic and chemical components cannot be separated out experimentally [13, 18, 19], they can be differentiated theoretically; allowing for the determination of a chemical interaction term that is independent of the adsorbent's surface charge [2]. The total free energy of an adsorption reaction can be written as Equation 2.8:

$$\Delta G^{o}_{tot} = \Delta G^{o}_{int} + \Delta G^{o}_{coul} \tag{2.8}$$

where ΔG^{o}_{tot} is the total free energy of the adsorption reaction at standard state conditions, ΔG^{o}_{int} is the intrinsic free energy of reaction, and ΔG^{o}_{coul} accounts for the electrostatic energy of reaction.

The ΔG^{o}_{int} term can be expanded out to Equation 2.9:

$$\Delta G^{o}_{int} = \Delta G^{o}_{chem} + RT\ln \prod_{i} a_{i}^{n_i} \tag{2.9}$$

where ΔG^{o}_{chem} is the Gibbs chemical free energy of reaction at standard state conditions; R is the universal gas constant (8.314 J/mol·K); T is the temperature in Kelvin; a_i is the activity of the i^{th} species; and n_i is the stoichiometric coefficient of the i^{th} species in the adsorption reaction. It should be noted that, for convenience, the ratio of activity

coefficients for surface species in adsorption reactions is assumed to be equal to one [2, 20]. For surface species, all deviations from ideal behavior are thought to result from the adsorbent's surface potential [2]. The ΔG^{o}_{coul} term can be expanded out to:

$$\Delta G^{o}_{coul} = \sum_{k} \Delta Z_{k} F \psi_{k} \tag{2.10}$$

where ΔZ_k is the change in charge on the k^{th} electrostatic plane in units of moles of charge; F is Faraday's constant (96,485 C/mol); and ψ_k is the electric potential (J/C) of the k^{th} electrostatic plane.

Writing out the overall Gibbs free energy of reaction results in Equation 2.11:

$$\Delta G_{rxn-ec} = \Delta G^{o}_{ch} + RT \ln \prod_{i} a_{i}^{n_i} + \sum_{k} \Delta Z_{k} F \psi_{k} \tag{2.11}$$

where ΔG_{rxn-ec} is the Gibbs electro-chemical free energy of reaction, and all other terms are as defined previously.

At equilibrium, $\Delta G_{rxn-ec} = 0$, which yields Equation 2.12:

$$0 = \Delta G^{o}_{ch} + RT \ln \prod_{i} a_{i}^{n_i} + \sum_{k} \Delta Z_{k} F \psi_{k} \tag{2.12}$$

Rearranging terms from Equation 2.12, gives Equation 2.13:

$$\exp\left(\frac{-\Delta G_{ch}^{o}}{RT}\right) = \prod_{i} a_i^{n_i} \cdot \exp\left(\frac{\sum_k \Delta Z_k F \psi_k}{RT}\right) \tag{2.13}$$

The exponential term possessing the Gibbs chemical free energy of reaction at standard state is termed the intrinsic equilibrium constant (Equation 2.14) and is independent of the adsorbent's surface charge [2].

$$K^{int} = \exp\left(\frac{-\Delta G_{ch}^{o}}{RT}\right) \tag{2.14}$$

The ratio of activities between products and reactants of the adsorption reaction, raised to powers equal to their stoichiometric coefficients, is termed the apparent equilibrium constant (Equation 2.15).

$$K^{app} = \prod_i a_i^{n_i} \tag{2.15}$$

Substituting Equations 2.14 and 2.15 into Equation 2.13 results in Equation 2.16:

$$K^{int} = K^{app} \cdot \exp\left(\frac{\sum_k \Delta Z_k F \psi_k}{RT}\right) \tag{2.16}$$

where the exponential term possessing the electrostatic energy of reaction, is labeled the coulombic correction factor. It is considered to be an activity coefficient that takes into account the electrostatic effects of the charged surface [2].

In surface complexation modeling, K^{int} values are optimized to achieve the best model fit of an experimental data set. The resulting optimized K^{int} value is considered the true K^{int} value for the adsorption reaction being considered. It should be noted that the K^{int} value calculated using the modeling software FITEQL 4.0 [21] and FITEQLC [22] is based on a mol/L concentration of each surface species; however, to accurately account for entropy contributions, the concentration of each surface species present in the K^{int} term must be expressed as a mole fraction [23]. Therefore, the K^{int} value reported in FITEQL 4.0 and FITEQLC must be converted from a mol/L K^{int} value (K_M^{int}) into a mole fraction K^{int} value (K_θ^{int}).

Hiemstra and van Riemsdijk [23] illustrated that for a monodentate surface complex, K_M^{int} is equivalent to K_θ^{int} (Equation 2.17), while for bidentate surface complexes, K_θ^{int} is equal to K_M^{int} multiplied by a conversion factor (Equation 2.18). For the sake of simplicity, the coulombic correction factor is left out of these examples. For a monodentate surface complex, the expression for K_θ^{int} is presented in Equation 2.17:

$$K_\theta^{int} = \frac{\theta_{Ads}}{\theta_{Ref}} \cdot \prod a_{i,sol}^{n_i} = \frac{\left(\frac{C_{Ads}}{C_s \cdot SSA \cdot 10^{18} \cdot N_{S,j}/N_A}\right)}{\left(\frac{C_{Ref}}{C_s \cdot SSA \cdot 10^{18} \cdot N_{S,j}/N_A}\right)} \cdot \prod a_{i,sol}^{n_i} = \frac{C_{Ads}}{C_{ref}} \cdot \prod a_{i,sol}^{n_i} = K_M^{int} \quad (2.17)$$

where θ_{Ref} and θ_{Ads} are the mole fraction concentrations of the reference and adsorbed surface species, respectively; $a_{i,sol}$ represents the activities of the i^{th} aqueous species; n_i is the stoichiometric coefficient for the i^{th} aqueous species; C_{Ref} and C_{Ads} are the concentrations of the reference and adsorbed surface species, respectively, in units of mol/L; C_S is the concentration of adsorbent in the system, in units of mol/L; SSA is the specific surface area of the adsorbent in m^2/g; 10^{18} is the conversion factor to go from units of m^2 to nm^2; $N_{S,j}$ is the site density of the j^{th} surface site type, in units of sites/nm^2; and N_A is Avogadro's number (6.023×10^{23}) used to convert from sites to moles of sites.

For a bidentate surface complex, the expression for K_θ^{int} is presented in Equation 2.18.

$$K_\theta^{int} = \frac{\theta_{Ads}}{\left(\theta_{Ref}\right)^2} \cdot \prod a_{k,sol}^{n_k} = \frac{\left(\frac{C_{Ads}}{C_s \cdot SSA \cdot 10^{18} \cdot N_{S,j}/N_A}\right)}{\left(\frac{C_{Ref}}{C_s \cdot SSA \cdot 10^{18} \cdot N_{S,j}/N_A}\right)^2} \cdot \prod a_{k,sol}^{n_k}$$

$$= \frac{C_s \cdot SSA \cdot 10^{18} \cdot N_{S,j}}{N_A} \times \left[\frac{C_{Ads}}{\left(C_{ref}\right)^2} \cdot \prod a_{k,sol}^{n_k}\right] = \frac{C_s \cdot SSA \cdot 10^{18} \cdot N_{S,j}}{N_A} \times K_M^{int} \quad (2.18)$$

2.3. Surface Complexation Reactions

Metal (hydr)oxide minerals have demonstrated the ability to adsorb and desorb protons, as well as complex with both cations and anions to form inner- and outer-sphere complexes at the mineral surface [24-55]. Here, an overview of these reactions and how they are generally described in surface complexation modeling is provided. Four surface complexation models are referenced in this section of the literature review. Further

discussion of the SCMs mentioned here will be provided in the next section of this literature review. In particular, the SCMs discussed are the Diffuse Layer Model (DLM) [2, 56, 57], the Constant Capacitance Model (CCM) [12, 58-61], the original and modified Triple Layer Model (TLM_o and TLM_m, respectively) [62-68], and the Charge Distribution Multi-Site Complexation (CD-MUSIC) Model [23-25].

As discussed above, a mineral surface can develop charge through interactions between surface sites and ions present in solution, including protons [14]. The adsorption and desorption of protons allows for a variable charge surface that is positively charged at lower pH values and becomes negatively charged as the pH of the system rises (Figure 2.2).

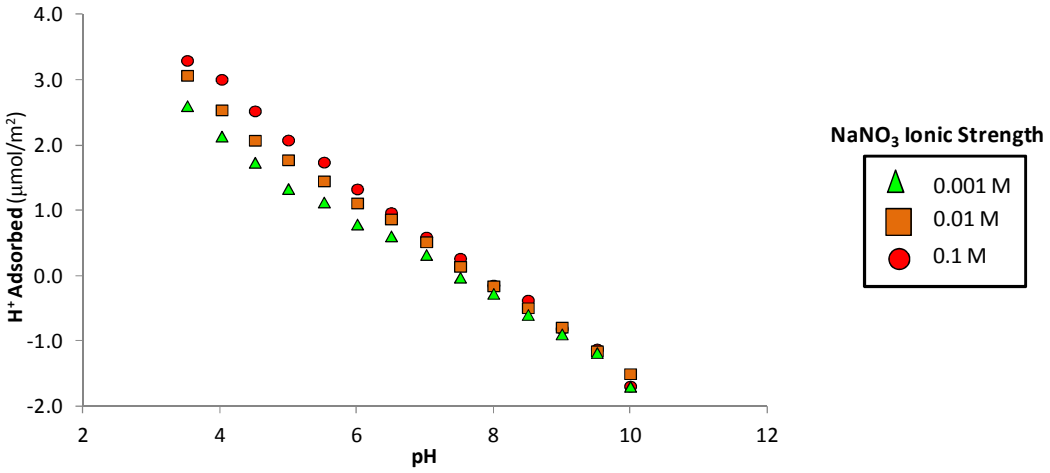

Figure 2.2 Potentiometric titration data for a goethite sample with a specific surface area (SSA) of 76 m^2/g using a $NaNO_3$ background electrolyte. Data taken from Barrow and Cox [69].

To describe the surface acidity of metal (hydr)oxide minerals, SCMs such as the DLM, CCM, TLM_o and TLM_m, utilize amphoteric surface sites ($\equiv SOH^0$) that are capable of being protonated and deprotonated (Equation 2.19 and Equation 2.20).

$$\equiv SOH^0 + H^+ \leftrightarrow \equiv SOH_2^+ \ (K_+^{int}, \text{ protonation reaction}) \tag{2.19}$$

$$\equiv SOH^0 \leftrightarrow \equiv SO^- + H^+ \ \ (K_-^{int}, \text{ deprotonation reaction}) \tag{2.20}$$

Using Equation 2.16, the mass action expression for surface protonation and deprotonation reactions, as depicted in Equation 2.19 and Equation 2.20, respectively, can be written as Equation 2.21 and Equation 2.22

$$K_+^{int} = \frac{[\equiv SOH_2^+]}{[\equiv SOH^0] \cdot (H^+)} \times \left(\frac{F \cdot \Psi_0}{RT}\right) \tag{2.21}$$

$$K_-^{int} = \frac{[\equiv SO^-] \cdot (H^+)}{[\equiv SOH^0]} \times \left(\frac{-F \cdot \Psi_0}{RT}\right) \tag{2.22}$$

where K_+^{int} and K_-^{int} are the intrinsic equilibrium constants for the protonation and deprotonation reactions in Equation 2.19 and Equation 2.20, respectively; $[\equiv SO^-]$, $[\equiv SOH^0]$, and $[\equiv SOH_2{}^0]$ are the concentrations of deprotonated, neutral, and protonated surface species, in units of mol/L; (H^+) is the activity of H^+ in solution; ψ_0 is the electric potential on the surface (electrostatic 0-plane) in units of J/C; and F, R, and T are as defined above.

Both metal cations and oxyanions have been observed to form inner-sphere surface complexes on metal (hydr)oxide surfaces [32, 39, 40, 45, 46, 49-54, 70-76]. Inner-sphere surface complexes are bound directly to the mineral surface; there are no waters of solvation present between the adsorbate and the adsorbent (Figure 2.3).

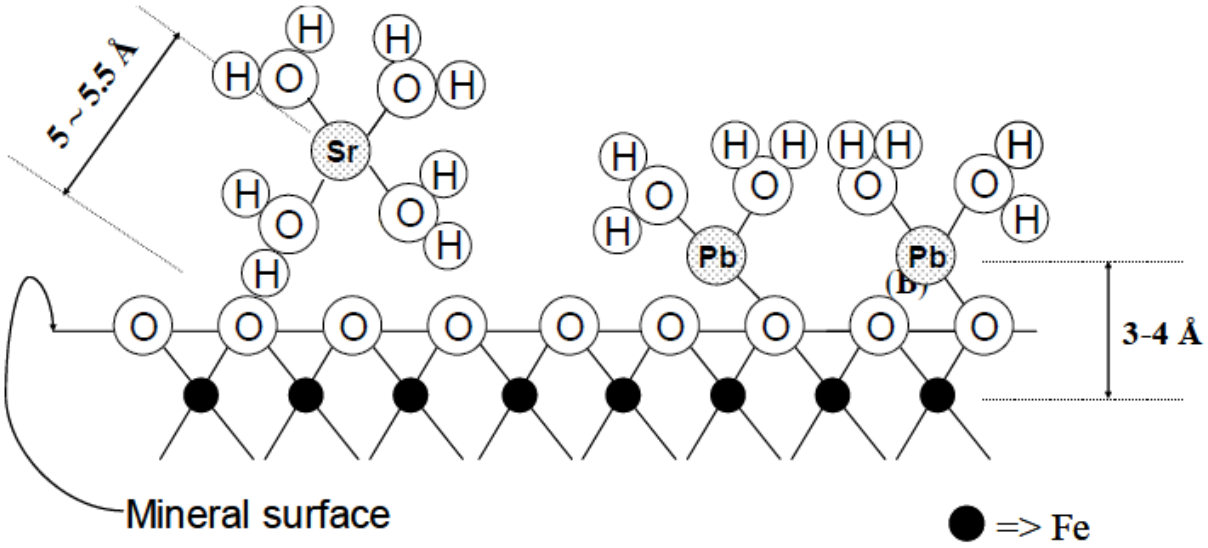

Figure 2.3 Inner- and outer-sphere surface complexation to an iron oxide mineral. Sr(II) forms an outer-sphere surface complex with a solvation shell of water surrounding the cation. Pb(II) binds directly to the mineral surface forming an inner-sphere surface complex. Taken from Chen [77].

For metal cations, inner-sphere surface complexation is achieved through the formation of bonds between the complexing metal cation and surface oxygen atoms [2, 27, 28, 33, 39, 40, 49, 53, 54, 78]. In the case of oxyanions, inner-sphere adsorption is achieved by means of a ligand exchange process in which surface hydroxyl groups are displaced by the adsorbing oxyanion [12, 34, 45, 79-81]. Most SCMs (the DLM, CCM,

TLM_m, and CD-MUSIC) are capable of describing inner-sphere surface complexation of metal cations (Me^{2+}) and oxyanions ($OxAn^{2-}$) using reactions similar to those presented here in Equation 2.23 and Equation 2.24, respectively.

$$\equiv SOH^0 + Me^{2+} \leftrightarrow \equiv SOMe^+ + H^+ \tag{2.23}$$

$$\equiv SOH^0 + H^+ + OxAn^{2-} \leftrightarrow \equiv S(OxAn)^{1-} + H_2O \tag{2.24}$$

As can be seen from Equation 2.23, adsorption of metal cations is promoted as the surface becomes more negatively charged and pH increases [33, 69, 82, 83]. In contrast, oxyanion adsorption (cf. Equation 2.24) is observed to increase with decreasing pH and the surface becomes more positively charged [45, 82, 84, 85]. The corresponding mass-law expressions for the inner-sphere surface complexation reactions in Equation 2.23 and Equation 2.24 are written here as Equation 2.25 and Equation 2.26:

$$K_{Me}^{int} = \frac{[\equiv SOMe^+] \cdot (H^+)}{[\equiv SOH^0] \cdot (Me^{2+})} \times \left(\frac{F \cdot \Psi_0}{RT}\right) \tag{2.25}$$

$$K_{OxAn}^{int} = \frac{[\equiv S(OxAn)^-]}{[\equiv SOH^0] \cdot (H^+) \cdot (OxAn^{2-})} \times \left(\frac{-F \cdot \Psi_0}{RT}\right) \tag{2.26}$$

where K_{Me}^{int} and K_{OxAn}^{int} are the intrinsic equilibrium constants for the inner-sphere adsorption reactions of metal cations and oxyanions described in Equation 2.23 and Equation 2.24, respectively; $[\equiv SOH^0]$, $[\equiv SOMe^+]$, and $[\equiv S(OxAn)^-]$ are the

concentrations of the neutral surface site, the metal cation inner-sphere complex, and, the oxyanion inner-sphere surface complex, in units of mol/L; (H^+), (Me^{2+}), and ($OxAn^{2-}$) are the aqueous activities of H^+ , the metal cation, and the oxyanion, respectively; and ψ_0, F, R, and T are as defined previously.

Metal cations, oxyanions, and background electrolytes present in solution are capable of forming outer-sphere surface complexes with metal (hydr)oxide minerals [45, 48, 86, 87]. Outer-sphere surface complexes are surrounded by a solvation shell of water that separates the adsorbate from the adsorbent and limits the ion's closest distance of approach to the mineral surface (Figure 2.3) [13, 43]. It should be noted that when background electrolytes such as Na^+ and NO_3^- form an outer-sphere complex with the mineral surface, it is termed an ion pair formation reaction. Outer-sphere surface complexation reactions for a cation (Cat^{z+}) or an anion (An^-) can be described in the TLM_o, TLM_m, and CD-MUSIC SCMs using reactions similar to those presented in Equations 2.27 and 2.28, respectively.

$$\equiv SOH^0 + Cat^{2+} \leftrightarrow \equiv SO^-\_Cat^{2+} + H^+ \quad (2.27)$$

$$\equiv SOH^0 + H^+ + An^- \leftrightarrow \equiv SOH_2^+\_An^- \quad (2.28)$$

In Equation 2.27, Cat^{2+} is used to represent all cations that can form outer-sphere complexes (e.g., Ca^{2+}, Mg^{2+}, Pb^{2+}, etc.) with the adsorbent surface. The charge of +2 was used strictly for illustrative purposes and will vary depending on the valence of the cation in question (e.g., Na^+ will have a +1 charge). In Equation 2.28, An^- is used as a general

term to denote all the anions that form outer-sphere surface complexes (e.g., NO_3^-, Cl^-, ClO_4^-). The -1 charge used for the aqueous anion species (An^-) is arbitrary and will vary depending on the charge of the complexing anion under consideration (e.g., SO_4^{2-} will have a -2 charge).

The corresponding mass-law expressions for the outer-sphere surface complexation reactions presented in Equation 2.27 and Equation 2.28 are written here as Equation 2.29 and Equation 2.30:

$$K_{Cat}^{int} = \frac{[\equiv SO^-\_Cat^{2+}] \cdot (H^+)}{[\equiv SOH^0] \cdot (Cat^{2+})} \times \left[\frac{F\left(-\Psi_0 + 2\Psi_\beta\right)}{RT}\right] \quad (2.29)$$

$$K_{An}^{int} = \frac{[\equiv SOH_2^+\_An^-]}{[\equiv SOH^0] \cdot (H^+) \cdot (An^-)} \times \left[\frac{F\left(\Psi_0 - \Psi_\beta\right)}{RT}\right] \quad (2.30)$$

where K_{Cat}^{int} and K_{An}^{int} are the intrinsic equilibrium constants for the cation and anion outer-sphere surface complexation reactions (Equation 2.27 and Equation 2.28), respectively; (H^+), (Cat^{2+}) and (An^-) are the aqueous activities of H^+, the cation, and the anion, respectively; ψ_0 and ψ_β are the electrostatic potentials for the electrostatic 0- and β-planes, respectively; and F, R, and T are as defined previously.

Unlike inner-sphere surface complexes, the adsorption behavior of outer-sphere surface complexes is observed to vary depending on the ionic strength of the solution (Figure 2.4). In particular, as ionic strength increases, the background electrolytes (e.g. $NaNO_3$, NaCl) will be present at higher concentrations in solution, meaning that it can increasingly compete with the adsorbate of interest (e.g., Ca^{2+}, SO_4^{2-}) to form outer-

sphere surface complexes with the mineral surface (Figure 2.4; Equation 2.27 and Equation 2.28). Since inner-sphere surface complexes are physically and chemically bound directly to surface oxygens, they are much stronger than outer-sphere complexes, and their adsorption behavior is not greatly affected by changes in ionic strength.

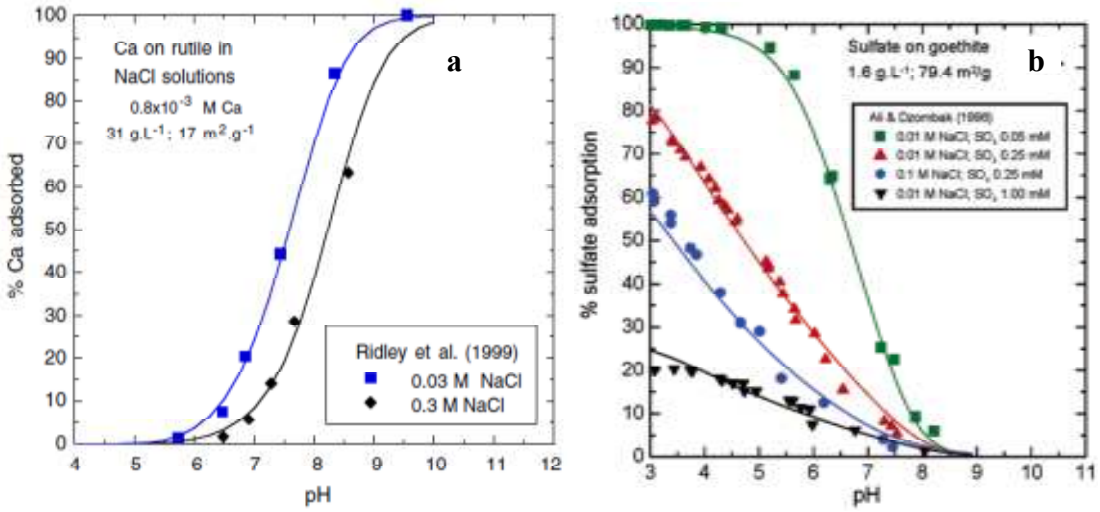

Figure 2.4 Affects of ionic strength on outer-sphere surface complexation of **(a)** calcium and **(b)** sulfate. Symbols represent experimental data and solid lines represent model predictions performed using the TLM_m. Experimental data taken from (a) Ridley et al. [88] and (b) Ali and Dzombak [89]. Figures and modeling data taken from (a) Sverjensky [90] and (b) Sverjensky and Fukushi [91].

2.4. Surface Complexation Models

SCMs describe the interaction between aqueous chemical species and the reactive sites present on the mineral's surface [6]. There are three basic principles applied to all SCMs [6]:

1. Adsorption/surface complexation of aqueous ions occurs at specific sites on the adsorbent's surface;
2. Surface complexation reactions can be described thermodynamically using mass law expressions that take into account the electrostatic effects of the EDL;
3. The electrostatic effects associated with adsorption (i.e., surface charge and surface potential) are accounted for.

A number of SCMs have been developed over the years including the Diffuse Layer Model (DLM) [2, 56, 57], the Constant Capacitance Model (CCM) [12, 58-61], the original and modified Triple Layer Model (TLM_o and TLM_m, respectively) [62-68], and the Charge Distribution Multi-Site Complexation (CD-MUSIC) Model [23-25]. These models primarily vary from one another in their description of the mineral-water interface. SCMs employing a simpler description of the mineral – water interface require less parameters to describe adsorption phenomena but are also less successful in predicting adsorption behavior in increasingly complex systems. While the more sophisticated SCMs have demonstrated a greater capability to describe ion adsorption over a broad range of experimental factors, they also require more input parameters. Thus there is a tradeoff between predictability and practicality that must be considered when selecting the appropriate SCM to use in modeling adsorption data.

2.4.1. Diffuse Layer Model (DLM)

The Diffuse Layer Model (DLM) was first introduced by Stumm et al. [57] and Huang and Stumm [56], and then further developed by Dzombak and Morel [2]. In the DLM, the mineral – water interface is thought to consist of two electrostatic planes, the surface and diffuse planes, referred to as the 0- and d-planes, respectively (Figure 2.5). Surface acidity is described using an amphoteric surface site ($\equiv SOH^0$) that can be both protonated and deprotonated (Equation 2.19 and Equation 2.20). Since only the 0- and d-planes are present in the DLM, all ion adsorption must be modeled as inner-sphere surface complexes binding directly to the mineral surface. In its original formulation, the DLM only had a single surface site type present on the mineral surface; however, to improve model predictions for cation adsorption, Dzombak and Morel [2] utilized two different site types that varied in bonding strength, termed type 1 (high affinity) and type 2 (low affinity) sites.

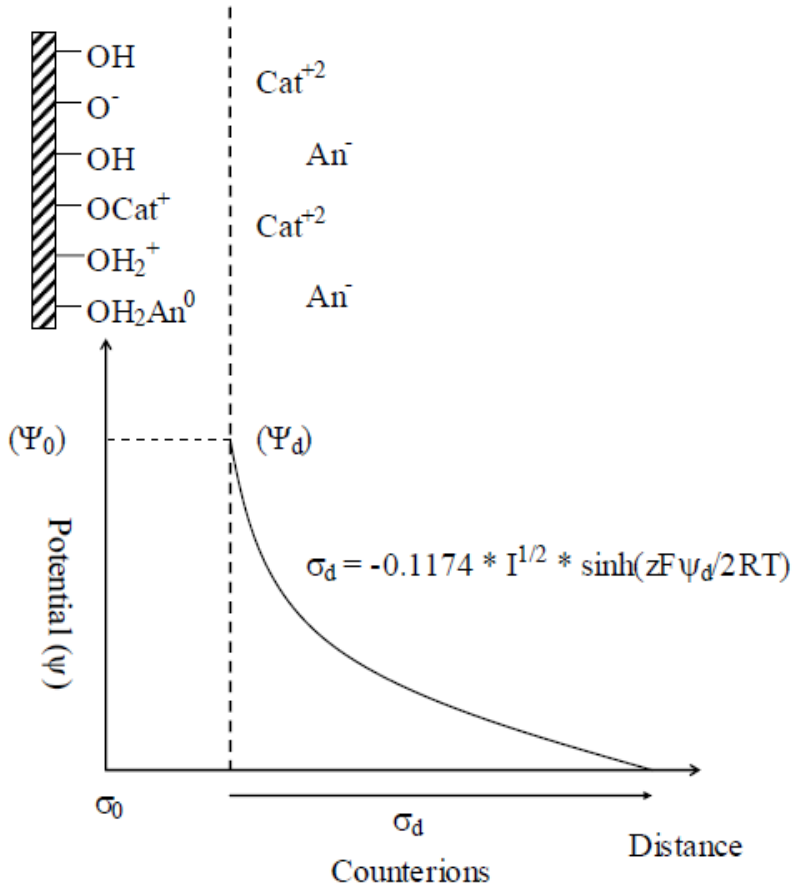

Figure 2.5 Illustration of the mineral – water interface as described in the Diffuse Layer Model (DLM). Taken from Vieira [92].

With only two electrostatic planes being considered in the model, electroneutrality is calculated using Equation 2.31:

$$\sigma_0 + \sigma_d = 0 \tag{2.31}$$

where σ_0 and σ_d are the surface charge densities of the 0- and d-planes, respectively, in units of C/m^2.

The relationship between the surface charge density of the diffuse plane (σ_d) and its electrostatic potential (ψ_d) is described using the Gouy-Chapman theory (Equation 2.7) [16, 17] which helps account for the effects of ionic strength on ion adsorption. The potential of the 0-plane (ψ_0) is equivalent to the potential of the d-plane (i.e., ψ_d).

In its simplest form (i.e., only one surface site type considered), the DLM requires four parameters to describe ion adsorption:

1. The surface protonation constant (K_+^{int});
2. The surface deprotonation constant (K_-^{int});
3. Surface site density (N_S);
4. The affinity constant for the adsorbate of interest (K_{Ads}^{int}).

2.4.2. Constant Capacitance Model (CCM)

In the Diffuse Layer Model (DLM), the electric double layer (EDL) can be approximated as a parallel plate capacitor when solutions of high ionic strength (> 0.1 M) are employed [6]. The constant capacitance model (CCM) [12, 58-61] is based on this special case of the DLM and describes the mineral – water interface as being composed of a single electrostatic plane (0-plane) located at the mineral surface (Figure 2.6). Between the mineral surface and bulk solution, a layer of constant capacitance (C_1) is thought to exist. The relation between surface charge and surface potential for the CCM is presented in Equation 2.32.

$$-\sigma_0 = \sigma_d = C_1 \cdot \psi_0 \tag{2.32}$$

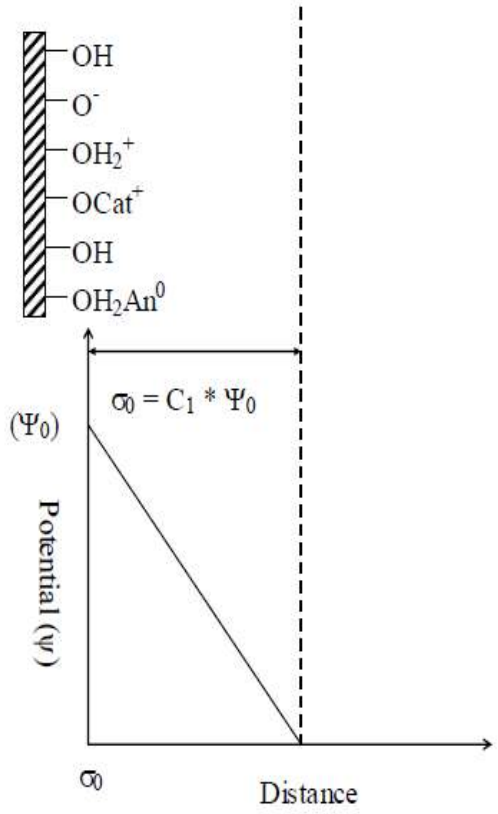

Figure 2.6 Illustration of the mineral – water interface as described in the Constant Capacitance Model (CCM). Taken from Vieira [92].

As in the DLM, the CCM utilizes amphoteric surface sites for describing surface acidity and models all ion adsorption as inner-sphere surface complexation reactions. While in theory the CCM is only valid at high and constant ionic strengths [6], the model can be used to fit adsorption data collected at variable ionic strengths if the C_1 capacitance value is considered a fitting parameter rather than a theoretically fixed value.

For the CCM, a total of five parameters are needed to predict ion adsorption:

1. The C_1 capacitance value;
2. The surface protonation constant (K_+^{int});

3. The surface deprotonation constant (K_{-}^{int});
4. Surface site density (N_S);
5. The affinity constant for the adsorbate of interest (K_{Ads}^{int}).

2.4.3. Triple Layer Model (TLM_o and TLM_m)

The Triple Layer Model (TLMo) was originally developed by Davis and coworkers [62-64] to model ion adsorption via outer-sphere surface complexation reactions. Blesa et al. [65] and Hayes and coworkers [66-68] later modified the Triple Layer Model (TLM_m) to allow for the formation of inner-sphere surface complexes as well. Herein, the modified version of the Triple Layer Model (TLM_m) will be discussed.

In the Triple Layer Model, the mineral – water interface is described using three electrostatic planes termed the 0-, β-, and d-planes (Figure 2.7). The 0-plane coincides with the mineral surface and is where H^+, OH^-, and inner-sphere complexing ions adsorb. The β-plane is located near the mineral surface and is where ion pairs and outer-sphere surface complexes are placed in the model. The d-plane used in the TLM is similar to the d-plane used in the DLM, and marks the closest distance of approach to the surface for counterions present in the diffuse layer. The 0-, β-, and d- planes are separated from each other by two charge free layers; resulting in an EDL that is electrically analogous to two parallel plate capacitors in series with capacitance values of C_1 and C_2, respectively.

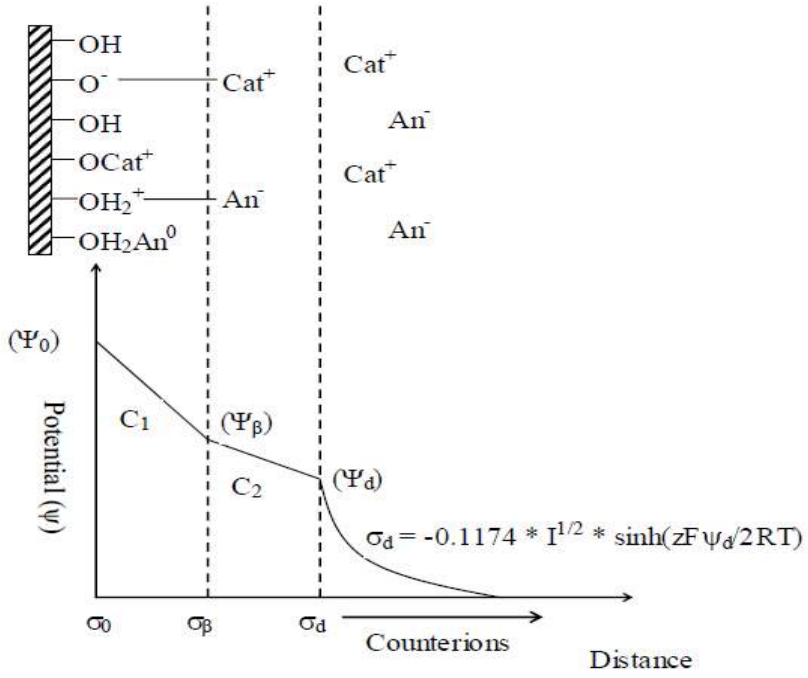

Figure 2.7 Illustration of the mineral – water interface as described in the modified Triple Layer Model (TLM_m). Taken from Vieira [92].

As with the CCM, the C_1 and C_2 capacitances used in the TLM_m are fixed and are used to describe the relation between surface charge density and electrostatic potential in Equations 2.33 – 2.35:

$$\sigma_0 + \sigma_\beta + \sigma_d = 0 \tag{2.33}$$

$$\sigma_0 = C_1 \cdot (\psi_0 - \psi_\beta) \tag{2.34}$$

$$\sigma_0 + \sigma_\beta = -\sigma_d = C_2 \cdot (\psi_\beta - \psi_d) \tag{2.35}$$

where σ_0, σ_β, and σ_d are the surface charge density of the electrostatic 0-, β-, and d-planes (C/m^2), ψ_0, ψ_β, and ψ_d are the electrostatic potentials of the 0-, β-, and d-planes (J/C), and

C_1 and C_2 are the capacitance values between the 0- and β-planes and the β- and d-planes, respectively (C^2/J). As in the DLM, the surface charge density of the diffuse layer (σ_d) is related to ψ_d via the Gouy-Chapman theory (Equation 2.6 and Equation 2.7).

Similar to the DLM and CCM, the TLM_m utilizes amphoteric surface sites to describe surface acidity (Equation 2.19 and Equation 2.20). However, unlike the other SCMs discussed up to this point, the TLM_m is capable of describing ion pair formation reactions (i.e., outer-sphere surface complexation reactions) between the background electrolyte and the mineral surface (Equation 2.29 and Equation 2.30).

For the TLM_m, a total of eight parameters are needed to predict ion adsorption:

1. The C_1 capacitance value;
2. The C_2 capacitance value;
3. The surface protonation constant (K_+^{int});
4. The surface deprotonation constant (K_-^{int});
5. The ion pair formation constant for the cation electrolyte (K_{Cat}^{int});
6. The ion pair formation constant for the anion electrolyte ($K_{An}^{int\ t}$);
7. Surface site density (N_S);
8. The affinity constant for the adsorbate of interest (K_{Ads}^{int}).

2.4.4. Charge Distribution Multi-Site Complexation (CD-MUSIC) Model

The Charge Distribution Multi-Site Complexation (CD – MUSIC) model describes the solid-water interface as being composed of three electrostatic planes (the 0-, 1-, and 2/d-plane) and two stern (charge free) layers [23-25, 93] (Figure 2.8). As in the case of

the TLM_m, the interface is considered to be electrically analogous to two parallel plate capacitors in series with the 0- and 1- electrostatic planes making up the first capacitor with capacitance C_1 and the 1- and 2-planes comprising the second capacitor with capacitance C_2. The equations governing the surface charge density and electrostatic potential relationships that were presented previously for the TLMm (i.e., Equation 2.6 , Equation 2.7, Equations 2.33 – 2.35) are all valid for the CD-MUSIC model.

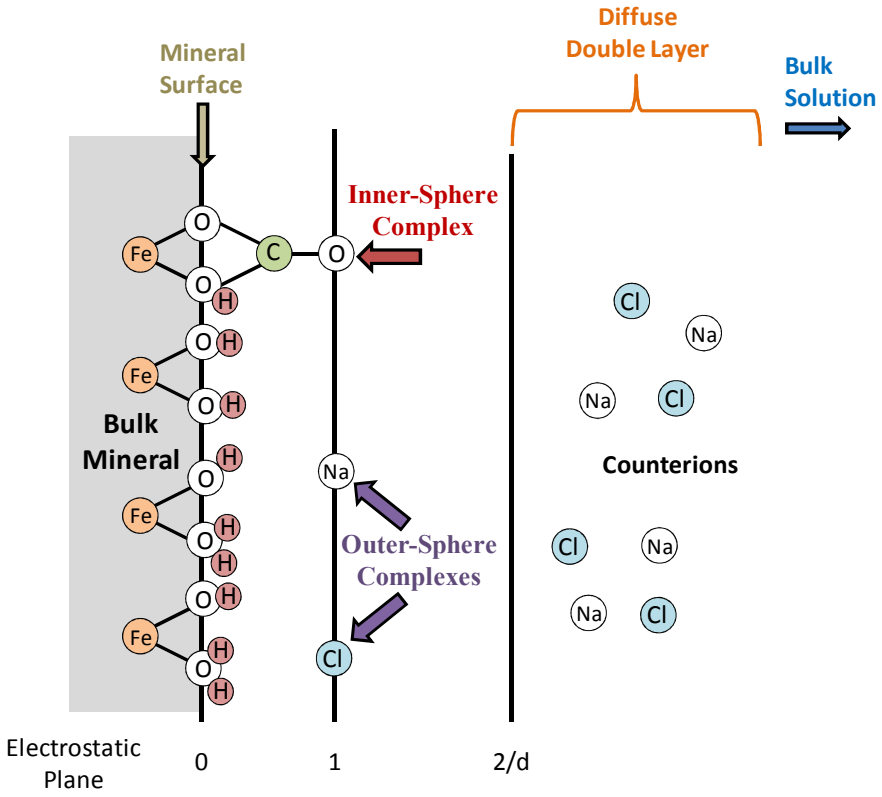

Figure 2.8 Illustration of the mineral – water interface as described by the CD-MUSIC model.

The 0-plane is located at the mineral surface where surface oxygen atoms can undergo protonation, de-protonation, and inner-sphere complexation reactions. The

charge from protons adsorbing to or desorbing from the mineral surface is all attributed to the 0-plane while the charge from an inner-sphere complex is distributed between the 0- and 1-planes. Positioned where outer-sphere complexes adsorb, the electrostatic 1-plane is separated from the 0-plane by approximately 0.35 nm, the radius of a hydrated cation [93]. As mentioned above, the charge of inner-sphere complexes is distributed between the 0- and 1-planes, therefore some of the charge from inner-sphere complexes along with all the charge from outer-sphere complexes is placed on the electrostatic 1-plane. Previously, outer-sphere complexes and ion pairs, formed by the interaction between electrolyte ions and the surface [94-96], were located on the 2/d-plane which designates the head end of the diffuse layer [23]. However, a more recent study by Rahnemaie et al. [86] provides evidence that there is charge separation between the minimum distance of approach for ion pairs and the head end of the diffuse layer [34, 86, 93]. Given this recent finding, current modeling practices for CD-MUSIC [34-36, 38, 93, 97, 98] place outer-sphere complexes and ion pairs on the 1-plane. The 2-plane also called the d- or diffuse plane marks the closest distance of approach for ions present in the diffuse double layer and is thought to be between 0.2 – 0.7 nm from the 1-plane [93].

The CD-MUSIC model tries to account for surface heterogeneity by considering the different surface site types that are present at the interface. The identity of these different surface site types and the quantity of each (i.e., N_S) is estimated using available crystallographic information for the mineral in question [23-29]. Microscopic image analysis of the mineral sample being studied can be used to approximate the contribution from each crystal face to the mineral surface (Figure 2.9) [23, 27, 99].

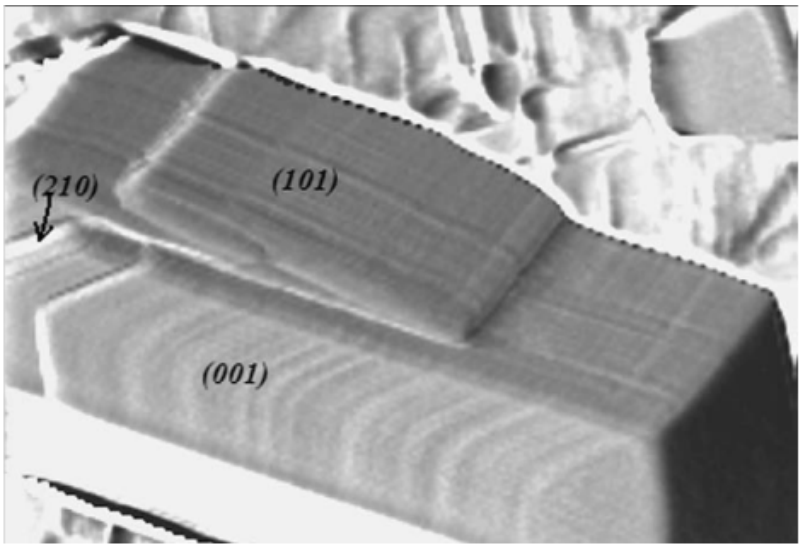

Figure 2.9 Image of a goethite crystal obtained using Atomic Force Microscopy. The contributions from three different crystal faces (see labeled) to the mineral surface can be observed. Taken from Villalobos et al. [85].

For metal (hydr)oxide minerals, the surface site types utilized in the CD-MUSIC model generally differ based on the number of metal ions they are bound to in the bulk mineral. In the case of the iron hydroxide mineral goethite (α-FeO(OH)), there are three different surface site types generally considered (Figure 2.10) [23, 27, 28]:

1. Singly coordinated (≡FeOH)
2. Doubly coordinated (≡Fe_2OH)
3. Triply coordinated (≡Fe_3O)

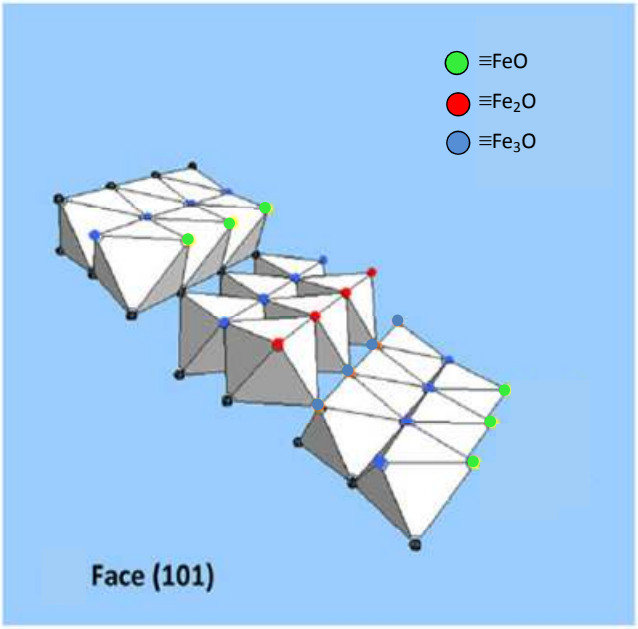

Figure 2.10 Illustration of the different site types present on the (101) crystal face of goethite. Adapted from Salazar-Camacho and Villalobos [84].

In CD-MUSIC, the charge of the different surface site types is calculated using Pauling's bond valence principle [100] to take into account the contribution from the bulk metal ions bound to the surface oxygen atom. The bond valence value is calculated using Equation 2.36:

$$v = \frac{z}{CN} \tag{2.36}$$

where v is the bond valence, z is the charge of the central cation, and CN is the coordination number for the cation.

Pauling's bond valence principle assumes that the charge of the central cation (present in the mineral's bulk) is evenly distributed between all ions that it is coordinated to. In the case of goethite (Figure 2.10), the charge of the central cation (Fe(III)) is +3, and the coordination number is six, yielding a bond valence value (v) of +0.5. Using a -2 value for the surface oxygen atom, a +1 value for every adsorbed proton, and the bond valence value of +0.5 for each Fe-O bond, the charge of each surface site type present on goethite can be calculated as -0.5, 0, and -0.5 for singly ($\equiv FeOH^{-1/2}$), doubly ($\equiv Fe_2OH^0$), and triply ($\equiv Fe_3O^{-1/2}$) coordinated sites, respectively.

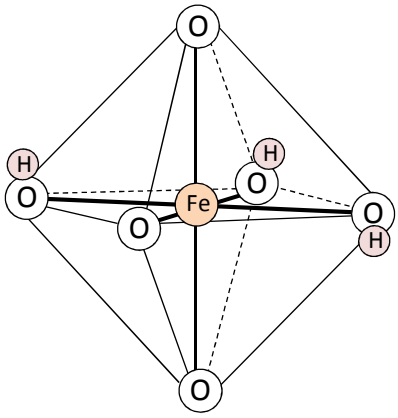

Figure 2.11 Illustration of Fe(III)'s coordination environment in goethite.

Using the site types reported from crystallographic studies, the acidity of the mineral surface is described in CD-MUSIC using a 1-pK approach in which there is only a single protonation step. In the case of goethite, doubly coordinated surface sites ($\equiv Fe_2OH^0$) have been predicted to be unreactive to protonation and deprotonation reactions in the environmentally relevant pH range [26, 27, 29, 85, 97]; hence only singly

and triply coordinated surface sites are considered in predicting goethite's surface charging behavior (Equation 2.37 – 2.42)

$$\equiv FeOH^{-0.5} + H^{+} \leftrightarrow \equiv FeOH_2^{+0.5} \quad (2.37)$$

$$\equiv FeOH^{-0.5} + H^{+} + An^{-} \leftrightarrow \equiv FeOH_2^{+0.5}\_An^{-} \quad (2.38)$$

$$\equiv FeOH^{-0.5} + Cat^{+} \leftrightarrow \equiv FeOH_2^{+0.5}\_Cat^{+} \quad (2.39)$$

$$\equiv Fe_3O^{-0.5} + H^{+} \leftrightarrow \equiv Fe_3OH^{+0.5} \quad (2.40)$$

$$\equiv Fe_3O^{-0.5} + H^{+} + An^{-} \leftrightarrow \equiv Fe_3OH^{+0.5}\_An^{-} \quad (2.41)$$

$$\equiv Fe_3O^{-0.5} + Cat^{+} \leftrightarrow \equiv Fe_3OH^{+0.5}\_Cat^{+} \quad (2.42)$$

Hiemstra and Van Riemsdijk [23] contend that when inner-sphere surface complexes form, only part of the adsorbate is actually incorporated into the mineral surface while the remainder is present in the "charge free" region between the 0- and 1-planes (Figure 2.8). In order to account for the spatial distribution of an inner-sphere surface complex's charge, the CD-MUSIC model utilizes charge distribution (CD) values [23, 93]. In particular, CD values are used to describe the change in charge on the 0- and 1- electrostatic planes (Δz_0 and Δz_1, respectively) that occur as the result of an inner-sphere surface complexation reaction. The Δz_0 and Δz_1 values are calculated using Equation 2.43 and 2.44:

$$\Delta z_0 = n_0 + n_{H0} - \phi(n_0 + n_{H0} + \Sigma n_{ref} z_{ref}) \quad (2.43)$$

$$\Delta z_1 = n_1 + n_{H1} + \phi(n_0 + n_{H0} + \Sigma n_{ref} z_{ref}) \quad (2.44)$$

where n_0 and n_1 denote the amount of adsorbate charge placed on the 0- and 1-planes, respectively, n_{H0} and n_{H1} are the charge from additional protons and/or other ligands involved in the reaction and located on the 0- and 1-planes, respectively, the symbol ϕ is a constant ($\phi \approx 0.17$), n_{ref} is the number of surface sites of a given type that are involved in the reaction, and z_{ref} is the reference state charge of those surface sites.

In the case of goethite, a total of 14 parameters are needed to predict ion adsorption in CD-MUSIC:

1. The C_1 capacitance value;
2. The C_2 capacitance value;
3. The surface protonation constant for ≡FeOH sites;
4. The surface protonation constant for $\equiv Fe_3O$ sites;
5. The ion pair formation constant for the cation electrolyte for ≡FeOH;
6. The ion pair formation constant for the anion electrolyte for ≡FeOH;
7. The ion pair formation constant for the cation electrolyte for $\equiv Fe_3O$;
8. The ion pair formation constant for the anion electrolyte for $\equiv Fe_3O$;
9. Surface site density of ≡FeOH;
10. Surface site density of $\equiv Fe_2OH$;
11. Surface site density of $\equiv Fe_3O$;
12. The affinity constant for the adsorbate of interest

13. The Δz_0 value for the inner-sphere surface complex

14. The Δz_1 value for the inner-sphere surface complex

2.5. Summary

There are a number of surface complexation models (SCMs) available for modeling adsorption processes. Given the small number of modeling parameters needed to employ the DLM and CCM, both are attractive in their simplicity; however, the simplicity of these models also limits their predictive capability, especially in complex, multi-solute systems. The TLM_m and CD-MUSIC models are better able to capture the complexity of the mineral-water interface by accounting for both inner- and outer-sphere surface complexes. These models are better suited than the DLM and CCM for predicting adsorption behavior over a broad range of conditions but require additional modeling parameters. Given the breadth of experimental conditions considered in this work (i.e., pH, surface loading, competing adsorbates), one of the more sophisticated SCMs is needed to develop a predictive tool capable of accurately simulating ion adsorption behavior under all conditions studied.

While the CD-MUSIC model requires more parameters than the TLM_m, it provides a more complete picture of the mineral – water interface by accounting for mineral surface heterogeneity. By accounting for the different site types physically present on the mineral surface, the CD-MUSIC model can employ surface complexes in closer agreement with molecular scale analyses (i.e., spectroscopic data and computational molecular modeling simulations) than the TLM_m. Furthermore, in

accounting for mineral surface heterogeneity, the CD-MUSIC model appears to be better suited for predicting adsorbate competition. In fact, more recent adaptations of the TLMm have started to employ multiple surface site types to improve model predictions of adsorption behavior [82, 84, 85].

Although CD-MUSIC requires the largest number of parameters of any of the SCMs considered, a number of these parameters can be estimated based on experimental and theoretical findings:

1. Hiemstra and Van Riemsdijk [93] along with Sverjensky [101] have reasoned that the outer layer capacitance (C_2) is approximately equal to the inner layer capacitance (C_1) based on theoretical considerations of the electrical double layer. This approximation that $C_1 \equiv C_2$ is currently used in modeling studies [34, 35, 38, 98];

2. The N_S values for the different surface site types can be determined using crystallographic information in conjunction with microscopic image analysis, surface saturation data, or surface charging data [23, 27, 28, 84, 85, 99];

3. The affinity constants for ion pair formation on the different surface site types are considered equivalent [26-29];

4. The protonation equilibrium constants for the different surface site types can be determined based on the formal charge of the surface oxygen; thus allowing for the acid – base properties of the adsorbent to be predicted theoretically [26, 29];

5. The Δz_0 and Δz_1 values can be calculated using bond valence analysis in conjunction with bond lengths obtained from spectroscopic analysis or computational molecular modeling simulations.

When all these parameter estimation techniques are employed, the number of fitting parameters that are needed to model ion adsorption using CD-MUSIC drops from 14 down to 4, making the CD-MUSIC model much more manageable to use. Therefore, given the low number of fitting parameters needed to run the model, its sophisticated description of the electrical double layer and the mineral surface, and its ability to predict ion adsorption behavior in simple and complex systems, the CD-MUSIC model appears to hold the most promise for modeling adsorption in increasingly complex systems.

With that being said, there are limitations to the CD-MUSIC model that have yet to be addressed. In particular, for the iron hydroxide goethite, researchers have assumed only the (101) and (210) crystal faces to be present on the mineral surface. In most cases, goethite's surface is thought to possess 90% (101) face and 10% (210) face, regardless of mineral sample in question (i.e., SSA and particle size) [27, 28, 34, 37, 86, 98, 102]. While this generalization of the goethite surface simplifies the modeling process, it fails to capture how the reactivity and crystal face composition (CFC) of goethite changes

between mineral samples [82, 84, 85, 99]. In fact, to sidestep this issue, researchers using CD-MUSIC have arbitrarily adjusted the specific surface area (SSA) of goethite samples, employed surface species not supported by spectroscopic data, utilized CD values not consistent with bond valence analysis, and used the CFC of goethite as a fitting parameter (i.e., adjusting the %(101) face to get the best model fit) [28, 33, 34, 102]. In this work, the variable CFC of goethite will be specifically addressed and techniques will be employed to determine the CFC for each goethite sample considered.

Chapter 3 : CHARACTERIZING MINERAL SURFACE HETEROGENEITY

3.1. Introduction

Ion interactions at the mineral – water interface can play a pivotal role in controlling a contaminant's migration and bioavailability in the subsurface [1-4]. Surface complexation models (SCMs) [2, 4, 6, 23-25] have been developed to describe these interactions between aqueous ions and mineral surfaces and have proven capable of predicting ion adsorption behavior over a range of environmental conditions [27, 28, 30, 31, 33-36, 38, 75, 82, 84, 87, 103-105]. While SCMs can vary in complexity and the number of adjustable parameters present in the model, one parameter common to all SCMs is surface site density (N_s). In numerous modeling studies, the adsorbent surface is thought to be composed of a single generic site type (e.g. [69, 75, 83, 101, 106-108]) or a distribution of high and low affinity site types (e.g. [2, 92, 104, 109, 110]); thereby requiring the model to have one or two N_s values, respectively. Although the models developed from this approach have proven capable of predicting adsorption in relatively simple, mono-solute systems [2, 27, 30, 33, 34, 69, 75, 83-85, 107, 108, 111], utilization of these models to describe more extensive data sets or more complex systems has proven difficult, and oftentimes requires incorporation of surface species into the model that are not consistent with molecular scale analysis [2, 28, 33, 34, 107, 108]. In this study, we contend that these observed deficiencies are, in part, a result of an oversimplification of the model's description of the mineral surface and in part due to inappropriate interpretation of the results from various techniques for estimating site density. We hypothesize that application of a surface complexation model that appropriately

characterizes the surface site distribution across different crystal faces of a mineral can be used to develop a unifying theory that appropriately incorporates data from different site density estimation techniques.

Mineral surfaces are comprised of crystal faces that are specific to a given mineral [85, 112-114]. These crystal faces possess surface functional groups (i.e. adsorption sites) that can vary in type and density (sites/nm^2) from one crystal face to another. Each type of surface functional group, herein referred to as surface site type, is thought to possess its own unique reactivity to adsorbing ions, including protons [26, 27, 29, 97]. Furthermore, adsorption studies utilizing spectroscopy, computational molecular modeling, bond valence analysis or some combination thereof, have revealed that site reactivity varies depending on the adsorbate, the surface site type, and the coordination environment [27, 34, 36, 39, 40, 42, 49-54, 70-72, 97]. Since the surface site type, site density, and coordination environment can vary depending on the crystal face considered, the mineral surface's morphology or crystal face composition (CFC), greatly affects its reactivity [24, 25, 82, 84, 85]. Given this information, it stands to reason that attempts to better quantify the mineral surface's heterogeneity by estimating its CFC and in turn, incorporating the different surface site types present on these crystal faces into a SCM, as done in the CD-MUSIC model [23-26] and some adaptations of the Triple Layer Model [84, 85], will improve model predictions in increasingly complex systems. Furthermore, this modeling strategy allows for better agreement between macro-scale models (SCMs) and molecular scale analysis by enabling selection of surface species employed in SCMs to be guided by spectroscopic data and computational molecular modeling simulations.

With the objective in mind of better describing mineral surface heterogeneity in SCMs via estimation of the mineral's CFC and incorporating the different surface site types present on these crystal faces into the SCM, the focus of this paper is on the iron hydroxide mineral goethite (α-FeO(OH)). Given its abundance in the environment, well researched crystal morphology, and thermodynamic stability under aerobic conditions [28, 92], goethite has been frequently used in adsorption experiments and modeling studies [26, 27, 29-35, 37, 38, 74, 82, 85, 92, 98, 99, 115-120], and is therefore well suited for our discussion.

SCMs that assume a single homogenous site type to be present on the mineral surface, or a distribution of high and low affinity sites, can estimate the N_S parameter utilizing techniques (discussed in detail below) such as crystallography, tritium exchange, surface saturation, and objective curve fitting for the mineral sample of interest [2, 106-108, 121-126]. Depending on the estimation technique used, site density values for goethite have been found to range between 0.5 and 20 sites/nm^2 [92]. SCMs utilizing a single homogenous site type, or a distribution of high and low affinity sites, cannot account for these different reported site density values and therefore must employ a single N_S value to represent the "true" site density of the mineral sample.

For SCMs such as CD-MUSIC that consider the surface heterogeneity of the mineral in more detail, the CFC of the mineral sample must be established in order to determine the N_S value for each surface site type considered in the model. In the case of the iron hydroxide mineral goethite, researchers have typically assumed the mineral surface to be composed of 90% (101) face and 10% (210) face, regardless of mineral

sample in question [27, 28, 34, 37, 86, 98, 102]. While this approach for estimating CFC provides a simple and straightforward method for determining the N_S of each surface site type considered, it fails to account for the differences in reactivity and CFC that have been observed for goethite both experimentally and through microscopic image analysis [23, 24, 82, 85, 99, 118, 127-130]. As a result, in order to attain satisfactory model fits using the 90% (101) and 10% (210) CFC, researchers have needed to adjust the SSA of goethite samples or utilize surface species not consistent with spectroscopic observations [28, 34, 102].

In this work, a methodology is developed for predicting the CFC of a mineral sample that unifies the different N_S values predicted from crystallography, microscopic image analysis, tritium exchange, surface saturation and surface charging data for the iron hydroxide mineral goethite. This methodology was applied to a goethite mineral sample to substantiate its ability to provide conformity among the different N_S values predicted from these different estimation techniques. For the methods presented here, CFC is calculated assuming only perfect crystal faces are present on the mineral surface. Experimental approaches discussed (i.e., tritium exchange and surface saturation) can be used to measure the number of reactive sites present on the mineral surface and help create a CFC capable of accounting for crystal face defects.

3.2. Crystal Morphology of Goethite

For goethite, the (101), (001), (210), and (010) crystal faces (using the Pnma space group) have been identified as the four principal crystal faces of the mineral [1, 27, 82, 85, 99, 118, 127, 129] through the use of different analytical techniques such as scanning electron microscopy (SEM), transmission electron microscopy (TEM), deflection mode atomic force microscopy (AFM), and deflection mode scanning force microscopy (SFM) [82]. The (101) and (001) crystal faces are commonly referred to as the "main" crystal faces while the (210) and (010) faces are referred to as the "capping/terminal" faces [85].

The surface of goethite is composed of oxygen ions bound to one, two, or three iron atoms present in the mineral's bulk [23]. These surface oxygens are termed singly, doubly, and triply coordinated sites, respectively, and constitute the surface functional groups present at the goethite – water interface (cf. Figure 3.1 and Figure 3.2). While all three site types can participate in adsorption reactions, their reactivity depends on the complexing ion and crystal face involved [27, 33, 34, 39, 40, 46, 54, 78]. Mounting evidence suggests that doubly coordinated sites on goethite are nonreactive to protons at environmentally relevant pHs; however, singly and triply coordinated surface oxygens are considered to be proton reactive, with log K_H's of ≈ 8 and 11.7, respectively [26, 27, 29, 82, 85, 97, 131]. Each surface site type present on goethite can be classified further and placed into subcategories based on whether the surface oxygen has a high or low proton affinity, labeled O_I and O_{II} respectively [26, 27, 29].

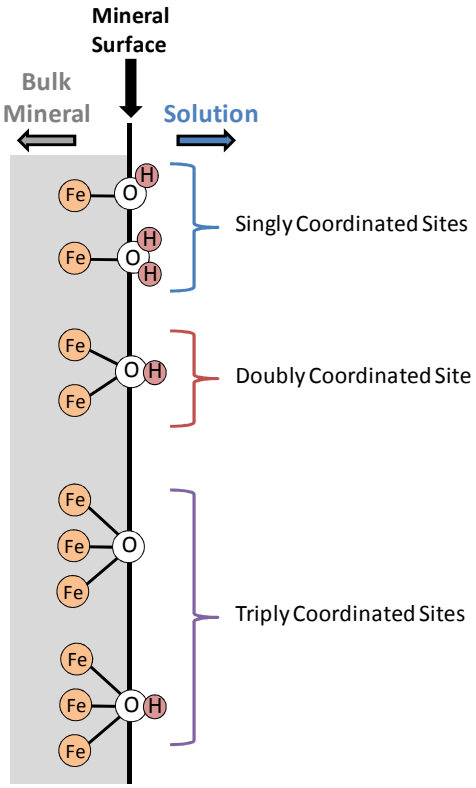

Figure 3.1 Surface functional groups present at the goethite – water interface with different protonation states. Note that for the environmentally relevant pH range, singly coordinated surface sites are either singly or doubly protonated, doubly coordinated sites are singly protonated, and triply coordinated sites are deprotonated or singly protonated [27, 30, 32, 86].

The (101) and the (001) crystal faces of goethite both possess singly, doubly, and triply coordinated surface sites (cf. Table 3.1) [99]. All singly and doubly coordinated sites present on these two crystal faces have a surface oxygen atom with a low proton affinity (O_{II}). In addition, one third of the triply coordinated sites found on the (101) and (001) faces also possess an O_{II} surface oxygen; the other two thirds are comprised of a surface oxygen with a high proton affinity (O_I) [26, 27, 29, 99]. The combination of two

triply coordinated sites, one with high and the other with low proton affinity ($\equiv Fe_3O_I$ and $\equiv Fe_3O_{II}$, respectively), has been found to render both surface sites inert [24]. For this reason, only one third of the triply coordinated sites present on the (101) and (001) crystal faces are considered reactive.

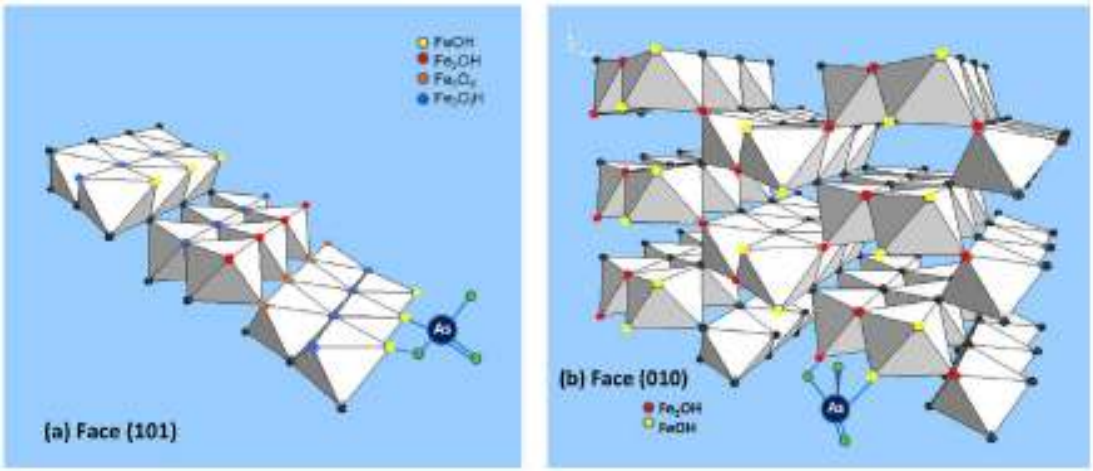

Figure 3.2 Arsenate surface complexation as a corner sharing complex (a) onto face (101) of goethite via two bonds to two singly coordinated surface groups located on adjacent octahedra; and (b) on face (010) of goethite via one bond to a singly coordinated surface group and a second bond to a doubly coordinated surface group located on an adjacent octahedron. Taken from Salazar-Camacho and Villalobos [84].

Table 3.1 Site types and site densities (sites/nm^2) present on the predominant crystal faces of goethite

Surface Site Type	Crystal Face N_s (sites/nm^2)			
	(101)[a]	(001)[b]	(210)[a]	(010)[c]
$\equiv FeO_I$	0	0	3.75	9.1
$\equiv FeO_{II}$	3.03	3.34	3.75	
$\equiv Fe_2O_I$	0	0	3.75	9.1
$\equiv Fe_2O_{II}$	3.03	3.34	3.75	
$\equiv Fe_3O_I$	6.06	6.68	0	0
$\equiv Fe_3O_{II}$	3.03	3.34	0	0

Site densities are taken from:
[a] Venema et al. [29]
[b] Gaboriaud and Ehrhardt [99]
[c] Lutzenkirchen et al. [129]

Similar to the (101) and (001) main faces, the (210) and (010) capping faces (using the Pnma space group) share many of the same attributes but do vary with respect to site density and their structural arrangement of surface sites. On these capping/terminal faces of goethite, only singly and doubly coordinated sites are present, and in the case of the (210) face both surface groups are comprised of equal amounts of low and high proton affinity oxygens [29]. To our knowledge, the distribution of sites with low and high proton affinity oxygens on the (010) face has not been determined.

For goethite, crystal faces can vary not only with respect to the number and type of surface sites present, but also in their structure/coordination environment; specifically in the arrangement of singly coordinated sites, which can significantly impact surface reactivity with respect to particular complexing ions [36, 78]. Singly coordinated surface sites present on the (101), (001), and (210) crystal faces are positioned at the corners of

adjacent octahedra allowing for double corner bidentate complexes to form via two singly coordinated sites [97]. On the (010) capping face, a subset of iron octahedra possess edges that are constructed from pairs of singly coordinated surface oxygens. This arrangement on the (010) crystal face permits the formation of edge sharing bidentate complexes utilizing two singly coordinated sites but at the same time renders the formation of double corner bidentate complexes utilizing two singly coordinated sites impossible (Figure 3.2) [97].

3.3. Describing Surface Heterogeneity in SCMs

Once a CFC is established for a given mineral sample, the different site types and their respective site density values can be determined for goethite using the crystallographic information presented in Table 3.1. Previous modeling studies that have estimated the CFC of goethite have typically considered only two crystal faces to be present on the mineral surface, either the (101) and (210) [27, 28, 33, 34, 38], the (101) and (001) [99], or the (101) and (010) [84, 85]; resulting in a total of eight, eight, and six possible site types, respectively. To make the SCM more manageable, certain assumptions regarding the site types present on the different crystal faces are employed. In particular, doubly coordinated sites on the (101) and (001) crystal faces are not considered reactive [26, 27, 85, 97, 99], the combination of one $\equiv Fe_3O_I$ site and one $\equiv Fe_3O_{II}$ site is thought to result in both sites being unreactive [24], $\equiv FeO_I$ and $\equiv FeO_{II}$ sites on the (210) and (010) crystal faces are equivalent [27, 28, 84, 85], and $\equiv Fe_2O_I$ and $\equiv Fe_2O_{II}$ sites on the (210) and (010) crystal faces are equivalent. These assumptions result in a simplified description of the interface (Table 3.2).

Table 3.2 Simplified site types and site densities (sites/nm^2) present on the predominant crystal faces of goethite

Surface Site Type	Crystal Face N_s (sites/nm^2)			
	(101)	(001)	(210)	(010)
≡FeO	3.03	3.34	7.5	9.1
≡Fe_2O	0	0	7.5	9.1
≡Fe_3O	3.03	3.34	0	0

Further simplification of the SCM's description of the mineral surface is possible depending on whether the site types present on each crystal face are considered independently [27, 28] or collectively [34, 35, 84, 85, 98, 132], termed the segregate and composite approaches, respectively. In the segregate approach, each surface site type, on each crystal face considered, is entered into the model as its own component; whereas in the composite approach, all sites of a given site type are considered equivalent to each other, irrespective of crystal face. For example, if a goethite sample was found to have a CFC consisting of the (101) and (210) crystal faces, eight (Table 3.1) or four (Table 3.2) surface site types would be used in the model's description of the mineral surface. However, if the composite approach was used for the same goethite sample, a total of six (Table 3.1) or three (Table 3.2) surface site types would be incorporated into the model. By considering each surface site type independently, the segregate approach allows for the model to achieve a high level of specificity regarding the identity of each surface complex employed. In comparison, SCMs utilizing the composite approach are unable to

distinguish between crystal faces; resulting in an ambiguous description of the mineral surface and surface complexes with unclear coordination environments.

In multi-solute systems, ion adsorption behavior is influenced by site competition between the different adsorbates present in solution, as well as electrostatic effects that result from different ions adsorbing to the mineral surface [28, 133-135]. By inputting the different site types found on the mineral surface into a SCM, surface species employed in the model can be guided by molecular scale analysis and more closely reflect the surface complex's actual identity (i.e., coordination environment), as predicted from spectroscopic data and computational molecular modeling simulations. With the SCM capable of specifying each surface complex's true coordination environment, the model will be better able to describe adsorption behavior in single solute systems and capture site competition effects between competing adsorbates in multi-solute systems. In addition, for SCMs such as CD-MUSIC that take into account the spatial distribution of an inner-sphere surface complex's charge, the model's ability to specify the true bonding environment of a surface complex will allow for better predictions concerning the electrostatic effects associated with adsorption reactions.

For example, consider Cd(II) surface complexation onto goethite. Spectroscopic evidence suggests that Cd(II) binds on goethite as an edge sharing complex to two singly and one doubly coordinated surface site on the (210) crystal face (using the Pnma space group), and as a corner sharing complex to two singly coordinated surface sites on the (101) crystal face [27, 39, 40]. In SCMs utilizing one generic surface site type (>SOH), the best description the model can give concerning the Cd(II) edge and corner sharing

complexes, with respect to agreeing with spectroscopic data, would be $(>SOH)_3Cd$ and $(>SOH)_2Cd$. In this instance, the Cd(II) edge sharing complex would compete with the Cd(II) corner sharing complex for the same (>SOH) surface sites; whereas in reality, no competition between these two species is thought to occur since the edge sharing complex forms only on the (210) face while the corner sharing complex is only found on the (101) face. Furthermore, the edge sharing complex $(>SOH)_3Cd$ is binding to three surface sites of the same type rather than two of one type (singly coordinated) and one of another type (doubly coordinated); thereby inflating site competition in the model for the one site type used (>SOH). This same line of reasoning can be extended to multi-solute systems as well, where the edge sharing complex $(>SOH)_3Cd$ is now competing with the Cd(II) corner sharing complex, as well as the surface complexes forming from other adsorbates.

To illustrate the potential impact that a one site model could have on electrostatics, consider the scenario described above in the context of the CD-MUSIC model. In CD-MUSIC, different inner-sphere surface complexes have different charge distribution (CD) values that are used to account for the spatial distribution of an inner-sphere surface complex's charge between the surface/0 and 1 electrostatic planes [23]. The amount of charge placed on the 0 and 1 electrostatic planes (Δz_0 and Δz_1, respectively) from an adsorption reaction varies depending on the surface complex formed. In the case of Cd(II) adsorption, the tridentate edge sharing complex has CD values of $\Delta z_0 = 1.15$ and $\Delta z_1 = 0.85$, while the bidentate corner sharing complex $\Delta z_0 = 0.82$ and $\Delta z_1 = 1.18$ (Table 3.6). Hence, if the model allows the tridentate edge sharing

complex to form on all surface sites, rather than only those on the (210) crystal face, the model could overestimate the positive charge present on the mineral surface. This could potentially cause the model to under predict other cations adsorbing to the surface due to the elevated electrostatic repulsion predicted to occur between the surface and the positively charged adsorbate. It should be noted that while the one site model is never used in CD-MUSIC, the scenario outlined above yields a two site model that assumes all surface sites of a given type are equivalent, regardless of the crystal face they are located on (i.e., the composite approach) [34, 35, 98, 132]. This approach essentially negates the robustness of the CD-MUSIC model and suggests that the potential electrostatic issue discussed above is a valid concern for the CD-MUSIC model.

3.4. CFC and N_S: Methods of Determination

A number of different approaches have been applied over the years to estimate the CFC and/or N_S of goethite [27, 29, 82, 92, 99, 115-117, 127, 136]. In this section, some of the more common practices for determining CFC are discussed.

3.4.1. Microscopic Image Analysis

The crystal face composition (CFC) of a mineral surface can be estimated through a number of analytical techniques such as atomic force microscopy (AFM), high resolution transmission electron microscopy (HRTEM), and scanning electron microscopy (SEM) [23, 29, 99, 114, 127]. By analyzing microscopy images of individual

mineral particles/crystals, the CFC of the mineral can be estimated. If the mineral's structure and crystallinity are known, the N_s of each surface site type can be determined.

While the utility of this technique is evident, there are drawbacks related to this procedure that must be considered. In particular, this approach assumes that the mineral is composed of perfect crystal faces, which is not usually true; crystal faces typically possess a number of defects [6, 115, 119, 137, 138]. Another difficulty with this method is that the CFC determined for a mineral sample is based on the analysis of a few individual crystals and their z-profiles/cross-sections. Furthermore, the CFC calculated for a single crystal can vary depending on the location of the cross-section analyzed [99]. Therefore, while this method does provide a reliable CFC of the mineral using analytical techniques, the value reported may not always reflect the average CFC for the mineral sample being studied. One additional difficulty in estimating the CFC of a mineral using microscopic image analysis is when there is a scarcity of information regarding the morphology, crystallinity, and grain size for the mineral of interest [119].

3.4.2. Tritium Exchange

Tritium exchange is a technique used to estimate the number of surface protons present on an oxide mineral. Using the method of Berube, Onoda, and de Bruyn (1967) [139], Yates (1975) and Yates et al. (1977) performed tritium exchange experiments on a number of metal oxides including goethite [115, 136].

The procedure employed by Yates (1975) involves initially placing an oxide sample into a centrifuge tube with tritiated water of known activity. The tube is then sealed and shaken continuously for a given amount of time, after which the resulting tritium labeled oxide is outgassed in a vacuum for 4 days to remove any physically adsorbed water. To extract the tritium from the mineral surface, the oxide is set in a centrifuge tube with ultra pure, unlabelled water. The tube is then sealed and shaken continuously for approximately 50 hours. At various times throughout the extraction process, the contents of the tube are centrifuged down and samples of the supernatant are taken and then measured for radioactivity. Plotting the results from the extraction process as radioactivity in solution versus time and then extrapolating that data back to time zero allows for the number of rapidly exchangeable protons (i.e. surface protons) to be determined [136]. Dividing the number of surface protons by the surface area of the oxide sample allows for the surface proton site density (N_{TRIT}) to be calculated.

Using the tritium exchange technique of Berube et al. (1967), Yates et al. (1977) found the N_{TRIT} for goethite samples with SSAs of 39, 48, and 54 m^2/g to range from 16.4 ± 0.7 up to 18 - 20 protons/nm^2 depending on the extraction times considered in extrapolating the data. The former value of 16.4 ± 0.7 protons/nm^2 was arrived at utilizing extraction times of less than 15 minutes whereas the latter values of 18 - 20 protons/nm^2 were determined from longer extraction times in which the first 15 minutes were ignored [136]. Yates et al. (1977) contends that the higher end N_{TRIT} values ranging between 18 - 20 protons/nm^2 provide a more accurate description of the goethite surface given that it may take several minutes before the labeled goethite is fully wetted; thus

warranting extrapolation of the tritium exchange data from longer extraction times. More recently however, a study by Rustad et al. [140] involving molecular statics calculations on the different crystal faces of goethite argues in favor of the N_{TRIT} value of 16.4 for goethites made up predominantly with the (101) and (210) crystal faces [140]. Given this finding, several adsorption modeling studies involving goethite over a range of SSAs from 45 - 86 m^2/g have set the total site density (N_{TOT}) of goethite in their models equal to 16.4 sites/nm^2 [92, 119]. It is important to note that in these modeling studies N_{TRIT} is assumed to be equal to N_{TOT} which is not necessarily true unless each surface site is considered to have only one rapidly exchangeable proton. This assumption seems questionable given the fact that N_{TOT} for the (101) and (210) crystal faces is 15.15 and 15 sites/nm^2, respectively (cf. Table 3.3). The only way that a goethite surface composed of the (101) and (210) crystal faces, as described by Rustad et al. (1996), can possess a N_{TRIT} value of 16.4 is if some of the sites on these crystal faces possess more than one surface proton. To that same point, if the value for N_{TRIT} is actually between 18 – 20 protons/nm^2, as suggested by Yates et al. (1977), certain surface sites must possess more than one surface proton.

While oxygen ligands typically have a total of four molecular orbitals available for bonding when part of a solution complex, this number can effectively decrease in the case of surface complexes due to heightened spatial constraints [26, 29]. When considering singly coordinated sites on goethite, both Venema et al. [29] and Hiemstra et al. [26] contend that, due to steric hindrance, these surface oxygens have three orbitals available for bonding, one of which is participating in the linkage between bulk iron and

the surface oxygen. Given this fact, the authors conclude that singly coordinated sites can bond with a maximum of two protons. The two studies additionally contend that deprotonated doubly coordinated sites (i.e. Fe_2O^{-1}) on the (101) face of goethite can form only one hydrogen bridge with water. This assertion by the authors implies that doubly coordinated surface oxygens possess three orbitals available for bonding, two of which are involved in iron – oxygen bonds, which in turn suggest that doubly coordinated sites can only be singly protonated. Additionally, bond valence analysis indicates that the $\equiv FeO_2H_2$ species does not exist on goethite due to oversaturation of the surface oxygen bond [54]. Given this information, doubly coordinated surface sites are considered to only be singly protonated in this study. In the case of triply coordinated surface oxygens, three out of the four available orbitals are being used in iron – oxygen bonds and hence only one orbital is available for proton binding. In addition, Hiemstra et al. [26] and Venema et al. [26] both concluded that the $\equiv Fe_3O_{II}$ surface site possesses a very low proton affinity constant (log K determined to be 0.2 and -0.2, respectively), and are therefore considered to be unprotonated under the experimental conditions employed.

In summary, singly, doubly, and triply ($\equiv Fe_3O_I$) coordinated surface sites present on goethite can bind a maximum of two, one, and one protons, respectively. Given this information, the predicted surface proton site density (N_{TRIT}) for each of the four crystal faces considered can be calculated (Table 3.3). To test the validity of the N_{TRIT} values presented in Table 3.3, the experimental value obtained by Yates et al. [136] for a goethite sample with a specific surface area (SSA) of 54 m^2/g was compared to the theoretical N_{TRIT} value for a well characterized goethite sample with a SSA of 49 m^2/g.

Using the CFC previously established from AFM image analysis (Gaboriaud and Ehrhardt [99]) of 30% (101) face and 70% (001) face, the goethite sample possessing a SSA of 49 m^2/g yielded a predicted N_{TRIT} value of 16.2 surface protons/nm^2; in good agreement with the experimental value of 16.4 surface protons/nm^2 obtained by Yates et al. [136] for the 54 m^2/g goethite sample.

Table 3.3 Total site density (N_{TOT}), surface proton site density (N_{TRIT}), and proton reactive site density (N_H) values for the principal crystal faces of goethite

Site Density	Crystal Face			
	(101)	(001)	(210)	(010)
N_{TOT} [a]	15.15	16.7	15	18.2
N_{TRIT} [b]	15.15	16.7	22.5	27.3
N_H [c]	6.06	6.68	7.5	9.1

[a] **N_{TOT}** (sites/nm^2) is the total site density for a crystal face calculated by summing all site types and their respective site densities from Table 3.1.
[b] **N_{TRIT}** (surface protons/nm^2) is the predicted number of rapidly exchangeable protons per nm^2 assuming that both singly coordinated site types (FeO_I and FeO_{II}) possess two rapidly exchangeable protons while doubly coordinated sites and $\equiv Fe_3O_I$ sites only possess one surface proton. $\equiv Fe_3O_{II}$ sites are not thought to be protonated under normal experimental conditions.
[c] **N_H** (proton reactive sites/nm^2) is the proton reactive sites present on each crystal face. Doubly coordinated sites are not considered to be proton reactive [26, 27, 29, 39, 82, 85, 97, 99, 131, 141]. The combination of two triply coordinated sites, one with high and the other with low proton affinity ($\equiv Fe_3O_I$ and $\equiv Fe_3O_{II}$, respectively) has been found to render both surface sites inert [24, 27, 85]; therefore, the number of triply coordinated sites that are considered proton reactive is determined by subtracting the $\equiv Fe_3O_{II}$ site density from that of $\equiv Fe_3O_I$. All singly coordinated sites are considered to be proton reactive [23, 29].

Estimating site density using tritium exchange is advantageous over other methods in that it can be applied to both amorphous and crystalline solids [92, 137]. In addition, tritium exchange uses H^+ (an adsorbate of interest in all aqueous environments)

and can account for crystal face defects since N_{TRIT} is determined experimentally rather than theoretically [115, 119]. To calculate the mineral's CFC from tritium exchange, Equation 3.1 is used:

$$N_{TRIT} = \sum_{k} [(\%\ Crystal\ Face)_i \cdot (N_{TRIT})_i] \tag{3.1}$$

where N_{TRIT} is the tritium exchange site density determined for the goethite sample in units of surface protons/nm^2, (% Crystal Face)$_i$ is the percent of the mineral surface comprised from the ith crystal face, $(N_{TRIT})_i$ is the tritium exchange site density for the ith crystal face in units of of surface protons/nm^2, and the summation is over all crystal faces k considered.

3.4.3. Isotherm/Surface Saturation Experiments

Site density estimation via surface saturation data utilizes adsorption isotherm experiments to determine the maximum surface coverage possible for a given constituent. In a number of studies, the adsorbate used was either arsenate As(V) or arsenite As (III), and conducted at pH values coincident with the maximum adsorption observed in sorption edge experiments, pH ≈ 4 and ≈ 7 - 8, respectively [122-126]. Previously, once the surface saturation value was determined, N_{TOT} was calculated using the solids concentration, the specific surface area of the mineral, and assuming only monodentate complexes form [122]. One of the deficiencies with this particular approach however is

that extended x-ray absorption fine structure (EXAFS) spectroscopy studies have revealed that both arsenate and arsenite complex with goethite to form monodentate and bidentate complexes, rather than strictly monodentate complexes as assumed in this method [41-44, 132, 142]. In addition, these EXAFS studies have shown that both adsorbates complex primarily to singly coordinated surface sites. This evidence suggests that the site density retrieved from these adsorption experiments is closer to the value for singly coordinated sites rather than N_{TOT}.

More recently, a similar approach was proposed by Villalobos and Perez-Gallegos [82] in which the CFC, and consequently the N_s of each surface site type, could be estimated from isotherm experiments employing chromate Cr(VI) as the adsorbate [82]. Fendorf et al. [42] showed that when conducting this experiment under the conditions prescribed by Villalobos and Perez-Gallegos [82], chromate complexes with the surface and no precipitation or reduction is observed. Villalobos et al. [85] utilized this particular method in looking at how site density varies with respect to specific surface area on goethite. In their analysis, simplified models of the goethite surface were employed in which only the mineral's principal crystal faces were considered [82, 85]. By using these models and assuming that chromate only forms bidentate surface complexes with singly and doubly coordinated sites on goethite, the CFC and site density for each surface site type can be determined [82].

While this approach put forth by Villalobos and co-workers is very promising for predicting the CFC of a mineral sample, there are shortcomings that need to be addressed. In particular, as was the case for surface saturation experiments using arsenate and

arsenite, chromate also has been found, via EXAFS spectroscopy, to complex with goethite in both a monodentate and bidentate fashion, rather than solely in a bidentate fashion as presumed in this approach [42]. In particular, the monodentate chromate surface complex is observed in EXAFS spectra at low surface coverages but disappears from the spectra as surface loading increases; a result indicative of adsorption to the more highly reactive (210) or (010) crystal faces [27, 39, 78, 114]. Furthermore, Fendorf et al. [42] observed two different bidentate surface complexes forming on goethite, mononuclear and binuclear, which bind to different surface site types.

To circumvent the complexities involved in estimating a mineral's CFC using surface saturation data for arsenate or chromate, both of which possess three unique surface complexes on goethite [42], the use of a different probing molecule is proposed here. Using EXAFS spectroscopy to investigate selenite adsorption onto goethite, Hayes et al. [45] observed a single selenite – iron distance of 3.38 Å, consistent with an inner-sphere binuclear bidentate complex forming on two singly coordinated surface sites [34, 45]. Combining this spectroscopic information with selenite surface saturation data provides a seemingly straight forward approach to estimating the CFC of a goethite sample using Equation 3.2:

$$\Gamma_{Se,Max} = \frac{\sum_k \left[(\%\ Crystal\ Face)_i \cdot \left(N_{s,\equiv FeOH}\right)_i\right]}{2} \times \frac{10^{18}}{N_A} \times 10^6 \qquad (3.2)$$

where $\Gamma_{Se,Max}$ is the surface saturation value of selenite on the goethite sample in units of μmol/m^2, (% Crystal Face)$_i$ is the percent of the mineral surface comprised from the ith crystal face, $(N_{s,\equiv FeOH})_i$ is the site density of singly coordinated sites present on the ith crystal face, in units of sites/nm^2, 2 is the number of singly coordinated sites occupied per one SeO_3^{2-} molecule adsorbed, 10^{18} is the conversion factor from nm^2 to m^2, N_A is Avogadro's number ($6.023 \cdot 10^{23}$), 10^6 is the conversion factor from mol to μmol, and the summation is over all crystal faces k considered. It should be noted that Equation 3.2 is only valid for goethite's crystal faces possessing singly coordinated sites on adjacent octahedra (the (101), (001), and (210) faces).

One potential shortcoming of using selenite in this surface saturation approach is that the spectroscopic studies performed by Hayes et al. [45] were conducted at relatively high surface coverages (Γ_{Se} > 1.25 μmol/m^2). As observed in EXAFS studies performed by Spadini et al. [39] and Fendorf et al. [42], with increasing surface coverage, certain surface complexes can become drowned out in the spectra due to either the dominance of a particular surface complex or unequal contributions to the EXAFS spectra resulting from differing bond lengths (the shorter the bond length, the greater the contribution to the spectra). For example, at a surface coverage of 0.22 μmol/m^2, Spadini et al. [39] observed an edge sharing complex that disappeared from their spectra once the surface coverage was raised to 1.35 μmol/m^2. Therefore, additional spectroscopic investigations for selenite adsorption onto goethite, performed at lower surface coverages than previously employed by Hayes et al. [45], would help resolve any uncertainty regarding additional selenite surface complexes present on goethite.

3.4.4. Generic Site Density Estimation Techniques

While the techniques discussed previously (i.e. crystallographic method, tritium exchange, and max adsorption experiments) can be useful for determining a mineral's CFC, they are not always employed in adsorption studies, thereby leaving modelers with limited options for estimating the mineral's CFC. For this reason a more generic means to estimating site density is sometimes desirable.

3.4.4.1. Objective Curve Fitting

To estimate N_S through objective curve fitting, potentiometric titration data collected for a given mineral sample at different ionic strengths are modeled using the desired SCM and a pre-selected site density value to obtain the best fit model parameters. The same modeling procedure is repeated at several different site density values, all of which are selected by the modeler. A comparison is then made between each of the model simulations to ascertain which one best fits the experimental data. The corresponding site density value of the best fit model is then labeled the "true" site density of the mineral. It should be noted that if more than one surface site type is being considered (e.g. singly, doubly, and triply coordinated surface sites) in the SCM, as in the case of the CD-MUSIC model, the procedure outlined above would have to be applied for each surface site type under consideration.

In a study performed by Christl and Kretzschmar [106], the 2-pK basic Stern model as well as the Triple Layer Model were both used to fit the acid-base titration data

of hematite via the objective curve fitting method. Site density values ranging from 2 - 20 sites/nm^2 were selected for use in this study. In performing this analysis, researchers discovered that the relative goodness of fit was virtually constant over the range of site densities tested (2 – 20 sites/nm^2) and no apparent minimum could be observed. Given this result and the fact that a number of SCM parameters (e.g. log K values for adsorption reactions) are often dependent upon the N_S value employed in the model, the authors concluded that determining N_S based on the objective curve fitting method for acid-base titration data is not suitable unless the titration curves demonstrated that the surface was clearly saturated with protons [92, 106]. Similar results were found previously by Hayes et al. [121].

3.4.4.2. Titration Congruency

The titration congruency method was developed by Salazar-Camacho and Villalobos [84] specifically for determining the CFC of goethite through the use of a sample's titration/surface charge data . In this approach, the titration data from two ideal goethite preparations, specifically GOE94 from Villalobos et al. [130] and HVR94 from Weng et al. [120] are used. Based on the work of Gaboriaud and Ehrhardt [99], both of these goethites were characterized as having 70% (101) crystal face and 30% (001) crystal face (using the Pnma space group) [84]. The CFC of these ideal goethite samples can be used in conjunction with the titration data to determine the proton reactive site coverage for each titration data point.

The phrase "proton reactive site coverage", originally stated in Salazar-Camacho and Villalobos [84], can be a bit ambiguous; leading to confusion as to what exactly is being calculated. To clarify, the "proton reactive site coverage" is the net protons adsorbed to the mineral's surface (NPA) divided by the total number of proton reactive sites present on the mineral's surface (PRS), both in units of $mol \cdot L^{-1}$. NPA values can be determined using the mineral sample's experimental titration data, while PRS can be calculated if the mineral's CFC is known. In addition, it should be noted that the NPA value will change with each titration data point because the number of protons adsorbed to the mineral's surface will either increase or decrease, depending on the addition of acid or base, respectively. PRS on the other hand, is a constant value that represents the total number of proton reactive sites (i.e. singly and triply coordinated surface sites) present on the mineral surface. If a mineral sample's CFC is known, the average number of proton reactive sites per nm^2, herein referred to as the proton reactive site density (N_H), can be determined which in turn leads to the mineral's PRS value as illustrated in Equation 3.3 and Equation 3.4:

.

$$N_H = \sum_k (\%\ Crystal\ Face_i)\left(N_{S,\equiv FeOH,i} + N_{s,\equiv Fe_3O,i}\right) \tag{3.3}$$

where N_H is in units of $sites \cdot nm^{-2}$, % Crystal $Face_i$ is the percent of the mineral surface comprised from the ith crystal face, $N_{s,\equiv FeOH,i}$ and $N_{s,\equiv Fe3O,i}$ are the site densities of singly

and triply coordinated sites, respectively, present on the ith crystal face, in units of sites·nm^{-2}, and the summation is over all crystal faces k considered.

$$PRS = \frac{(N_H)(10^{18})(SSA)(C_S)}{N_A} \tag{3.4}$$

where PRS is in units of mol·L^{-1}, N_H is in units of sites·nm^{-2}, 10^{18} is the conversion factor from nm^2 to m^2, SSA is in units of m^2·g^{-1}, C_S is the solid's concentration in units of g·L^{-1}, and N_A is Avogadro's number ($6.023 \cdot 10^{23}$).

Once the proton reactive site coverage for the ideal goethite preparations (i.e. GOE94 or HVR94) has been calculated for each titration data point, the proton reactive site coverage data for the goethite of interest, with an as yet unknown CFC, can be plotted against the ideal goethite's data. In these plots, the x and y axes are pH and proton reactive site coverage, respectively. Furthermore, it is important to note that the titration data of the ideal goethite employed in this method must have similar or identical electrolytes and ionic strength as the titration data being used for the goethite of interest. Recall that the proton reactive site coverage used in this approach has two components, NPA and PRS. For the goethite of interest, the NPA value can be calculated at each data point using the goethite's titration data, while in order to calculate its PRS (assuming SSA and C_S are known), the N_H of the sample must first be guessed and then adjusted until the two graphs of proton reactive site coverage vs. pH converge [84]. Hence, the N_H for the goethite of interest is obtained in an iterative fashion. Using the fitted N_H value and the values presented in Table 3.3, the CFC for the goethite of interest can be

calculated using Equation 3.3. Further information regarding the titration congruency approach can be found in the appendix.

3.5. Methodology and Application

Utilizing the techniques discussed above, a methodology is developed here to determine a goethite sample's CFC that allows for harmonization of the different N_S values reported from crystallography, microscopic image analysis, tritium exchange, surface saturation and surface charging data.

3.5.1. Experimental Data

3.5.1.1. Goethite preparation

The experimental data used in this work was collected by Vieira [92]. Goethite (GOE63, specific surface area of 62.9 m^2/g) was produced in accordance with the procedure of Schwertmann et al. [32] and further developed by Peak et al. [33]. In a CO_2 free glove box (Labconco model 50700-00), 50 mL of 1 M ferric nitrate [$Fe(NO_3)_3 \cdot 9H_2O$] was added to 450 mL of 1 M potassium hydroxide (KOH). Both solutions were constructed using carbonate free Millipore water while being housed within a nitrogen-purged glove box. Upon the addition of ferric nitrate to the potassium hydroxide solution, ferrihydrite proceeded to precipitate out and was aged for two weeks at 25^oC over which time the solid converted into goethite. The goethite was then put through five wash cycles in which the solid was centrifuged for 10 minutes at 3,000 rpm

and the supernatant was then replaced with carbonate free Millipore water. To ensure that the goethite surface was free of any remaining ferrihydrite, the solid was placed in a 0.4 M hydrochloric acid (HCl) solution and tumbled for two hours inside a mechanical tumbler. The goethite suspension was then washed and centrifuged five times or until the supernatant had a conductivity reading of roughly 50 μS/cm, whichever came first, in order to remove aqueous iron and chloride ions present in the solution. The washed solids were next placed inside the nitrogen-purged glove box and inserted into dialysis tubing (SpectraPor 1000 MWCO). Dialysis was subsequently performed by placing the tubing inside a 2-L bottle of nitrogen purged Millipore water that was replaced every 6 – 8 hours for 36 hours or until the conductivity of the solution read between 4 and 10 μS/cm. A magnetic stir bar was placed inside the 2-L bottle to provide mixing for the solution. After dialysis, the solid slurry was freeze dried and set aside until needed. The formation of goethite was verified through X-ray diffraction (XRD) analysis and the surface area was estimated to be 62.9 m^2/g with a Micromeritics ASAP 2010 BET analyzer using nitrogen gas adsorption.

3.5.1.2. Potentiometric Titrations

All potentiometric titrations on goethite were conducted at 25 ± 0.5 ^oC in a temperature controlled room. The solids slurry was held in a 400-mL Para film covered beaker and purged using nitrogen (N_2) gas to prevent CO_2 contamination. The slurry was kept well mixed using a magnetic stir bar coated in Teflon. Slurries of known solids concentration were amended with nitrate salts (reagent grade) to achieve ionic strengths

of 0.01, 0.08, and 0.31 M $NaNO_3$ and then titrated using an automatic titrimeter, built in-house, to yield a set of potentiometric titration curves. Software created by Dr. George Redden (INEEL, Utah) controlled the acid-base delivery system via two 2,500 μL digital syringes (Gilmont GS 3200-S). In addition the software recorded all pertinent information including run time, total volume, volume of titrant added, and solution pH.

3.5.1.3 Adsorption Experiments

Goethite slurries with specific solids concentrations were prepped inside a nitrogen-purged glove box using freeze dried goethite (described previously), $NaNO_3$ as the background electrolyte, and carbonate free Millipore water. All slurries were given an ionic strength of 0.1 M $NaNO_3$. To confirm the concentration of goethite in the slurry, three 10 mL samples of diluted solids slurry were taken and analyzed gravimetrically. The slurry was acidified to around pH 3 and then 10 mL aliquots were placed in 15 mL VWR polypropylene centrifuge tubes which acted as batch equilibrium reactors, with each reactor representing one data point for the pH adsorption edge (constant metal concentration, varying pH) or adsorption isotherm (constant pH, varying metal concentration) to be constructed. Cd(II) was then added to each reactor bottle to attain the metal(s) concentration desired. In order to avoid local metal hydroxide precipitation, each centrifuge tube was forcefully shaken prior to raising the reactor's pH via the addition of nitrogen purged 1N NaOH. To test for any losses in the system and/or precipitation of the metal(s) in each experiment, reactor tubes devoid of goethite (metal blanks) were also prepared.

Once the samples were prepared they were placed in a tumbler for 48 hours at 25^{o}C, which had been determined from preliminary experiments to be sufficient time for the batch reactors to reach equilibrium. For the adsorption isotherm experiments, the pH of each reactor tube was checked and, if necessary, adjusted via the addition of either carbonate free 1N HNO_3 or carbonate free 1N NaOH every 4 – 6 hours in order to sustain a constant pH throughout the experimental run. After 2 days time, the reactor tubes were placed back inside the nitrogen-purged glove box and their final pH was recorded. The samples were then removed from the glove box and placed in a constant temperature centrifuge (Beckman J2-21) for 10 minutes at 3000 rpm. Each reactor's supernatant was subsequently filtered using a 0.2 μm Supor polyethersulfone membrane filter (Pall Corporation) and, to prevent metal precipitation and adsorption onto the container, was then acidified to 1.5% HNO_3 (Ultrex Ultrapure Reagent, JT Baker, NJ). To ascertain the amount of adsorbate remaining in solution, the supernatant was then analyzed using inductively coupled plasma (ICP) optical emission spectroscopy (Spectro CirosCCD). A mass balance on each batch reactor was conducted to determine the quantity of metal adsorbed to goethite.

3.5.2. Modeling Approach

Both natural and synthetic goethite surfaces have been found to be comprised primarily of four crystal faces: the (101), (001), (210), and (010), using the Pnma space group [23, 26, 85, 97, 99, 114, 127, 129]. However, of these crystal faces, the (101), (001), and (210) are most commonly observed, with the (101) and/or (001) crystal face

typically dominating and the (210) face making up a smaller portion of the mineral's surface [99, 114, 143-145]. Based on this information, the surface of the goethite sample GOE63 was considered to be comprised of some combination of the (101), (001), and (210) crystal faces (Equation 3.5):

$$1 = \sum_{k} (\%\ Crystal\ Face)_i \tag{3.5}$$

where $(\%\ \text{Crystal Face})_i$ is the percent of the mineral surface comprised from the ith crystal face and the summation is over all crystal faces k considered. Using Equation 3.5 along with GOE63's selenite surface saturation data and its proton reactive site density (N_H), the CFC of the goethite sample can be estimated.

Cd(II) adsorption onto GOE63 was described using the CD-MUSIC model and the computer software FITEQLC [22] and FITEQL 4.0 [21]. The CD-MUSIC model presented in this paper was developed in three steps: (1) Fitting the potentiometric titration data collected for GOE63 to determine the proton affinity, ion pair formation constants, and capacitance values (C_1 and C_2) of the electrical double layer; (2) fitting Cd(II) pH adsorption edge experimental data conducted on GOE63 to obtain the surface complex formation constants for the different Cd(II) surface species considered; and (3) simulating of Cd(II) isotherm adsorption data collected for GOE63 using the surface species and equilibrium constants determined in step 2. In summary, the potentiometric titration data and pH adsorption edge data for Cd(II) were used to calibrate the CD-

MUSIC model while the Cd(II) isotherm adsorption data was used to test the model's predictive capability.

Aqueous Cd(II) speciation was calculated in FITEQLC [22] using the equilibrium constants supplied in MINEQL+ 4.5 [146, 147] at 25^{o}C. The model's performance in predicting adsorption edge and isotherm data was quantified for each data set by calculating the weighted sum of squares divided by degrees of freedom (WSOS/DF). WSOS/DF values between 0.1 and 20 are considered to be satisfactory model fits of the experimental data [21].

Mass balance residuals computed in FITEQL [21] and FITEQLC [22] are defined as the difference between the calculated and experimental concentrations for each component in which both the total and free concentrations are known (termed Type II components in FITEQL). For the adsorption experiments discussed here, both the total and free concentrations of the adsorbate component are known; hence, in model simulations of pH adsorption edge and isotherm experiments, the mass balance residual calculated in FITEQL and FITEQLC is for the adsorbate.

These mass balance residuals are used to help determine the goodness of fit that a model has with the experimental data. To account for uncertainties in the experimental data, the residual values calculated at each data point are weighted using estimates of the absolute and relative experimental error. In conducting an extensive modeling study on cation and anion adsorption to the iron hydroxide mineral ferrihydrite, Dzombak and Morel [2] established a set of error estimates to be utilized for all potentiometric titration and adsorption data based on an exhaustive review of available literature (Table 3.4).

These estimates of the relative and absolute error are assumed to be valid for a given component (e.g., H+, adsorbate) and experimental data set. It should be noted that utilizing fixed error values can lead to data points where low concentrations of adsorbate (e.g., the plateau of an adsorption edge; the lower end of an adsorption isotherm) are weighted more heavily than other points in a data set. However, in the absence of individual error estimates for each data point, this approach of using fixed error estimates has been deemed the best alternative for weighting the mass balance residuals [2, 21]. In this work, the fixed absolute and relative error estimates presented in Dzombak and Morel [2] were utilized (Table 3.4). The WSOS value used in FITEQL and FITEQLC is calculated by summing the square of the weighted mass balance residuals over all data points. The degrees of freedom (DF) is calculated by multiplying the number of data points in a data set times the number of Type II components minus the number of adjustable parameters.

Table 3.4 Error estimates used in CD-MUSIC modeling. Taken from Dzombak and Morel [2].

Measurement [a]	s[rel] [b]	s[abs] [c]
X_H	0.05	0.0
X_H	0.10	0.0
T_H	0.01	0.01 x min T_H
X_M	0.05	0.0
T_M	0.01	0.01 x min T_M
X_A	0.05	0.0
T_A	0.01	0.01 x min T_A

[a] H, hydrogen ion (H^+); M, cation; A, anion; T, Total Concentration; X, Free Concentration
[b] s[rel] is the relative experimental error. s_H[rel] = 0.05 used for pH measurements in sorption experiments; s_H[rel] = 0.10 used for pH measurements in titration experiments
[c] s[abs] is the absolute experimental error

In considering the (101), (001), and (210) crystal faces to be present on GOE63, there are a total of twelve possible surface components that can be input into the CD-MUSIC model (cf. Table 3.1). However, the computer software used to run the CD-MUSIC model (FITEQLC) can only handle a maximum of four surface components; therefore, certain assumptions concerning the site types present on the different crystal faces must be applied in order to model the goethite surface under these constraints.

The (101) and (001) crystal faces are believed to have comparable reactivity given that they possess the same site types and coordination environments as one another and only vary with respect to the quantity of sites present (i.e., site density); hence, surface complexes that form on the (101) crystal face are assumed to also form on the (001) face [39, 97]. From this reasoning, singly and triply coordinated sites on the (101) face are considered to be equivalent to those on the (001) crystal face in the CD-MUSIC model.

Utilizing this reasoning along with the assumptions discussed in section 3.3 (Table 3.2), the number of surface components used in the model can be reduced down to four.

3.5.2.1. Selenite surface saturation data

For the GOE63 goethite sample, a surface saturation value of 3.17 μmol/m^2 was obtained for selenite using a surface loading of 7.85 μmol/m^2 and a slightly acidic pH of 6.6. As mentioned previously, spectroscopic evidence from Hayes et al. [45] along with molecular modeling simulations performed by Hiemstra et al. [34] suggests that selenite binds to goethite via two singly coordinated surface oxygens to form a double corner bidentate surface complex. With this information regarding selenite's coordination environment on goethite, in conjunction with the oxyanion's surface saturation value for GOE63, Equation 3.2 (previously developed and presented in section 3.4.3.) can be utilized.

For all three crystal faces considered in this study (i.e., the (101), (001), and (210) faces), singly coordinated surface sites are present on the corners of adjacent octahedra, allowing for the formation of a double corner bidentate complex [97]. Hence, Equation 3.2 is in agreement with the findings from molecular scale analyses concerning selenite's adsorption onto goethite.

3.5.2.2 Proton reactive site density

In the 1-pK CD-MUSIC model of goethite, doubly coordinated surface sites are nonreactive to protons at environmentally relevant pHs; however, singly and triply

coordinated sites are considered to be proton reactive, with log K_H's of ≈ 8 and 11.7, respectively [26, 27, 29, 97]. Hence, the sum of singly and triply coordinated surface sites ($N_{S,\equiv FeOH} + N_{S,\equiv Fe3O}$) is termed the proton reactive site density (N_H) of the goethite sample. Using titration congruency method proposed by Salazar-Camacho and Villalobos [84], the potentiometric titration data of GOE63 was compared with a second goethite sample, previously produced by Weng et al. [120], labeled HVR94 and possessing a specific surface area (SSA) of 94 m^2/g. Based on Gaboriaud's and Ehrhardt's (2003) work using atomic force microscopy (AFM) imaging to characterize goethite surfaces with varying SSAs, the HVR94 goethite sample was determined to have a CFC consisting of 70% (101) crystal face and 30% (001) crystal face (using the Pnma space group) [84, 99]. Alignment of GOE63's potentiometric titration data with that of HVR94 revealed a proton reactive site density value of 6.6 sites/nm^2 for GOE63 (Figure 3.3).

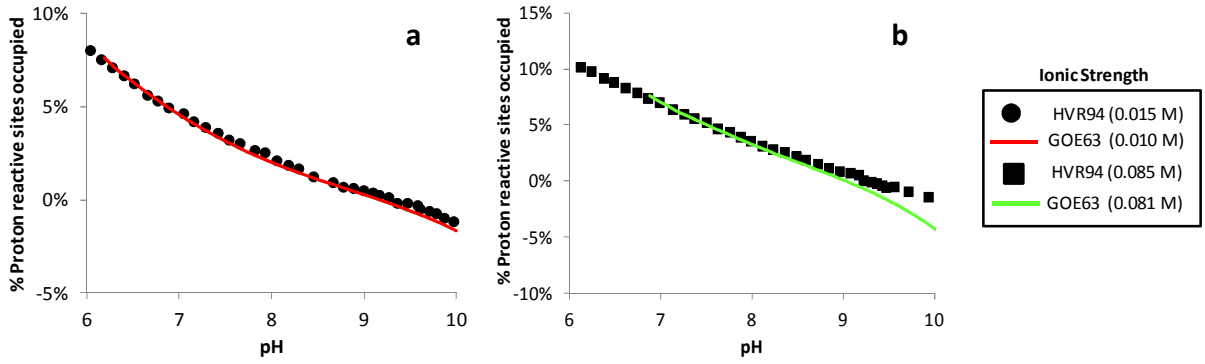

Figure 3.3 Fits from titration congruency method for GOE63 and HVR94 potentiometric titration data. N_H for GOE63 was adjusted until the HVR94 and GOE63 data sets aligned for a given ionic strength **(a)** ≈ 0.01 M and **(b)** ≈ 0.08 M. The background electrolyte used in each case was $NaNO_3$.

Using the N_H value of 6.6 sites/nm^2 for GOE63, and the fact that only singly and triply coordinated surface sites are considered to be proton reactive on goethite, allows for utilization of Equation 3.3 (presented earlier in section 3.4.4.2.).

3.5.3. CFC of GOE63

Utilizing the selenite surface saturation value observed for GOE63, along with the N_H value determined for the goethite sample, and recalling that the (101), (001), and (210) crystal faces are considered to be present on mineral surface, Equation 3.5, Equation 3.2, and Equation 3.3 can be solved simultaneously to estimate the CFC of GOE63. The CFC that results for GOE63 is 31% (101), 55% (001), and 14% (210). This CFC is in good agreement with the findings of Gaboriaud and Ehrhardt [99] who, using AFM images, found a CFC of 30% (101) and 70% (001) for a goethite sample possessing a SSA of 49 m^2/g. Furthermore, using the CFC presented here, GOE63's predicted tritium exchange site density (N_{TRIT}) was found to be 17.0 surface protons/nm^2 utilizing the N_{TRIT} values presented in Table 3.3. This value is in good agreement with the experimental and theoretical values obtained by Yates et al. [136] of 16.4 ± 0.7 and 16.8 surface protons/nm^2, respectively, for goethite samples with SSAs ranging from 39 to 54 m^2/g. Hence, the resulting CFC for GOE63 provides conformity among the different site density values predicted using crystallography, microscopic image analysis, surface saturation data, surface charging data, and tritium exchange. With the CFC for GOE63

determined, the N_S value for each different site type considered in the CD-MUSIC model can be calculated (Table 3.5).

Table 3.5 Site types and N_S used in the CD-MUSIC model for GOE63

Site Type	Crystal Face	CFC (%)	N_S (sites/nm^2)	
			Individual [a]	Model [b]
≡FeOH	(101)	31	0.94	2.79
	(010)	55	1.85	
	(210)	14	1.03	1.03
≡Fe_2OH	(101)	31	-	-
	(010)	55	-	
	(210)	14	1.03	1.03
≡Fe_3O	(101)	31	0.94	2.79
	(010)	55	1.85	
	(210)	14	-	-

[a] "Individual" Ns values were calculated for each site type by multiplying the CFC percentage by the respective crystal face's reactive site density (cf. Table 3.2)

[b] Values under the column labeled "model" represent the site densities used in CD-MUSIC for GOE63. For the (101) and (001) crystal faces, the Ns value for a given site type is calculated by summing the Ns values presented in the "Individual" column for the (101) and (001) faces. For the (210) crystal face, the site densities in the "model" column are equivalent to those presented in the "individual" column.

3.5.4. Surface Protonation and Ion pair formation

The intrinsic affinity constants for surface protonation and ion-pair formation reactions, along with the capacitance values (C_1 and C_2) for the goethite sample, were achieved through optimization of the CD-MUSIC model's fits to GOE63's potentiometric titration data (Table 3.6). The capacitance values of GOE63 were considered equivalent to one another (i.e., $C_1 \equiv C_2$) based on the findings of Hiemstra and van Riemsdijk [93] and Sverjensky [101].

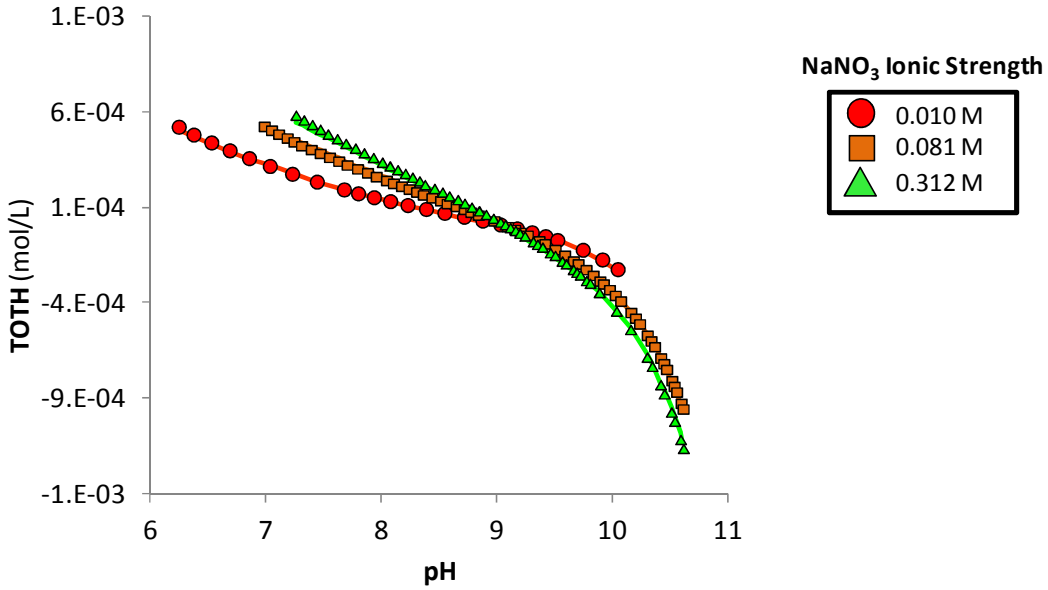

Figure 3.4 CD-MUSIC model fits of GOE63's potentiometric titration data. Symbols denote experimental data points and the solid lines represent CD-MUSIC model simulations. Model simulations were conducted using the reactions and affinity constants listed in Table 3.6. Capacitance values (C1 = C2) used were 1.05 F/m^2.

Table 3.6 Surface complexation reactions used in the CD-MUSIC model

Adsorbate	Crystal Face	Surface Complex	Linkage [a]	Δz_0	Δz_1	log K_{in}
H^+	(101), (001) & (210)	$\equiv FeOH^{-0.5} + H^+ \rightarrow \equiv FeOH_2^{+0.5}$	-	1	0	8.50
		$\equiv FeOH^{-0.5} + H^+ + NO_3^- \rightarrow \equiv FeOH_2^{+0.5}\_NO_3^-$	-	1	-1	8.00
		$\equiv FeOH^{-0.5} + Na^+ \rightarrow \equiv FeOH^{-0.5}\_Na^+$	-	0	1	-0.10
	(101) & (001)	$\equiv Fe_3O^{-0.5} + H^+ \rightarrow \equiv Fe_3OH^{+0.5}$	-	1	0	11.70
		$\equiv Fe_3O^{-0.5} + H^+ + NO_3^- \rightarrow \equiv Fe_3OH^{+0.5}\_NO_3^-$	-	1	-1	11.20
		$\equiv Fe_3O^{-0.5} + Na^+ \rightarrow \equiv Fe_3O^{-0.5}\_Na^+$	-	0	1	-0.10
Cd(II)	(101) & (001)	$2(\equiv FeOH^{-1/2}) + Cd^{2+} \rightarrow (\equiv FeOH)_2\text{-}Cd$	Corner	0.82	1.18	2.69
		$2(\equiv FeOH^{-1/2}) + Cd^{2+} + H_2O \rightarrow (\equiv FeOH)_2\text{-}CdOH + H^+$	Corner	0.82	0.18	-4.90
		$\equiv FeOH^{-1/2} + Cd^{2+} + 2H_2O \rightarrow (\equiv FeOH)\text{-}Cd(OH)_2 + 2H^+$	Vertex	0.41	-0.41	-11.96
	(210)	$2(\equiv FeOH^{-1/2}) + \equiv Fe_2OH^0 + Cd^{2+} \rightarrow (\equiv FeOH)_2\text{-}Cd\text{-}(\equiv Fe_2OH)$	Edge	1.15	0.85	8.04
		$2(\equiv FeOH^{-1/2}) + \equiv Fe_2OH^0 + Cd^{2+} + H_2O \rightarrow (\equiv FeOH)_2\text{-}CdOH\text{-}(\equiv Fe_2OH) + H^+$	Edge	1.15	-0.15	0.91

[a] "Linkage" denotes the way in which the adsorbate binds to the surface sites (e.g., corner, edge, vertex)

$C_1 = C_2 = 1.05$ F/m^2

3.5.5. Cd(II) Single solute Adsorption Modeling

Once the surface protonation and ion-pair affinity constants were determined, the CD-MUSIC model could be calibrated for Cd(II) adsorption through model fitting of experimental single solute pH adsorption edge and used to predict isotherm data collected on GOE63 (Table 3.7). CD values (Δz_0 and Δz_1) were determined using an approach similar to the one described by Hiemstra et al. [34] and is discussed in detail in Chapter 4.

Table 3.7 Single solute adsorption experiments performed on GOE63 with corresponding model fits

Adsorbate	Experiment	Ionic Strength or Surface Loading [a]	Model Fit (WSOS/DF)
H^+	Potentiometric Titration	0.01	1.4
		0.081	0.2
		0.312	0.3
Cd(II)	Adsorption Edge	0.31	3.9
		0.44	4.7
		2.22	1.8
		9.08	2.6
	Isotherm [b]	-	7.0

[a] For the H^+ adsorbate, ionic strength (mol/L) is reported. For all other adsorbates, surface loading (μmol/m2) is reported.
[b] Cd(II) isotherm experiment conducted at pH 6.89

3.5.6. Cd(II) Adsorption

Using extended x-ray absorption fine structure (EXAFS) spectroscopy, Spadini et al. [39] investigated cadmium surface complexes forming on goethite's surface at pH 7.5 for surface coverages ranging from 0.22 to 2.02 μmol Cd adsorbed/m^2. At the lowest surface coverage studied, two surface complexes with cadmium – iron distances of ≈ 3.3

Å and ≈ 3.7 – 3.8 Å, assigned to edge and corner linkage complexes respectively, were observed [39]. It should be noted that the cadmium - iron distance of ≈ 3.5 Å originally reported by Spadini et al. [39] and attributed to a corner linkage complex was later corrected by the authors; the actual cadmium – iron distance is ≈ 3.7 – 3.8 Å [40, 78].

As the cadmium surface loading was increased, the surface complex possessing a cadmium – iron distance of ≈ 3.3 Å could not be discerned in the EXAFS spectra. This disappearance was attributed to cadmium complexing in an edge linkage structure to the higher affinity sites located on the capping face(s) of goethite. At elevated surface coverages, available sites on the capping face(s) become scarce, and cadmium adsorbs in a corner linkage fashion to the more abundant low affinity sites present on the main face(s) of goethite. Hence, the corner linkage complex dominates as the Cd/Fe ratio increases; thereby diminishing the contribution of the edge linkage complex and rendering the proportion of Cd adsorbed through this mechanism too small to be observed using EXAFS [39, 78].

To explain the cadmium – iron distance of 3.3 Å, Venema et al. [27] proposed two tridentate edge sharing complexes, titled “Tridenate A” and “Tridentate B”, that could form on the (210) crystal plane of goethite. For both complexes considered, cadmium is bound to one doubly and two singly coordinated surface sites, however “Tridentate A” is made up of two edge linkages whereas “Tridentate B” possesses one edge and two corner linkages. Given its arrangement on the mineral surface, “Tridentate A” was assumed to be the more thermodynamically favorable of the two complexes considered and thus deemed the cadmium edge sharing complex [27]. Density

Functional Theory (DFT) calculations presented in Randall et al. [40] provide further evidence supporting the "Tridentate A" structure; specifically concerning the complex's cadmium – iron bond length (3.34 Å) and its stability [40]. Based on this information, the "Tridentate A" surface species is the only cadmium edge linkage complex considered in this study.

Two possible configurations for the cadmium corner linkage surface complex, possessing a cadmium-iron distance of ≈3.7 – 3.8 Å, have been theorized to form on the (101) face of goethite [27, 39]. In one configuration cadmium forms a monodentate complex with a doubly coordinated surface group. In the other arrangement, a bidentate complex is formed via two adjacent singly coordinated surface groups and cadmium. Given that the bidentate complex is thermodynamically favored over the monodentate species due to the number of bonds involved [39], and the fact that singly coordinated sites are more reactive than doubly coordinated ones [39, 148], the bidentate configuration is considered to be the sole corner linkage complex formed [27, 33, 39]. Additionally the cadmium - iron distances based on DFT calculations reported by Randall et al. (1999) and Parkman et al. (1999) of ≈3.7 - 3.8Å supports the double corner bidentate configuration [40, 149].

At the highest surface coverage studied by Spadini et al. [39] at pH 7.5 (2.02 μmol Cd adsorbed/m^2), the authors observed a third surface complex to form possessing a cadmium – iron distance of ≈ 4.0 Å. This third complex is thought to bind to singly coordinated surface oxygens on the (101) and (001) crystal faces in a monodentate fashion via a vertex linkage [28, 39]. However, the results of a second EXAFS study,

conducted by Randall et al. [40], seem to dispute the existence of this monodentate complex since the authors never observed this cadmium – iron distance of 4.0 Å and concluded that Cd(II) only binds to the (101) crystal face as a bidentate corner sharing complex. Examination of the experimental conditions employed by Randall et al. [40] reveals that the highest surface coverages investigated by the authors were 1.48 μmol/m^2 at pH 6.3 and 1.23 μmol/m^2 at pH 7.7. Under similar conditions (pH 7.5 and a surface coverage of 1.35 μmol/m^2), Spadini et al. [39] did not observe the presence of the monodentate cadmium complex in their EXAFS spectra either. Therefore, the results of Randall et al. [40] do not necessarily preclude the formation of this proposed monodentate Cd(II) complex, but rather, they provide guidance as to what experimental conditions (i.e., pH and surface coverage) this monodentate complex should not significantly contribute to cadmium adsorption onto goethite.

In summary, cadmium is thought to bind to goethite as: (1) a tridentate edge sharing complex to the (210) crystal face; (2) a bidentate corner sharing complex to the (101) and (001) crystal faces; and (3) a monodentate complex to the (101) and (001) crystal faces. All spectroscopic data collected by Spadini et al. [39] and Randall et al. [40] reveal that adsorbed cadmium complexes possess six first-shell oxygen atoms present as either O, OH, or OH_2 [33]. Therefore, the presence of hydroxyl ligands bound to cadmium surface complexes on the solution side of the mineral – water interface was considered when developing the CD-MUSIC model.

Bond valence analysis (described in detail in Chapter 4) can be helpful, when used in conjunction with spectroscopic data and molecular modeling simulations, in

elucidating a surface complex's identity. In particular, bond valence analysis is useful in ascertaining which protonation states of a surface oxygen atom are feasible for surface complex formation to occur (Table 3.8). To reduce the number of potential surface complexes considered in modeling cadmium adsorption onto GOE63, only the surface sites classified as "stable" in Table 3.8 were used.

Table 3.8 Bond valence analysis for Cd(II) adsorbing onto goethite

Surface species/bonds	Σs_i at surface oxygen (v.u.)		Prediction
	No H-bonds	With H-bonds	
≡**Fe-O-Cd**	0.75 - 0.99	1.01 - 1.49	**Plausible**
≡**Fe-OH-Cd**	1.43 - 1.87	1.56 - 2.12	**Stable**
≡Fe-OH_2-Cd	2.11 - 2.75	2.11 - 2.75	Doesn't Occur
≡**Fe_2-O-Cd**	1.16 - 1.59	1.29 - 1.84	**Plausible**
≡**Fe_2-OH-Cd**	1.84 - 2.47	1.84 - 2.47	**Stable**
≡**Fe_3-O-Cd**	1.57 - 2.19	1.57 - 2.19	**Stable**

Bond valence values calculated using the values listed in Table 4.3. If the range of "Σsi at surface oxygen" contains 2 ± 0.05 (i.e., |Zion| ± 0.05), the surface species is stable. If "Σsi at surface oxygen" < 1.95, the surface species is plausible. If "Σsi at surface oxygen" > 2.05, the surface species does not occur.

Cadmium adsorption onto GOE63 was simulated using CD-MUSIC and the surface complexes reported in Table 3.6. The CD-MUISC model was able to accurately describe (0.1 < WSOS/DF < 20) cadmium adsorption in pH adsorption edge and isotherm experiments (Figure 3.5). Under all experimental conditions simulated, cadmium adsorbed preferentially to the (210) crystal face (Figure 3.5b - Figure 3.5d), which is in agreement with other researchers [27, 39, 78, 114] contend that the (210) face possesses higher affinity surface sites than the (101) and (001) crystal faces. In other words, the

surface sites on the (210) face are used up first prior to Cd(II) complexing with the less reactive sites on the (101) and (001) crystal faces. For the two pH adsorption edges with Cd(II) surface loadings of 0.31 and 0.44 μmol/m^2, over 90% of Cd(II) was adsorbed as an edge sharing surface complex on the (210) crystal face at all data points modeled. Similarly, over 95% of Cd(II) was predicted to adsorb to the (210) face of GOE63 at the lower end of the isotherm (lowest three data points in Figure 3.5d) prior to all (210) sites becoming occupied.

The contribution of the monodentate cadmium surface complex (≡FeOH-$Cd(OH)_2$) in the CD-MUSIC model (Figure 3.5b - Figure 3.5d) agrees well with what has been spectroscopically observed [39, 40]. For pH adsorption edge experiments, the monodentate surface complex was found to make up less than 1% of the total Cd(II) adsorbed at the lower surface loadings modeled (0.31 and 0.44 μmol/m^2). However, for the two higher surface loadings of 2.22 μmol/m^2 (Figure 3.5c) and 9.08 μmol/m^2 (Figure 3.5b), the monodentate surface complex was observed to comprise approximately 15% and 25% of Cd(II)'s surface speciation around pH 7.5, respectively. That percentage continued to rise as pH increased, up to 50% and 70%, respectively. For the isotherm adsorption experiment conducted around pH 7, CD-MUSIC predicted the monodentate complex to account for less than 3% of total cadmium adsorbed at the upper end of the isotherm.

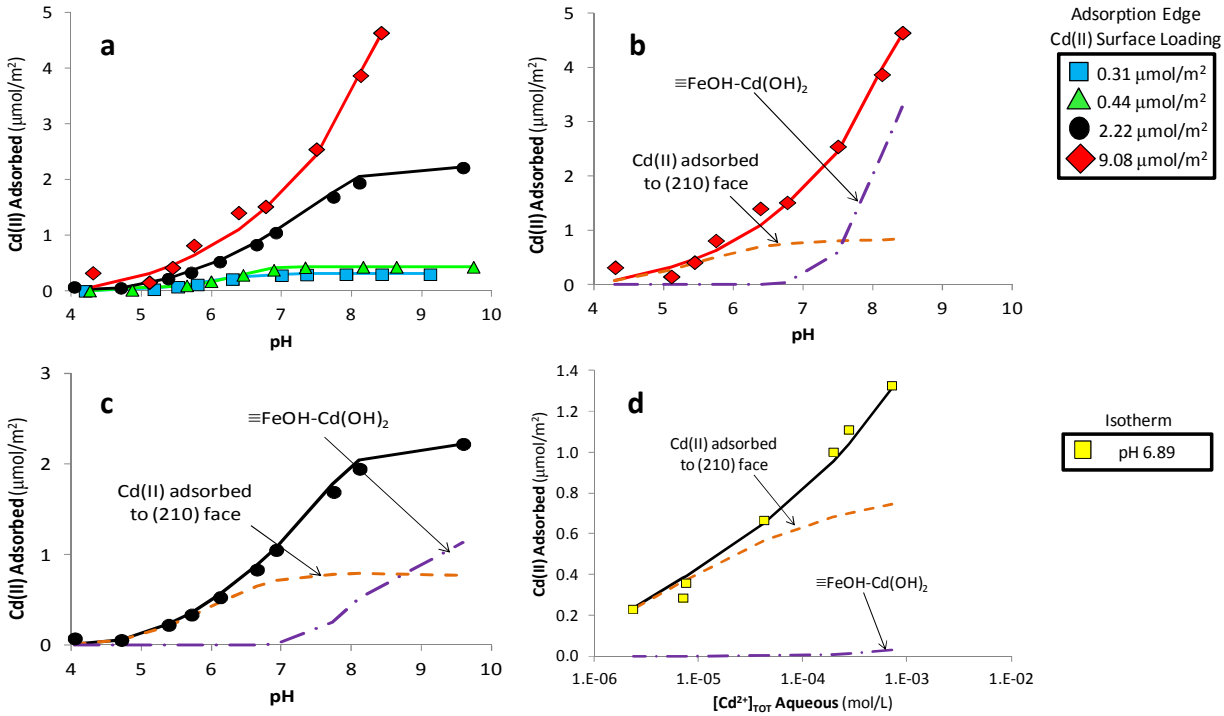

Figure 3.5 **(a)** Cd(II) pH adsorption edge data for GOE63 at four different Cd(II) surface loadings. **(b)** and **(c)** Cd(II) pH adsorption edge data for GOE63 at a Cd(II) surface loading of **(b)** 9.08 µmol/m^2 and **(c)** 2.22 µmol/m^2. **(d)** Cd(II) isotherm adsorption data for GOE63 at pH 6.89. In plots (a) – (d), symbols denote experimental data points while solid lines represent model simulations of total Cd(II) adsorbed. The dashed orange line in plots (b) - (d) represents the amount of Cd(II) adsorbed to the (210) crystal face while the dotted and dashed purple line denotes the amount of Cd(II) adsorbed as the monodentate surface complex that binds via a vertex linkage to the (101) and (001) crystal faces.

3.6. Conclusions

Using the methodology developed in this work, the disparate N_S values determined from the different estimation techniques discussed are collapsed into a single unified theory. Application of this methodology to the GOE63 goethite sample considered in this study resulted in a CFC that allowed for harmonization between the different N_S values obtained using crystallography, microscopic image analysis, tritium exchange, surface saturation data, and surface charging data. Utilizing this calculated

CFC for GOE63, the CD-MUSIC model was able to accurately predict Cd(II) adsorption onto goethite under all experimental conditions tested. By considering each surface site type independently in the model via the segregate approach, the CD-MUSIC model was able to utilize surface species consistent with spectroscopic data and molecular modeling simulations. To our knowledge, this is the first model capable of describing Cd(II) adsorption onto goethite that utilizes all Cd(II) surface complexes previously reported in EXAFS studies and is capable of predicting the distribution of these surface species in agreement with spectroscopic findings.

The difficulties currently encountered by researchers in accurately predicting adsorption for large experimental data sets and complex, multi-solute systems are believed to be, in part, a consequence of the mineral surface being described in too general/homogeneous of terms. Mineral surface reactivity is greatly influenced by its CFC because of the varying site types, site densities, and coordination environments that are found on these different crystal faces [24, 25, 82, 84, 85, 97]. Determination of the crystal faces present on a mineral surface, and incorporation of the various surface site types found on these crystal faces into SCMs, will allow for better agreement between the surface complexes employed in these models and molecular scale analyses. Furthermore, in utilizing a more meticulous description of the mineral surface, it is believed that SCMs will be better able to predict adsorption in multi-solute systems and describe the site competition effects between competing adsorbates.

A number of methods are available for estimating the CFC of a mineral surface. For the iron hydroxide mineral goethite, microscopic image analysis, tritium exchange

(Equation 3.1), and surface saturation (Equation 3.2) are all attractive techniques for estimating the mineral's CFC, although each method possesses some drawbacks/limitations. Ideally all three of these techniques could be performed on each mineral sample studied; however, this is not often practical and even when done so the data must be integrated in a way that properly quantifies the distribution of proton and metal ion sorption sites. The titration congruency method (Equation 3.3) only requires mineral surface charging data, data that is normally collected in adsorption studies already. Therefore, a more feasible approach to characterizing the goethite surface may be to employ only one of the three techniques listed above (i.e., microscopic image analysis, tritium exchange, or surface saturation) in conjunction with the titration congruency method, to calculate a CFC for the goethite sample of interest.

Chapter 4 : CD-MUSIC MODELING OF SINGLE AND BI-SOLUTE ADSORPTION DATA

4.1. Introduction

In natural aqueous systems the bioavailability of trace elements relies heavily upon their interaction with the mineral – water interface [1-4]. Surface complexation models (SCMs) have been developed to help describe the interactions occurring at the mineral – water interface and better predict ion adsorption behavior in the environment [6]. Of the surface complexation models available, the charge distribution multi-site complexation (CD-MUSIC) model is attractive in that it accounts for mineral surface heterogeneity and the spatial distribution of an inner-sphere surface complex's charge [23-26]. While a number of modeling studies predicting ion adsorption in single solute systems have been conducted [27, 30, 32-34, 38, 69, 75, 83, 84, 128], fewer studies have attempted to model more complex systems possessing multiple anion adsorbates [34, 85, 102], cation adsorbates, or a combination of both [28, 36, 87, 103]. Modeling adsorption in these more complex, multi-solute environments, has proven difficult because the model must be able to take into account site competition and electrostatic effects that are caused by the presence of multiple adsorbates in the system [27, 133-135]. Successful prediction of adsorption in these multi-solute systems has required the use of surface species not supported by spectroscopic evidence and/or adjustment of other model parameters such as the specific surface area (SSA) of the mineral sample [28, 33, 34, 102, 104]. As discussed in Chapter 3, we hypothesize that the reason for this shortcoming is due, in part, to SCMs utilizing an oversimplified description of the mineral surface and

inadequate interpretation of data quantifying the number of available sites for proton and metal ion adsorption.

To substantiate this hypothesis, we build on the work presented in Chapter 3 in which the surface heterogeneity of the GOE63 goethite sample was established using a new methodology that unifies the different N_S values predicted from crystallography, microscopic imaging, tritium exchange, surface saturation data, and surface charging data. The crystal face composition (CFC) of GOE63 determined via this new methodology was used to develop a CD-MUSIC model capable of predicting Cd(II) adsorption onto goethite in single solute systems. In this chapter, the CD-MUSIC model is further developed through fitting of Pb(II) and Se(IV) single solute adsorption edge data. The resulting model is tested using single solute isotherm data for Pb(II) and Se(IV) and bi-solute adsorption edge data for Cd(II), Pb(II), and Se(IV). Accurate model predictions of this adsorption data will provide support for: (1) GOE63's crystal face composition (CFC); (2) the methodology developed to determine GOE63's CFC; and, (3) our hypothesis regarding the need for a more rigorous accounting of the mineral surface in SCMs.

Spectroscopic data and computational molecular modeling simulations found in the literature were used to guide the selection of surface complexes employed in the CD-MUSIC model. Bond valence analysis as described by Bargar et al. [51], was also be used to help elucidate the identity of each surface species used in the model.

4.2. Materials and Methods of Adsorption Experiments

Data from this work was collected by Vieira [92]. Preparation of the goethite sample (GOE63) used in this work and the procedure used for conducting potentiometric titration experiments were presented previously in Chapter 3. The materials and methods used in conducting Pb(II) and Se(IV) single solute adsorption experiments and Cd(II), Pb(II), and Se(IV) bi-solute adsorption experiments are identical to those previously discussed in Chapter 3 for Cd(II) adsorption onto GOE63. For convenience, the materials and methods section describing adsorption experiments in Chapter 3 is repeated here.

Goethite slurries with specific solids concentrations were prepped inside a nitrogen-purged glove box using freeze dried goethite (described previously), $NaNO_3$ as the background electrolyte, and carbonate free Millipore water. All slurries were given an ionic strength of 0.1 M $NaNO_3$. To confirm the concentration of goethite in the slurry, three 10 mL samples of diluted solids slurry were taken and analyzed gravimetrically. The slurry was acidified to around pH 3 and then 10 mL aliquots were placed in 15 mL VWR polypropylene centrifuge tubes which acted as batch equilibrium reactors, with each reactor representing one data point for the pH adsorption edge (constant metal concentration, varying pH) or adsorption isotherm (constant pH, varying metal concentration) to be constructed. Cd(II), Pb(II), and/or Se(IV) was then added to each reactor bottle to attain the metal(s) concentration desired. In order to avoid local metal hydroxide precipitation, each centrifuge tube was forcefully shaken prior to raising the reactor's pH via the addition of nitrogen purged 1N NaOH. To test for any losses in the

system and/or precipitation of the metal(s) in each experiment, reactor tubes devoid of goethite (metal blanks) were also prepared.

Once the samples were prepared they were placed in a tumbler for 48 hours at 25^{o}C, which had been determined from preliminary experiments to be sufficient time for the batch reactors to reach equilibrium. For the adsorption isotherm experiments, the pH of each reactor tube was checked and, if necessary, adjusted via the addition of either carbonate free 1N HNO_3 or carbonate free 1N NaOH every 4 – 6 hours in order to sustain a constant pH throughout the experimental run. After 2 days time, the reactor tubes were placed back inside the nitrogen-purged glove box and their final pH was recorded. The samples were then removed from the glove box and placed in a constant temperature centrifuge (Beckman J2-21) for 10 minutes at 3000 rpm. Each reactor's supernatant was subsequently filtered using a 0.2 μm Supor polyethersulfone membrane filter (Pall Corporation) and, to prevent metal precipitation and adsorption onto the container, was then acidified to 1.5% HNO_3 (Ultrex Ultrapure Reagent, JT Baker, NJ). To ascertain the amount of adsorbate remaining in solution, the supernatant was then analyzed using inductively coupled plasma (ICP) optical emission spectroscopy (Spectro CirosCCD). A mass balance on each batch reactor was conducted to determine the quantity of metal adsorbed to goethite.

4.3. Modeling Approach

The crystal faces present on a mineral surface greatly impact the adsorption behavior of ions in solution [24, 25, 82, 84, 85]. Therefore, in predicting ion adsorption

in solid – solution systems, it is imperative that the crystal face composition (CFC) of the mineral surface be quantified. For the goethite sample employed in this study (GOE63), the CFC of the mineral was determined using a new methodology employing selenite surface saturation data and potentiometric titration data (see Chapter 3). The resulting CFC of 31% (101) face, 55% (001) face, and 14% (210) was in agreement with crystallography, microscopic image analysis, tritium exchange, surface saturation data, and surface charging data. The CD-MUSIC model was used to simulate Cd(II), Pb(II), and Se(IV) adsorption onto GOE63 via the computer software FITEQLC [22] and FITEQL 4.0 [21]. The site types and their respective site densities used in the CD-MUSIC model for describing the GOE63 surface were originally reported in Chapter 3 but are reprinted here for convenience in Table 4.1.

Table 4.1 Site types and N_S used in the CD-MUSIC model for GOE63

Site Type	Crystal Face	CFC (%)	N_S (sites/nm^2)	
			Individual [a]	Model [b]
≡FeOH	(101)	31	0.94	2.79
	(010)	55	1.85	
	(210)	14	1.03	1.03
≡Fe_2OH	(101)	31	-	-
	(010)	55	-	
	(210)	14	1.03	1.03
≡Fe_3O	(101)	31	0.94	2.79
	(010)	55	1.85	
	(210)	14	-	-

[a] "Individual" Ns values were calculated for each site type by multiplying the CFC percentage by the respective crystal face's reactive site density (cf. Table 3.2)
[b] Values under the column labeled "model" represent the site densities used in CD-MUSIC for GOE63. For the (101) and (001) crystal faces, the Ns value for a given site type is calculated by summing the Ns values presented in the "Individual" column for the (101) and (001) faces. For the (210) crystal face, the site densities in the "model" column are equivalent to those presented in the "individual" column.

The CD-MUSIC model presented in this chapter was developed in several distinct steps: (1) simulation of the potentiometric titration data for GOE63 to determine the intrinsic surface protonation and ion pair formation equilibrium constants; (2) fitting the single solute Cd(II), Pb(II), and Se(IV) pH adsorption edge experimental data conducted on GOE63 to obtain the equilibrium constants for each ion's surface complexes; (3) simulating of the single solute Cd(II), Pb(II), and Se(IV) isotherm adsorption experiments and the bi-solute adsorption edge experiments conducted on GOE63 utilizing the same parameters, surface species, and affinity constants previously determined in steps 1 and 2. In summary, the potentiometric titration data and single solute pH adsorption edge data were used for each ion to calibrate the CD-MUSIC model. The single solute isotherm

data and bi-solute adsorption edge data were used to substantiate the model's predictive capability. Fitting of the potentiometric titration data (Step 1) and the Cd(II) single solute pH adsorption edge data (Step 2) were previously presented in Chapter 3. In addition, the CD-MUSIC model's prediction of Cd(II)'s isotherm adsorption data (Step 3) was presented in Chapter 3.

The quality of the model fit for each data set was quantified by calculating the weighted sum of squares divided by degrees of freedom (WSOS/DF). Model fits resulting in a WSOS/DF value between 0.1 and 20 are considered acceptable [21]. The absolute and experimental errors used in the model were taken from previous research investigating metal ion adsorption onto an iron oxide mineral [2] (see Chapter 3).

4.3.1. Bond valence analysis

Bond valence analysis is a means for assessing the comparative strength of cation – oxygen bonds in crystalline structures [51]. Bond valence is defined by Brown and Altermatt [150] as Equation 4.1:

$$s_i = \exp\left(\frac{r_0 - r}{0.37}\right) \tag{4.1}$$

where s_i is the bond valence value in valence units (v.u.), r_0 is an empirically determined parameter with units of Å, and r is the cation – oxygen bond length in units of Å.

Pauling's electrostatic valence principle states that for a given ion in a crystal structure, the sum of bond valences around that ion equals the absolute value of the ion's charge (i.e., $\Sigma s_i = |Z_{ion}|$) [151]. This principle ($\Sigma s_i = |Z_{ion}|$), along with Brown's and Altermatt's [150] bond valence equation (Equation 4.1), was originally developed and utilized for investigating the structure of amorphous and crystalline solids [150, 152, 153]. Bargar et al. [51] reasoned that this bond valence concept could be extended to surface complexes present at the solid – solution interface, and the stability of proposed surface species can be predicted by determining whether the surface oxygen is coordinatively oversaturated ($\Sigma s_i > |Z_{ion}| \pm 0.05$), saturated ($\Sigma s_i = |Z_{ion}| \pm 0.05$), or undersaturated($\Sigma s_i < |Z_{ion}| \pm 0.05$) [49-51, 54, 71]. Surface species resulting in saturation of the surface oxygen atom are considered to be stable, while species resulting in under or over-saturation of the surface oxygen are considered to be plausible and unstable/non-existent, respectively [51]. By using the bond valence approach outlined by Bargar et al. [51], in addition to the spectroscopic data and molecular modeling simulations found in the literature, the identity of surface complexes present on the goethite surface can be further elucidated.

In this study, bond valence analysis was used to aid in determining the surface site types involved in surface complexation reactions as well as their protonation states. For the sake of clarity, the results from this analysis for each adsorbate considered (Cd(II), Pb(II), and Se(IV)) are included in their respective sections discussing single solute adsorption onto GOE63. In all bond valence calculations performed, the surface oxygen atom was considered to have a maximum coordination number of four, including

hydrogen bonds; in agreement with the maximum coordination number observed for oxygen in aqueous solutions and crystalline hydrates [154]. With this constraint on oxygen's coordination number, there are three, two, and one possible protonation states for the singly, doubly, and triply coordinated surface sites to complex with an adsorbate, respectively (Table 4.2).

Table 4.2 Possible protonation states of each surface site type when complexing with an adsorbate

Protonation State		
Non	Singly	Doubly
≡Fe-O-Ads	≡Fe-OH-Ads	≡Fe-OH_2-Ads
≡Fe_2-O-Ads	≡Fe_2-OH-Ads	–
≡Fe_3-O-Ads	–	–

"Ads" denotes the adsorbate complexed to the surface oxygen

The parameters reported in Table 4.3 were used in all bond valence calculations presented in this chapter. For hydroxyl and hydrogen bonds, bond valence contributions reported in Table 4.3 were calculated using the relationship developed by Bargar et al.[51] and presented here as Equation 4.2:

$$s_{OH} = \frac{0.241}{r_{OH} - 0.677} \tag{4.2}$$

where s_{OH} is the bond valence contribution from a hydroxyl or hydrogen bond in valence units (v.u.), and r_{OH} is the length of the hydroxyl or hydrogen bond in Å.

Table 4.3 Bond valence contributions for pertinent surface oxygen bonds

Bond	r (Å)	r_0 (Å) [a]	s_i (v.u.)
Fe - O	1.95 - 2.09 [b]	1.759	0.60 - 0.41
Cd - O	2.25 - 2.30 [c]	1.904	0.39 - 0.34
Pb - O	2.26 - 2.30 [d]	2.04	0.55 - 0.50
Se - O	1.70 [e]	1.811	1.35
O - H	0.95 - 1.03 [f]	-	0.88 - 0.68
O---H	1.65 - 2.50 [f]	-	0.13 - 0.25

[a] All r_0 values taken from Brown and Altermatt [150]
[b] Fe – O bond lengths in goethite as reported in [155]
[c] Cd – O bond length range for first shell O atoms observed by [39, 40] using EXAFS spectroscopy
[d] Pb – O bond length range for first shell O atoms observed by [49, 54] using XAFS and EXAFS spectroscopies
[e] Se – O bond length for first shell O atoms observed by [45]
[f] Hydroxyl and hydrogen bond lengths taken from [51]
Bond valence values for Fe-O, Cd-O, Pb-O, and Se-O bonds calculated using Equation 4.1. Bond valence values for O-H and O---H bonds calculated using Equation 4.2.

4.3.2. Charge Distribution (CD) values

For inner-sphere surface complexes, charge distribution (CD) values, Δz_0 and Δz_1, employed in this work were determined using an approach similar to the one described by Hiemstra et al. [34]. The values Δz_0 and Δz_1 were calculated using Equation 4.3 and Equation 4.4, developed by Hiemstra and Van Riemsdijk [93].

$$\Delta z_0 = n_0 + n_{H0} - \phi(n_0 + n_{H0} + \Sigma n_{ref} z_{ref}) \quad (4.3)$$

$$\Delta z_1 = n_1 + n_{H1} + \phi(n_0 + n_{H0} + \Sigma n_{ref} z_{ref}) \quad (4.4)$$

where n_0 and n_1 are the amount of adsorbate charge allocated to the 0- and 1-planes, respectively, n_{H0} and n_{H1} represent the charge from additional protons, or other ligands, participating in the surface complexation reaction and positioned in the 0- and 1-planes, respectively, the symbol ϕ is a proportionality constant ($\phi \approx 0.17$), n_{ref} represents the number of sites from a particular surface group participating in the reaction, and z_{ref} denotes the charge for the reference state of the surface group(s) involved in the reaction [93].

CD values were determined by first calculating n_0, the amount of charge distributed from the adsorbing cation (Pb(II), Cd(II), and Se(IV)) to the mineral surface. The n_0 value was calculated by utilizing the bond valence equation (Equation 4.1) developed by Brown and Altermatt [150] in conjunction with the cation – surface oxygen bond lengths observed in previously published EXAFS studies (Table 4.3) [39, 40, 45, 49, 54].

Inputting the spectroscopically observed bond length, r, into Equation 4.1, along with r_0 values taken from Brown and Altermatt [150], results in a bond valence value (s_i) for a single cation – surface oxygen bond. This bond valence value s_i, is thought to represent the amount of charge supplied from the cation to the mineral surface for a single bond between the adsorbate and adsorbent [34]. Thus, for a mono, bi, and tridentate surface species, the total amount of charge supplied from the cation to the surface (i.e., n_0) is equal to s_i, $2s_i$, and $3s_i$, respectively. Once n_0 is known, n_1 can be calculated by subtracting n_0 from the formal charge of the complexing cation. For

instance, if $n_0 = 1.2$ for a Cd(II) surface complex, then $n_1 = Z_{Cd} - n_0$. Since Cd(II) has a formal charge of +2, $n_1 = 2 - 1.2 = 0.8$.

The n_{H0} value in Equation 4.3 is determined based on the resulting protonation state of the surface oxygen atom(s) involved in the adsorption reaction compared to their reference state. For example, if ≡FeOH was used as the reference surface component for singly coordinated surface sites, then a surface complex bound to a ≡FeO or ≡$FeOH_2$ site would have an n_{H0} value of -1 or +1, respectively. The n_{H1} value takes into account any protons, as well as hydroxide or oxygen ions that are bound to the surface complex on the solution side of the mineral – water interface. Selenite's adsorption onto goethite is a useful illustration of how n_{H1} is calculated. Selenite (SeO_3^{2-}) forms a bidentate surface complex with goethite, meaning that one of its three oxygen ligands is on the solution side of the interface and located in the electrostatic 1 plane of the CD-MUSIC model. This oxygen ligand located in the electrostatic 1 plane has a formal charge of -2; hence $n_{H1} = -2$. If the oxygen atom in question was protonated, then the value of n_{H1} would equal -1.

4.4. Results and Discussion

4.4.1. Cd(II), Pb(II), and Se(IV) aqueous species

Equilibrium constants provided in MINEQL+ 4.5 at 25°C were used to determine the aqueous speciation for Cd(II), Pb(II), and Se(IV) in FITEQLC [146, 147]. The formation constants for $CdSeO_3$, $Cd(SeO_3)_2$, and $PbSeO_3$ aqueous complexes were taken

from Feroci et al. [156], Toropova [157], and Feorci et al. [158], respectively. Formation constants for these three aqueous complexes were not provided in the MINEQL+4.5 database.

4.4.2. Surface Protonation and ion pair formation

The equilibrium constants for the surface protonation and ion pair formation reactions, as well as the capacitance values of GOE63 were determined via model fitting of the mineral sample's potentiometric titration data using the methodology developed in Chapter 3 (see Chapter 3). The values are summarized in Table 4.4.

4.4.3. Single Solute Modeling

Once the surface protonation and ion pair equilibrium constants were determined, the CD-MUSIC model could be calibrated for Cd(II), Pb(II), and Se(IV) adsorption through model fitting of experimental single solute pH adsorption edge data collected on GOE63 (Table 4.4 and Table 4.5)

Table 4.4 Surface complexation reactions used in the CD-MUSIC model

Adsorbate	Crystal Face	Surface Complex	Linkage [a]	Δz_0	Δz_1	log K_{in}
H^+	(101), (001) & (210)	$\equiv FeOH^{-0.5} + H^+ \rightarrow \equiv FeOH_2^{+0.5}$	-	1	0	8.50
		$\equiv FeOH^{-0.5} + H^+ + NO_3^- \rightarrow \equiv FeOH_2^{+0.5}\_NO_3^-$	-	1	-1	8.00
		$\equiv FeOH^{-0.5} + Na^+ \rightarrow \equiv FeOH^{-0.5}\_Na^+$	-	0	1	-0.10
	(101) & (001)	$\equiv Fe_3O^{-0.5} + H^+ \rightarrow \equiv Fe_3OH^{+0.5}$	-	1	0	11.70
		$\equiv Fe_3O^{-0.5} + H^+ + NO_3^- \rightarrow \equiv Fe_3OH^{+0.5}\_NO_3^-$	-	1	-1	11.20
		$\equiv Fe_3O^{-0.5} + Na^+ \rightarrow \equiv Fe_3O^{-0.5}\_Na^+$	-	0	1	-0.10
Cd(II)	(101) & (001)	$2(\equiv FeOH^{-1/2}) + Cd^{2+} \rightarrow (\equiv FeOH)_2\text{-}Cd$	Corner	0.82	1.18	2.69
		$2(\equiv FeOH^{-1/2}) + Cd^{2+} + H_2O \rightarrow (\equiv FeOH)_2\text{-}CdOH + H^+$	Corner	0.82	0.18	-4.90
		$\equiv FeOH^{-1/2} + Cd^{2+} + 2H_2O \rightarrow (\equiv FeOH)\text{-}Cd(OH)_2 + 2H^+$	Vertex	0.41	-0.41	-11.96
	(210)	$2(\equiv FeOH^{-1/2}) + \equiv Fe_2OH^0 + Cd^{2+} \rightarrow (\equiv FeOH)_2\text{-}Cd\text{-}(\equiv Fe_2OH)$	Edge	1.15	0.85	8.04
		$2(\equiv FeOH^{-1/2}) + \equiv Fe_2OH^0 + Cd^{2+} + H_2O \rightarrow (\equiv FeOH)_2\text{-}CdOH\text{-}(\equiv Fe_2OH) + H^+$	Edge	1.15	-0.15	0.91
Pb(II)	(101) & (001)	$\equiv FeOH^{-1/2} + Fe_3O^{-1/2} + Pb^{2+} + H_2O \rightarrow (\equiv FeO)\text{-}PbOH\text{-}(\equiv Fe_3O) + 2H^+$	Edge	0.25	-0.25	-4.13
		$2(\equiv FeOH^{-1/2}) + Fe_3O^{-1/2} + Pb^{2+} \rightarrow (\equiv FeOH)_2\text{-}Pb\text{-}(\equiv Fe_3O)$	Edge	1.5	0.5	12.34
	(210)	$\equiv FeOH^{-1/2} + \equiv Fe_2OH^0 + Pb^{2+} + H_2O \rightarrow (\equiv FeOH)\text{-}PbOH\text{-}(\equiv Fe_2O) + 2H^+$	Edge	0.17	-0.17	-5.20
		$2(\equiv FeOH^{-1/2}) + \equiv Fe_2OH^0 + Pb^{2+} \rightarrow (\equiv FeOH)_2\text{-}Pb\text{-}(\equiv Fe_2OH)$	Edge & Corner	1.4	0.6	10.93
Se(IV)	(101) & (001)	$2(\equiv FeOH^{-1/2}) + SeO_3^{2-} + 2H^+ \rightarrow (\equiv FeO)_2\text{-}SeO + 2H_2O$	Corner	0.75	-0.75	19.85
	(210)	$2(\equiv FeOH^{-1/2}) + SeO_3^{2-} + 2H^+ \rightarrow (\equiv FeO)_2\text{-}SeO + 2H_2O$	Corner	0.75	-0.75	21.25
		$2(\equiv FeOH^{-1/2}) + SeO_3^{2-} + 3H^+ \rightarrow (\equiv FeO)_2\text{-}SeOH + 2H_2O$	Corner	0.75	0.25	29.83
Cd(II) and Se(IV)	(101) & (001)	$2(\equiv FeOH^{-1/2}) + SeO_3^{2-} + Cd^{+2} \rightarrow (\equiv FeOH)_2\text{-}CdOSeO_2$	Corner	0.82	-0.82	11.54
Pb(II) and Se(IV)	(210)	$\equiv FeOH^{-1/2} + \equiv Fe_2OH^0 + Pb^{2+} + SeO_3^{2-} \rightarrow (\equiv FeOH)\text{-}PbOSeO_2\text{-}(\equiv Fe_2OH)$	Edge	0.92	-0.92	19.73

[a] "Linkage" denotes the way in which the adsorbate binds to the surface sites (e.g., corner, edge, vertex)

$C_1 = C_2 = 1.05$ F/m^2

Table 4.5 Single solute adsorption experiments performed on GOE63 with corresponding model fits

Adsorbate	Experiment	Ionic Strength or Surface Loading [a]	Model Fit (WSOS/DF)
H^+	Potentiometric Titration	0.01	1.4
		0.081	0.2
		0.312	0.3
Cd(II)	Adsorption Edge	0.31	3.9
		0.44	4.7
		2.22	1.8
		9.08	2.6
	Isotherm [b]	-	7.0
Pb(II)	Adsorption Edge	0.27	17
		0.36	3.7
		1.86	3.0
		7.34	2.3
	Isotherm [c]	-	3.1
Se(IV)	Adsorption Edge	0.38	1.5
		2.10	5.8
		7.84	4.9
	Isotherm [d]	-	15

[a] For the H^+ adsorbate, ionic strength (mol/L) is reported. For all other adsorbates, surface loading (μmol/m2) is reported.
[b] Cd(II) isotherm experiment conducted at pH 6.89
[c] Pb(II) isotherm experiment conducted at pH 4.89
[d] Se(IV) isotherm experiment conducted at pH 9.89

4.4.3.1. Cd(II) Adsorption

Cd(II) adsorption was modeled on goethite utilizing a tridentate edge sharing complex forming on the (210) crystal face, and a bidentate corner sharing complex and monodentate surface complex, both forming on the (101) and (001) crystal faces of goethite. The resulting model fits for the pH adsorption edge experiments were satisfactory and the model proved capable of accurately predicting GOE63's Cd(II) isotherm adsorption data. A detailed discussion of the Cd(II) surface complexes used in

the CD-MUSIC model and the model fits for Cd(II) single solute data is presented in Chapter 3.

4.4.3.2. Pb(II) Adsorption

The same approach used to select surface complexes and to calibrate the CD-MUSIC model for Cd(II) in Chapter 3 was applied to Pb(II) adsorption to goethite. However, previous attempts to model Pb(II) adsorption has been confounded by an inability to resolve spectroscopic data with the surface complexes and corresponding equilibrium reactions used in SCMs [33, 104]. EXAFS investigations concerning lead adsorption onto goethite have resulted in two primary lead – iron distances being observed at ≈3.3 Å and ≈3.9 Å [50, 54]. The edge sharing complex associated with the lead – iron distance of 3.3 Å was found to exist over the entire pH range investigated (pH 5 – 7) while the corner sharing complex, characterized by the lead – iron distance of 3.9 Å, was only detected in samples with a pH below 6 [54]. Above pH 6, the contribution from the corner sharing complex to Pb(II) adsorption was found to greatly diminish and the only Pb-Fe distance observed spectroscopically was ≈3.3 Å [54]. To ascertain whether or not the disappearance of the corner sharing complex at pH values above 6 from their spectra was simply the result of higher surface coverages, Ostergren et al. [54] analyzed the spectra of several samples taken from adsorption experiments conducted at pH 7 using low Pb(II) surface loadings between 0.5 and 1 μmol/m^2. The resulting spectra from these experiments revealed only one Pb-Fe distance at 3.34 Å, indicative of an edge sharing complex rather than a corner sharing one. This finding supports the idea that the

corner sharing complex, observed below pH 6, becomes less thermodynamically favorable as pH rises and is replaced by/converts into an edge sharing complex.

Based on the lead – oxygen bond lengths observed for these surface complexes, two possible first shell configurations exist: a trigonal pyramidal structure consisting of three nearest neighbor oxygens or a square arrangement made up of four oxygen atoms [49, 51, 52, 54, 159, 160]. In determining which of the two first shell geometries was more probable, Ostergren et al. [54] acknowledged that the coordination numbers associated with lead binding and derived from EXAFS fitting could differ between 3 and 4 depending on the scale factor used in fitting the data. However, a scale factor of approximately 0.5, too low to be considered realistic, was necessary in arriving at a coordination number of four [54, 160]. Additionally, comparison of X-ray absorption near-edge structure (XANES) spectra for lead adsorbed onto goethite with that of the $Pb_4(OH)_4^{+4}$ solution complex, which possesses a trigonal pyramidal geometry, suggests that the coordination environment of the Pb(II) surface complexes is similar to that of the $Pb_4(OH)_4^{+4}$ solution complex [50, 54]. Furthermore, both EXAFS studies investigating Pb(II) adsorption onto goethite [49, 54] observed first shell Pb - O distances of 2.26 – 2.30 Å for all samples studied. In comparing these Pb – O bond lengths to those found in Pb(II)- hydrates, hydroxides, oxides, and oxysalts, Bargar et al. [50] found that Pb-O bond lengths $\leq$ 2.35 Å are indicative of Pb(II) having a trigonal pyramidal coordination with oxygen atoms or hydroxide ions. While water molecules are present near the adsorbed Pb(II) ion and are even thought to act as ligands with the adsorbate, none of the three first shell oxygens of adsorbed Pb(II) are thought to be from water due to the fact

that Pb – O_{water} bond distances are > 2.75 Å [50]. For these reasons, lead surface complexes in this study are considered to have a trigonal pyramidal first shell coordination, with a coordination number of three, consisting of some combination of surface oxygen atoms and hydroxide ions.

To summarize, Pb(II) binds to goethite as: (1) an edge sharing complex over all pH values; and (2) a corner sharing complex at pH values below 6. In addition, adsorbed Pb(II) has three nearest neighbor oxygen atoms that are either surface oxygen atoms or OH ligands. Bond valence analysis reveals that Pb(II) adsorption can occur on all three surface site types (Table 4.6). As in the case of Cd(II) adsorption, only the surface sites classified as "stable" in Table 4.6 were used in modeling Pb(II) adsorption onto GOE63 in this work.

Table 4.6 Bond valence analysis for Pb(II) adsorbing onto goethite

Surface species/bonds	Σs_i at surface oxygen (v.u.)		Prediction
	No H-bonds	With H-bonds	
≡Fe-O-Pb	0.91 - 1.15	1.17 - 1.65	**Plausible**
≡Fe-OH-Pb	1.59 - 2.03	1.72 - 2.28	**Stable**
≡Fe-OH_2-Pb	2.27 - 2.91	2.27 - 2.91	Doesn't Occur
≡Fe_2-O-Pb	1.32 - 1.75	1.45 - 2.00	**Stable**
≡Fe_2-OH-Pb	2.00 - 2.63	2.00 - 2.63	**Stable**
≡Fe_3-O-Pb	1.73 - 2.35	1.73 - 2.35	**Stable**

Bond valence values calculated using the values listed in Table 4.3. If the range of "Σsi at surface oxygen" contains 2 ± 0.05 (i.e., |Zion| ± 0.05), the surface species is stable. If "Σsi at surface oxygen" < 1.95, the surface species is plausible. If "Σsi at surface oxygen" > 2.05, the surface species does not occur.

To explain the pH dependence of the corner sharing complex (Pb – Fe distance ≈3.9 Å), Ostergren et al. [54] hypothesized that the complex forms on the (101) main face of goethite via two singly coordinated sites on adjacent octahedra. As pH rises above 6, the bidentate corner sharing complex transforms into a tridentate edge sharing complex composed of two singly and one triply coordinated site. The tridentate edge sharing complex is thought to be increasingly stable as pH increases thereby suggesting that a pH dependence exists between Pb(II) and the triply coordinated surface sites involved in the formation of the tridentate complex. According to Ostergren et al. [54], as the pH drops below 6, the number of triply coordinated sites that are protonated rises considerably thereby making it increasingly hard for Pb(II) to bind to these surface sites because of increased competition with protons.

Pb(II) adsorption onto GOE63 was originally modeled in CD-MUSIC using the bidentate corner sharing complex, and the tridentate edge sharing complex that it is thought to evolve at higher pH values, proposed by Ostergren et al. [54]. Additional edge sharing complexes proposed by Bargar et al. [49] and Ostergren et al. [54] were used to help improve model fits. In the end, no model utilizing the corner sharing complex proposed by Ostergren et al. [54] was capable of accurately predicting Pb(II) adsorption onto GOE63 while conforming to EXAFS findings; specifically that the Pb(II) corner sharing complex is only prevalent below pH 6. The incongruence between the models and the spectroscopic data stems from the fact that practically all triply coordinated sites (≈99%) on GOE63 are already protonated at pH 10 (recall that triply coordinated sites are thought to have a log K_H of 11.7 [23, 29], and are modeled as such in this study). Hence,

at pH 6, Pb(II) is unable to bind to these triply coordinated sites in the manner described by Ostergren et al. [54].

An alternative surface complex is proposed in this work that, when used in CD-MUSIC, allows for the model to predict Pb(II) adsorption onto GOE63 while also agreeing with spectroscopic evidence [49, 54]. The proposed surface species forms on the (210) crystal face as a tridentate complex, consisting of two singly and one doubly coordinated surface site (Figure 4.1). The complex is edge sharing with one octahedra and corner sharing with a second octahedra, identical to the "Tridentate B" species discussed by Venema et al. [27] for Cd(II) adsorption onto goethite. As pH increases, the corner sharing linkage to the singly coordinated surface site on the second octahedra (right octahedra in Figure 1) is thought to break, transforming the tridentate complex into an edge sharing bidentate complex (Table 4.4).

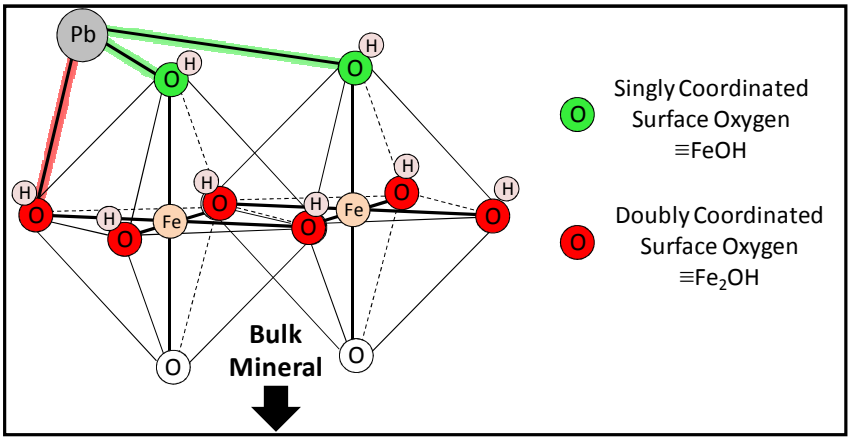

Figure 4.1 Proposed Pb(II) surface complex on the (210) crystal face of goethite. The ion is complexed to the mineral surface via an edge and corner linkage.

A similar tridentate complex can be proposed to form on the (101) and (001) crystal faces of goethite, bound to two singly and one triply coordinated site. However, the low surface coverages (0.5, 0.4, and 1.3 μmol/m^2 at pH 5.0, 5.0, and 5.2) at which Ostergren et al. [54] observed the Pb – Fe distance of 3.9 Å, coupled with the fact that the (210) face possesses higher affinity surface sites than the (101) and (001) crystal face [27, 39, 78, 114], supports the idea of this tridentate complex forming on the (210) crystal face of goethite.

Using the tridentate edge and corner sharing complex proposed above (Figure 4.1), along with three additional edge sharing surface complexes (cf. Table 4.4), one on the (210) face and two on the (101) and (001) faces, the CD-MUSIC model was able to successfully predict Pb(II) adsorption onto GOE63 (Figure 4.2). All of the surface complexes used in the CD-MUSIC model agree with spectroscopic evidence and bond valence analysis [49, 54]. Furthermore, the newly proposed tridentate complex's contribution to Pb(II) adsorption (Figure 4.2b - Figure 4.2d), as predicted by CD-MUSIC, agrees well with the spectroscopic evidence available [49, 54]. Additionally, as in the case of Cd(II) adsorption, Pb(II) adsorbed preferentially to the (210) crystal face of GOE63 (Figure 4.2b - Figure 4.2d).

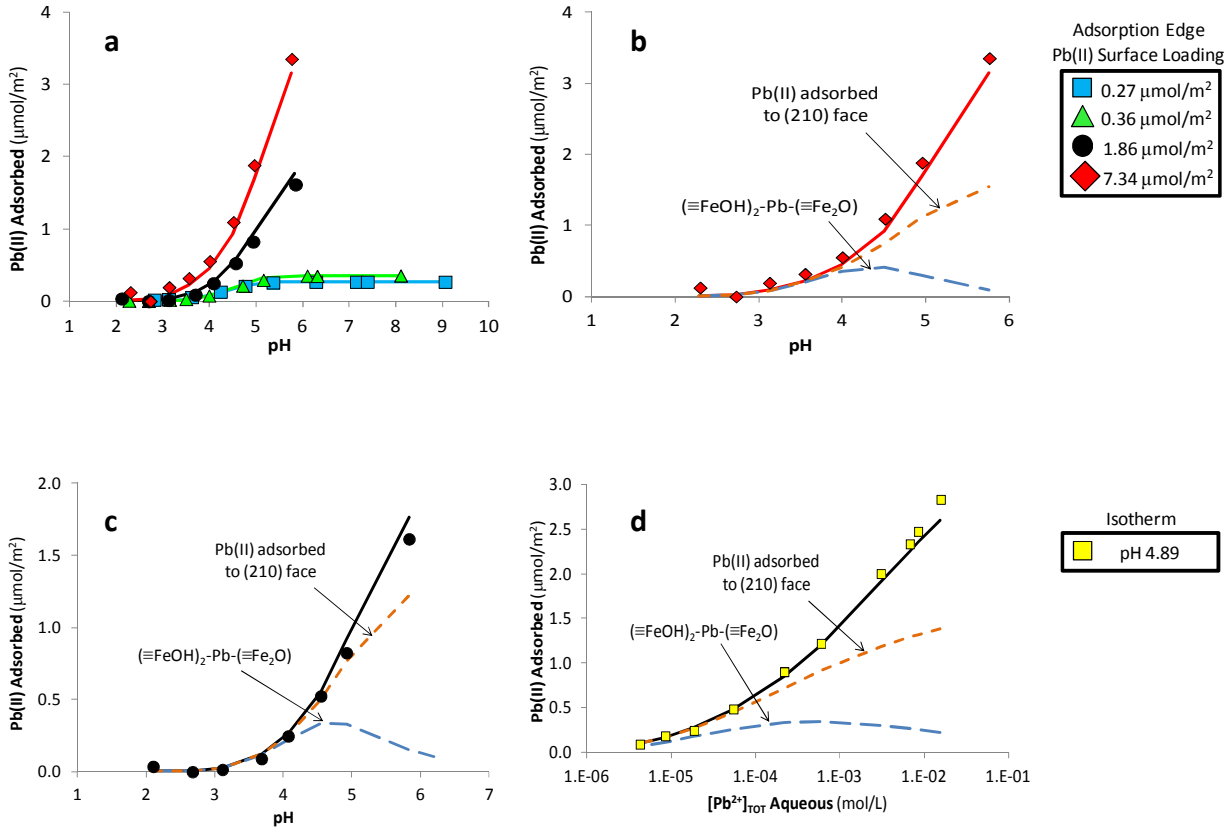

Figure 4.2 **(a)** Pb(II) pH adsorption edge data for GOE63 at four different Pb(II) surface loadings. **(b) and (c)** Pb(II) pH adsorption edge data for GOE63 at a Pb(II) surface loading of **(b)** 7.34 µmol/m^2 and **(c)** 1.86 µmol/m^2. **(d)** Pb(II) isotherm adsorption data for GOE63 at pH 4.89. In plots **(a) – (d)**, symbols denote experimental data points while solid lines represent model simulations of total Pb(II) adsorbed. The dashed orange line in plots **(b) - (d)** represents the amount of Pb(II) adsorbed to the (210) crystal face while the long dash blue line denotes the amount of Pb(II) adsorbed as the $(\equiv FeOH)_2$-Pb-$(\equiv Fe_2O)$ surface complex that binds via a corner and edge linkage to the (210) crystal face.

4.3.3.3. Se(IV) Adsorption

To our knowledge there has been only one EXAFS study on selenite adsorbing to goethite, performed by Hayes et al. [45], in which selenite was found to bind to goethite as an inner-sphere binuclear bidentate complex possessing an iron – selenium distance of 3.38 Å.

In a modeling study conducted by Hiemstra et al. [34], the optimized geometry of four proposed selenite surface complexes forming on goethite were calculated using density functional theory (DFT). Bond valence analysis for Se(IV) adsorbed onto goethite reveals that only deprotonated singly coordinated sites are capable of complexing with selenite (Table 4.7); therefore, the four complexes considered were: 1) a non-protonated bidentate complex $(\equiv FeO)_2SeO$; 2) a protonated bidentate complex $(\equiv FeO)_2SeOH$; 3) a non-protonated monodentate complex $\equiv FeOSeO_2$; and 4) a protonated monodentate complex $\equiv FeOSeOOH$. All DFT calculations performed by Hiemstra et al. [34] were conducted on the (101) face of goethite; therefore both bidentate complexes modeled had a double corner bidentate structure. Once the geometry and corresponding bond lengths of a proposed surface complex were established, the authors could then calculate the complex's corresponding charge distribution (CD) factor via bond valence analysis, and then employ that CD factor into the CD-MUSIC model.

Table 4.7 Bond valence analysis for Se(IV) adsorbing onto goethite

Surface species/bonds	Σs_i at surface oxygen (v.u.)		Prediction
	No H-bonds	With H-bonds	
≡Fe-O-Se	1.76 - 1.95	2.02 - 2.45	**Stable**
≡Fe-OH-Se	2.44 - 2.83	2.57 - 3.08	Doesn't Occur
≡Fe-OH_2-Se	3.12 - 3.71	3.12 - 3.71	Doesn't Occur
≡Fe_2-O-Se	2.17 - 2.55	2.30 - 2.80	Doesn't Occur
≡Fe_2-OH-Se	2.85 - 3.43	2.85 - 3.43	Doesn't Occur
≡Fe_3-O-Se	2.58 - 3.15	2.58 - 3.15	Doesn't Occur

Bond valence values calculated using the values listed in Table 4.3. If the range of "Σsi at surface oxygen" contains 2 ± 0.05 (i.e., |Zion| ± 0.05), the surface species is stable. If "Σsi at surface oxygen" < 1.95, the surface species is plausible. If "Σsi at surface oxygen" > 2.05, the surface species does not occur.

To determine which of the proposed selenite complexes exist on the goethite surface, Hiemstra et al. [34] used CD-MUSIC to model single and bi-solute data for selenite and phosphate adsorption onto goethite using the four proposed selenite complexes with their corresponding CD values determined using a combination of DFT and bond valence calculations. Through their modeling work, Hiemstra et al. [34] concluded that the non-protonated bidentate complex was the dominant selenite surface species present on goethite, in agreement with spectroscopic evidence. Furthermore, the iron-selenium distance calculated for the non-protonated bidentate complex using DFT (3.35 Å) was found to be very close to the EXAFS value observed by Hayes et al. [45] of 3.38 Å.

At high pH values the model could describe selenite adsorption well using only the non-protonated bidentate complex; however, as the SeO_3^{2-} surface loading increased and pH decreased, a second selenite surface complex, specifically the protonated

monodentate complex, was necessary to accurately model the adsorption data. Given these results, the authors reasoned that the protonated monodentate surface complex also forms on goethite, but to a lesser extent than the non-protonated bidentate complex. This conclusion by Hiemstra et al. [34] that both a protonated and non-protonated selenite surface species exists agrees well with the findings of Zhang and Sparks [161]; who, using pressure-jump relaxation techniques, found evidence of both protonated and non-protonated selenite surface complexes adsorbed to goethite.

Given the EXAFS results of Hayes et al. [45], along with the evidence provided by Zhang and Sparks [161] using pressure-jump relaxation techniques and the DFT and CD-MUSIC modeling results of Hiemstra et al. [34], there is strong evidence supporting the formation of selenite forming a non-protonated bidentate double corner surface complex. Additionally, the studies by Zhang and Sparks [161] and Hiemstra et al. [34] both suggest the presence of a protonated selenite complex present on goethite's surface. While the CD-MUSIC modeling results presented by Hiemstra et al. [34] point towards this protonated surface species binding in a monodentate fashion, the Fe – Se distance predicted for that complex via DFT calculations is 3.55 Å, a value that is not observed spectroscopically. However, in the same study by Hiemstra et al. [34], DFT calculations reveal that the resulting Fe – Se distance of a protonated bidentate complex (3.42 Å) agrees well with the spectroscopically observed value of 3.38 Å. To summarize, the Fe – Se distances calculated by Hiemstra et al. [34] using DFT for the protonated and non-protonated *bidentate* selenite surface complexes are in good agreement with the spectroscopically observed value reported by Hayes et al. [45]. The DFT calculations of

Hiemstra et al. [34] also show that the protonated *monodentate* selenite surface complex that was employed in their CD-MUSIC model does not possess a Fe – Se distance in agreement with EXAFS data.

Therefore, in this current modeling work, only protonated and non-protonated binuclear bidentate corner sharing complexes were considered (Table 4.4). Using a protonated and non-protonated bidentate corner sharing complex on the (210) face, along with a non-protonated bidentate corner sharing complex on the (101) and (001) crystal faces, the CD-MUSIC model was able to successfully predict Se(IV) adsorption onto GOE63 over all experimental conditions tested (Figure 4.3). Similar to the results obtained for Cd(II) and Pb(II), the CD-MUSIC model predicts Se(IV) to adsorb preferentially to the (210) crystal face of GOE63 (Figure 4.3b - Figure 4.3d), in agreement with [27, 39, 78, 114].

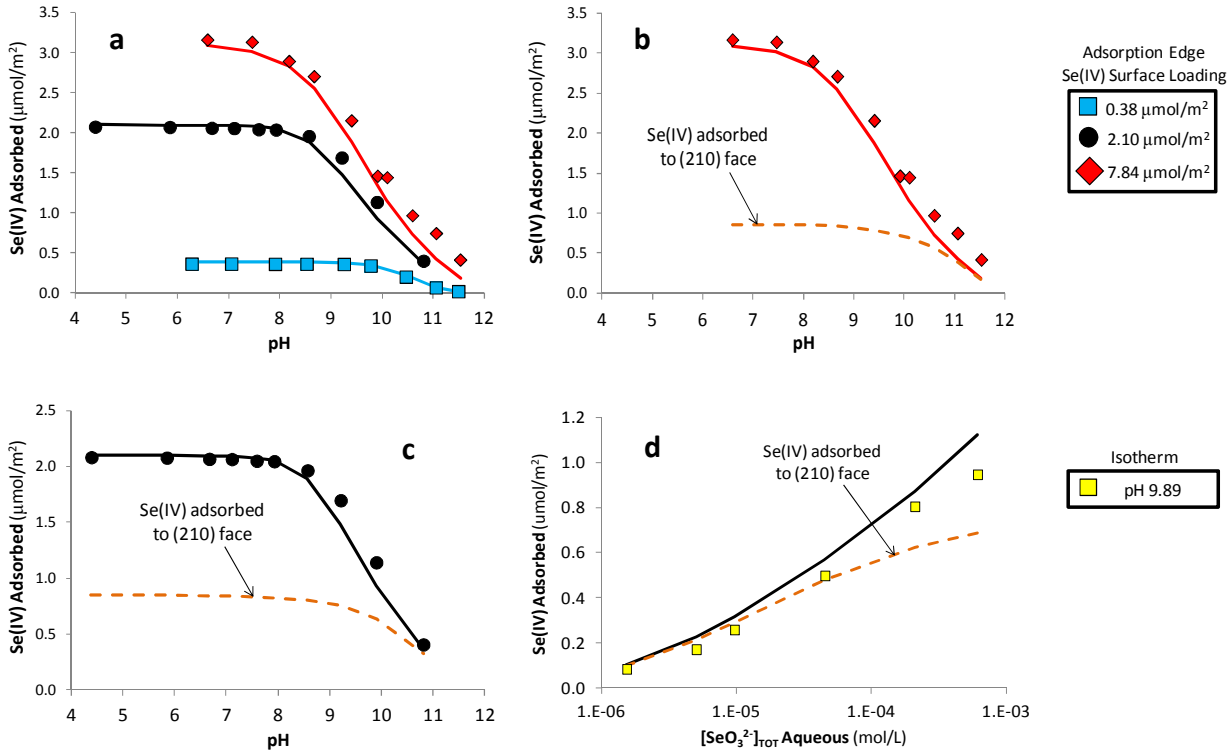

Figure 4.3 **(a)** Se(IV) pH adsorption edge data for GOE63 at four different Se(IV) surface loadings. **(b) and (c)** Se(IV) pH adsorption edge data for GOE63 at a Se(IV) surface loading of **(b)** 7.84 µmol/m^2 and **(c)** 2.10 µmol/m^2. **(d)** Se(IV) isotherm adsorption data for GOE63 at pH 9.89. In plots **(a) – (d)**, symbols denote experimental data points while solid lines represent model simulations of total Se(IV) adsorbed. The dashed orange line in plots **(b) - (d)** represents the amount of Se(IV) adsorbed to the (210) crystal face.

4.4.4. Bi-Solute Modeling

All bi-solute adsorption experiments were modeled using the surface species and equilibrium constants determined through model fitting of the single solute adsorption experiments and listed in Table 4.4. Adsorption edge experiments were conducted at two different surface loadings, classified as "Low" and "Medium" (Table 4.8), for each bi-solute system considered, specifically Cd(II)/Pb(II), Cd(II)/Se(IV), and Pb(II)/Se(IV).

Table 4.8 Bi-solute adsorption experiments performed on GOE63 with corresponding model fits

Bisolute Experiment	Experiment Name [a]	Adsorbate	Surface Loading ($\mu mol/m^2$)	Model Fit (WSOS/DF) No T.C. [b]	Model Fit (WSOS/DF) With T.C. [c]
Cd(II) and Pb(II)	Low	Cd(II)	0.31	4.7	4.7
		Pb(II)	0.26		
	Medium	Cd(II)	2.15	7.2	7.2
		Pb(II)	1.87		
Cd(II) and Se(IV)	Low	Cd(II)	0.43	34	12
		Se(IV)	0.49		
	Medium	Cd(II)	1.98	217	11
		Se(IV)	1.97		
Pb(II) and Se(IV)	Low	Pb(II)	0.34	14	14
		Se(IV)	0.39		
	Medium	Pb(II)	2.24	200	19
		Se(IV)	2.10		

[a] pH adsorption edge experiments were conducted for each bi-solute system at two different surface loadings categorized as “Low” and “Medium”. In this column, "Low" and "Medium" denotes the bi-solute pH adsorption edge experiment being considered.
[b] Model fit determined for the experimental data *without* any ternary surface complexes (T.C.) considered
[c] Model fit determined for the experimental data *with* ternary surface complexes (T.C.) considered

Comparison of Pb(II) and Cd(II) single solute adsorption edges (Figure 4.2 and Figure 3.5) suggests that the former cation binds more strongly to goethite than the latter, based on the fact that Pb(II) adsorption is observed to begin around pH 2 whereas Cd(II) uptake starts closer to pH 4. The Cd(II) and Pb(II) bi-solute pH adsorption edges obtained in this study (Figure 4.4a and Figure 4.4b) lend further support to this idea that Pb(II) binds more strongly to goethite than Cd(II). In particular, at both low and medium surface coverages, nearly all Pb(II) is observed to be adsorbed onto goethite prior to Cd(II) adsorption beginning (Figure 4.4).

At the low surface loading bi-solute experiment, both Cd(II) and Pb(II) adsorption appear to mirror their behavior in single solute systems (Figure 4.4c). However, for the medium surface loading bi-solute adsorption edge experiment, Pb(II) uptake continues to reflect its adsorption behavior in the single solute system, whereas Cd(II) uptake is retarded in comparison to its single solute adsorption edge (Figure 4.4d). Since Cd(II) and Pb(II) surface complexes both utilize the same surface sites on the (101), (001), and (210) crystal faces (Table 4.4), this suppression of Cd(II) adsorption to goethite is believed to be a consequence of competition between the two adsorbates for a limited number of surface sites. Furthermore, if Pb(II) binds more strongly to goethite than Cd(II), it stands to reason that the site competition affects observed for Cd(II) would not be as pronounced for Pb(II) since it can outcompete Cd(II) for surface sites. Comparison of pH adsorption edges for single and bi-solute systems, conducted at a medium surface loading, supports this line of reasoning (Figure 4.4d).

For the Cd(II)/Pb(II) bi-solute system, the CD-MUSIC model was capable of accurately predicting ($0.1 < WSOS/DF < 20$) adsorption of both cations onto GOE63 and in so doing, appears to capture the competition for surface sites between the two adsorbates (Figure 4.4a and Figure 4.4b).

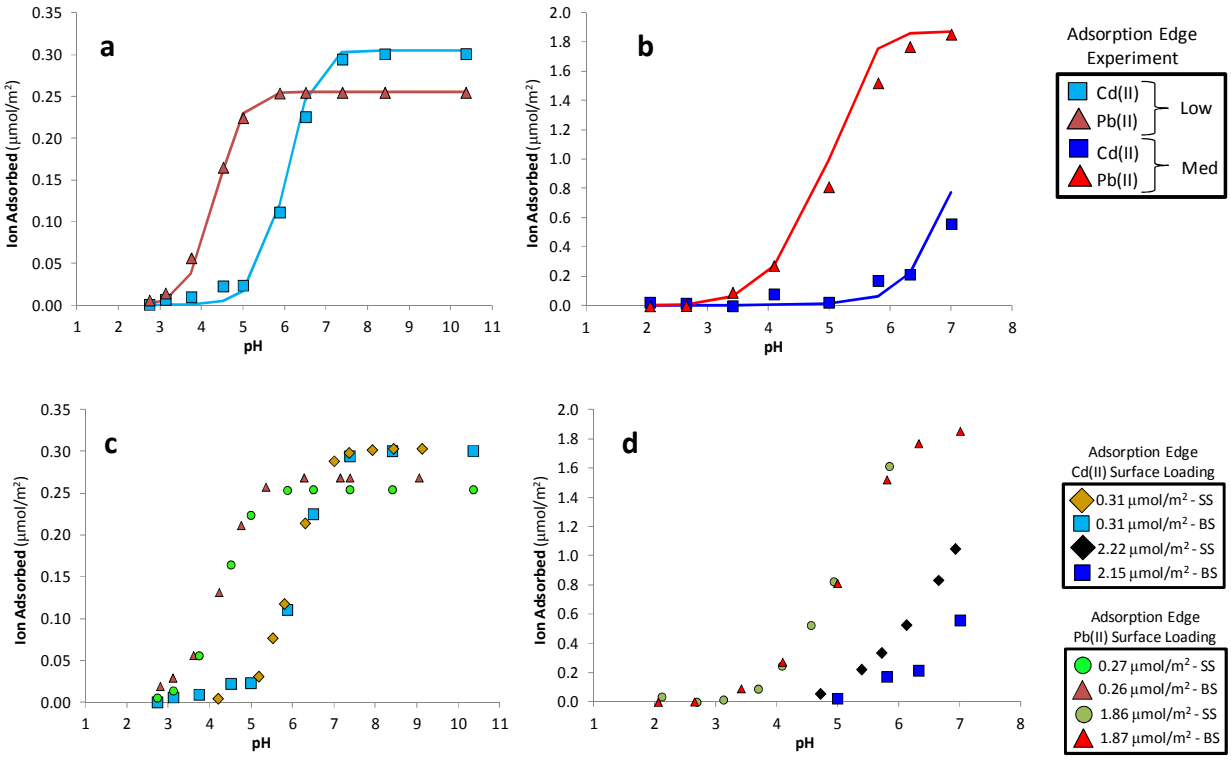

Figure 4.4 **(a) and (b)** Cd(II) and Pb(II) bi-solute pH adsorption edge data for the GOE63 goethite sample with surface loadings of **(a)** 0.31 and 0.26 µmol/m^2, respectively ("Low" surface loading); and **(b)** 2.15 and 1.87 µmol/m^2, respectively ("Medium" surface loading). **(c) and (d)** Comparison of Cd(II) and Pb(II) adsorption in single solute "SS" and bi-solute "BS" systems at **(c)** "Low" and **(d)** "Medium" surface loadings. In all plots, symbols denote experimental data and solid lines denote CD-MUSIC model predictions.

Cd(II)/Se(IV) and Pb(II)/Se(IV) bi-solute systems were initially modeled using only the surface species employed in the single solute portion of this study (Figure 4.5a and Figure 4.5b; Figure 4.6a and Figure 4.6b). In this instance, the CD-MUSIC model was unable to accurately predict the adsorption behavior of the Cd(II)/Se(IV) and Pb(II)/Se(IV) bi-solute systems for the medium surface loading experiments (Figure 4.5b; Figure 4.6b). Further inspection of the experimental data reveals that under the CFC considered, GOE63 does not possess a sufficient number of surface sites to accommodate

all ions removed from solution in the bi-solute pH adsorption edge experiments conducted at medium surface loadings.

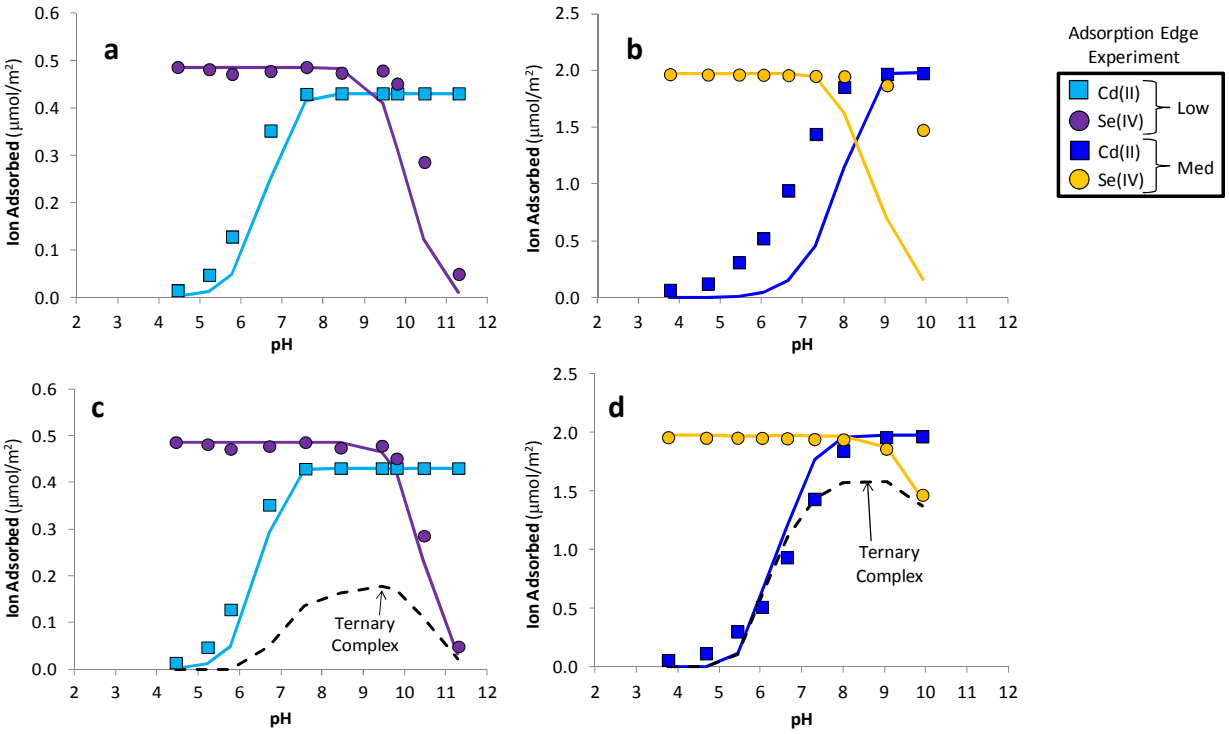

Figure 4.5 Cd(II) and Se(IV) bi-solute pH adsorption edge data for the GOE63 goethite sample with surface loadings of **(a) and (c)** 0.43 and 0.49 µmol/m^2, respectively ("Low" surface loading); and **(b) and (d)** 1.98 and 1.97 µmol/m^2, respectively ("Medium" surface loading). CD-MUSIC model simulations were conducted assuming ternary surface complexes were **(a) and (b)** absent; and **(c) and (d)** present. Symbols denote experimental data and solid lines denote CD-MUSIC model predictions. The black dashed line in plots **(c) and (d)** represents the amount of Cd(II) and Se(IV) adsorbed to the (101) and (001) crystal faces via the proposed $(\equiv FeOH)_2$-$CdOSeO_2$ ternary surface complex.

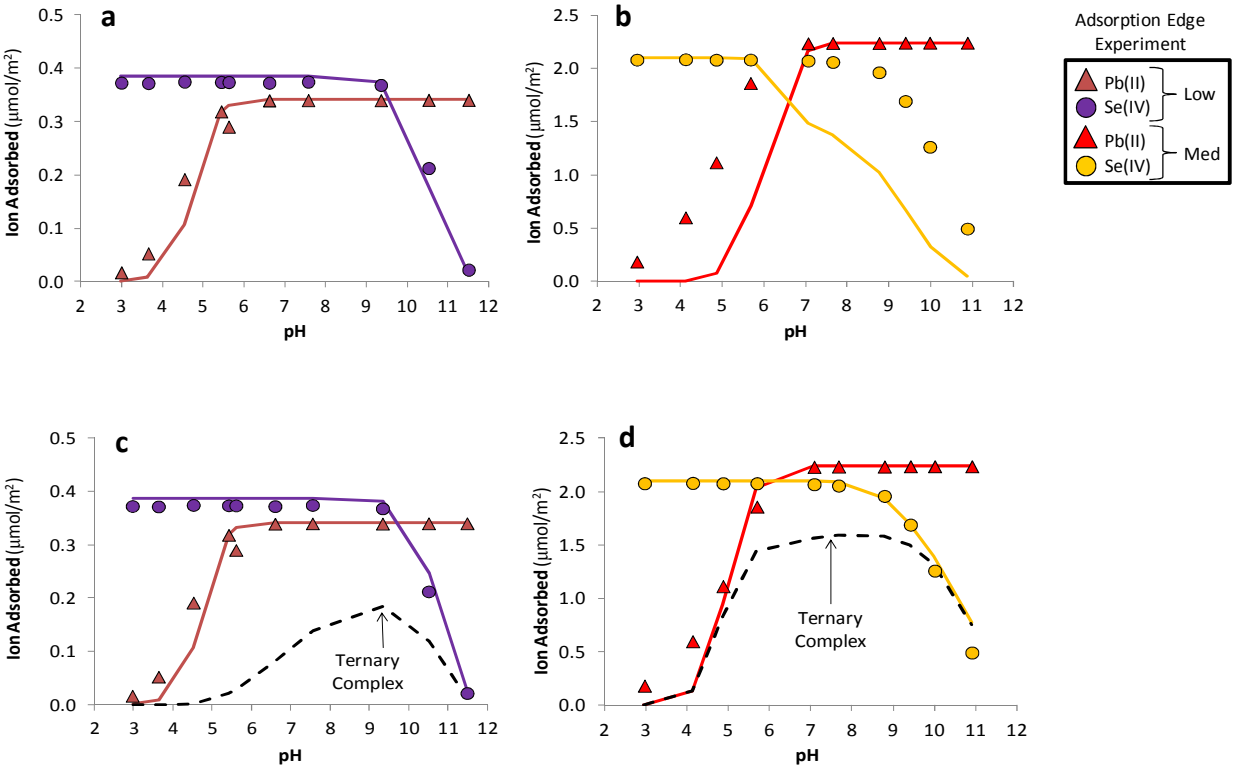

Figure 4.6 Pb(II) and Se(IV) bi-solute pH adsorption edge data for the GOE63 goethite sample with surface loadings of **(a) and (c)** 0.34 and 0.39 µmol/m^2, respectively ("Low" surface loading); and **(b) and (d)** 2.24 and 2.10 µmol/m^2, respectively ("Medium" surface loading). CD-MUSIC model simulations were conducted assuming ternary surface complexes were **(a) and (b)** absent; and **(c) and (d)** present. Symbols denote experimental data and solid lines denote CD-MUSIC model predictions. The black dashed line in plots **(c) and (d)** represents the amount of Pb(II) and Se(IV) adsorbed to the (210) crystal face via the proposed (≡FeOH)-$PbOSeO_2$-(≡Fe_2OH) ternary surface complex.

To account for this discrepancy between sites available and ions adsorbed, metal-selenite ternary complexes forming on the mineral surface were considered. To date, no spectroscopic studies have investigated the possible existence of $PbSeO_3$ and $CdSeO_3$ surface complexes on goethite. Therefore, justification for the formation of these metal-selenite complexes was based on spectroscopic evidence that supports the existence of $PbSO_4$ and $CdSO_4$ ternary complexes on goethite's surface [53, 104, 162, 163] and the

fact that aqueous phase stability constants for $CdSeO_3$ and $PbSeO_3$ are approximately two orders of magnitude greater than for the corresponding sulfate complexes [156, 158].

Given the dearth of information available regarding metal-selenite ternary complexes, the proposed complexes used in this study were modeled after their metal-sulfate counterparts, for which a number of studies have been published. Attenuated total reflectance Fourier transform infrared (ATR-FTIR) and EXAFS spectroscopies both suggest that $PbSO_4$ and $CdSO_4$ ternary complexes form with the metal ion bound directly to the mineral surface and the sulfate ligand bound to the metal on the solution side of the mineral water interface, creating what is called a "Type A" ternary surface complex [53, 162, 163]. $CdSeO_3$ and $PbSeO_3$ ternary surface complexes were modeled in CD-MUSIC in the same "Type A" fashion with selenite bound to the metal ion which in turn is bound to the goethite surface. The $CdSeO_3$ complex was modeled as forming on the (101) and (001) crystal faces as a double corner bidentate complex to two singly coordinated sites; identical to how Cd(II) binds to goethite in single solute systems (Table 4.4), and in agreement with the findings of Zhang and Peak [163] concerning the formation of the $CdSO_4$ ternary surface complex. In CD-MUSIC, the $PbSeO_3$ ternary complex was modeled as forming on the (210) crystal face as an edge sharing complex, binding to one singly and one doubly coordinated surface site; mirroring the Pb(II) edge sharing surface species that forms on the (210) face in the absence of selenite (Table 4.4). CD values for the CdSeO3 and PbSeO3 ternary surface complexes were calculated assuming that the Cd – surface oxygen and Pb – surface oxygen distances observed for Cd(II) and Pb(II) adsorbed onto goethite in single solute systems (Table 4.3) were valid for the ternary

surface complexes as well. The charge from the SeO_3^{2-} ligand was placed on the electrostatic 1 plane (n_{H1} = -2 in Equation 4.4).

Inclusion of the CdSeO3 and PbSeO3 ternary surface complexes into the CD-MUSIC model simulations of the Cd(II)/Se(IV) and Pb(II)/Se(IV) bi-solute systems, respectively, greatly improved the model's fit of both cation and anion adsorption data, especially at medium surface loadings (Table 4.8; Figure 4.5; Figure 4.6). In order to achieve acceptable model fits (0.1 < WSOS/DF < 20) for both the Cd(II)/Se(IV) and Pb(II)/Se(IV) bi-solute systems, the ternary surface complex considered in each case had to account for a substantial portion of the ions adsorbed to goethite.

4.4. Conclusions

The CFC of GOE63 was previously determined in Chapter 3 utilizing a newly developed methodology that unifies the different N_S values predicted from crystallography, microscopic imaging, tritium exchange, surface saturation data, and surface charging data. This CFC was used to develop a CD-MUSIC model capable of describing GOE63's surface heterogeneity and reactivity with ions in solution. In Chapter 3, the CD-MUSIC model was calibrated for acid-base surface reactions and Cd(II) surface complexation reactions. In this chapter, the CD-MUSIC modeling effort and evaluation of the CFC methodology discussed in Chapter 3 was expanded to include two additional probe ions, Pb(II) and Se(IV), in single solute and bi-solute systems . All surface complexes employed in CD-MUSIC for modeling single solute systems were completely consistent with the CD-MUSIC parameters developed in Chapter 3,

spectroscopic data and molecular modeling simulations. The CD values for each surface complex were calculated using cation – surface oxygen bond lengths observed in EXAFS studies and the bond valence equation developed by Brown and Altermatt [38].

Utilizing a newly proposed Pb(II) tridentate surface complex, CD-MUSIC's simulated surface speciation of Pb(II) on GOE63 is in agreement with spectroscopic findings [42, 44] over the entire pH range studied. To our knowledge, this is the first model that is capable of describing Pb(II) ion adsorption to goethite over the pH range from 3 to 11.

In Cd(II)/Pb(II) bi-solute systems, competition between the adsorbates for surface sites affects the adsorption behavior of Cd(II) relative to what is observed in single solute systems. The CD-MUSIC model developed in this study is able to predict the effects of this site competition and correctly describe the adsorption behavior of both cations in the Cd(II)/Pb(II) bi-solute system. Similar attempts to model cation/cation competition with simpler models has often lead to over prediction of the extent of competition [67].

In both the Cd(II)/Se(IV) and Pb(II)/Se(IV) bi-solute adsorption experiments, total ion adsorption exceeded the site capacity of the goethite. In contrast to the Cd(II)/Pb(II) bi-solute system where evidence for competition was observed in Cd(II)'s adsorption edge shift (Figure 4.4d), comparison of single and bi-solute experimental adsorption data for the cation/oxyanion systems revealed that no reduction in sorption occurred for any of the adsorbates (i.e., Cd(II), Pb(II), and Se(IV)) considered. These differences between the cation-cation and cation-oxyanion bi-solute systems can be attributed to the reduction in charge associated with adsorption of counter-ion solutes

and/or the formation of ternary complexes. Based on comparison with similar bi-solute systems (i.e., Cd(II)/S(IV) and Pb(II)/S(IV)), the formation of ternary complexes is expected. Incorporation of ternary surface complexes did lead to excellent simulations of the bi-solute data for both systems. Further confirmation of these species through molecular modeling and/or spectroscopy should be conducted to confirm the presence of these complexes within the range of conditions implicated by the modeling results.

In summary, the combination of CD-MUSIC modeling with an appropriate interpretation of site density experimental results (i.e., a unifying theory) and selection of surface complexes that are consistent with spectroscopic data across a range of pH and surface coverages represents a significant improvement in single-solute and bi-solute adsorption modeling of metal ions and oxyanions.

Chapter 5 : CD-MUSIC MODELING OF MERCURY ADSORPTION TO GOETHITE

5.1. Introduction

Mercury pollution has resulted from a number of industrial operations such as coal burning power plants and chlor alkali plants [164]. Given its negative health effects on humans and other animals, mercury's migration through the environment is of great concern to scientists and engineers. In the subsurface, ion adsorption at the mineral – water interface can play an important role in controlling the fate and transport of contaminants such as mercury [165]. Of the inorganic adsorbents most frequently encountered in aqueous environments, metal (hydr)oxide minerals such as goethite have demonstrated the strongest affinity for metal ions present in the solution phase [166].

Hg(II) uptake onto both natural and synthetic adsorbents has been studied by a number of researchers [69, 83, 167-173]. From these studies, it has been observed that in the absence of chloride, Hg(II) adsorption peaks around pH 4, coincident with $Hg(OH)_2$ becoming the dominant aqueous Hg(II) species [171, 174]. In the presence of chloride however, Hg(II) adsorption has been found to be inhibited at lower pH values, resulting in a shift in its adsorption edge to more alkaline pHs [69, 174]. Previous research efforts have attempted to model Hg(II) adsorption onto different adsorbent surfaces as a function of pH and in the presence and absence of chloride, using surface complexation models (SCMs) [69, 83, 173]. In these modeling studies, Hg(II) adsorption was either inaccurately predicted or required the use of hypothetical surface species that are not consistent with spectroscopic observations. Furthermore, the presence of carbonate in the

experimental solid – solution systems studied was not accounted for in these models despite evidence suggesting carbonate contamination [69, 83]. Hence, there is a need for a surface complexation model to be developed that can describe Hg(II) adsorption behavior over the entire range of experimental conditions tested utilizing surface species that are in agreement with molecular scale analysis (i.e., spectroscopy and molecular modeling simulations).

In this study, Hg(II) adsorption onto the iron hydroxide mineral goethite was described using the Charge Distribution Multi-Site Complexation (CD-MUSIC) Model. Hg(II) uptake onto two different goethite samples was simulated in the presence and absence of chloride as well as carbonate utilizing surface complexes consistent with spectroscopic observations, molecular modeling studies, and bond valence analysis.

5.2. Materials and Methods

5.2.1. Experimental data employed

Previously published adsorption data taken from Villalobos and Leckie [74, 75], Barrow and Cox [69], and Bonnissel-Gissinger et al. [83] was used in this modeling study. Carbonate adsorption data taken from Villalobos and Leckie [74, 75] was used to calibrate the CD-MUSIC model to account for carbonate's undocumented presence in the experimental systems of both Barrow and Cox [69] and Bonnissel-Gissinger et al. [83]. The specific surface area (SSA) for the goethite sample used by Villalobos and Leckie [74, 75] was measured by BET analysis to be 70 ± 2 m^2/g.

Experimental data from Barrow and Cox [69] was used to evaluate Hg(II) adsorption onto goethite as a function of mercury surface loading, chloride concentration, and pH. The authors performed batch equilibrium adsorption studies utilizing sodium hydroxide and nitric acid to adjust the system's pH. The mercury and chloride sources were mercury(II) nitrate and sodium chloride, respectively. Sodium nitrate ($NaNO_3$) was used in all adsorption experiments to keep the ionic strength of the solid – solution systems constant at 0.1 M. The solid concentration for each adsorption experiment was not reported but could be approximated via a mass balance approach utilizing the total, aqueous, and sorbed concentrations of Hg(II) reported. The solids concentration of goethite used was found to range between 4.02 and 4.51 g/L. Ethylene glycol monoethyl ether was used to determine the goethite sample's SSA to be 76 m^2/g.

Hg(II) adsorption onto goethite was also investigated by Bonnissel-Gissinger et al. [83] using batch equilibrium adsorption experiments for a goethite sample with a SSA of 15 m^2/g (determined via BET analysis). For all adsorption experiments conducted, goethite's concentration in solution was set at 10 g/L. Sodium hydroxide and nitric acid were used to vary the system's pH. Both sodium chloride and sodium nitrate were employed as background electrolytes in the adsorption experiments. A mercury nitrate ($Hg(NO_3)_2$) stock solution was used as the mercury source. A summary of the three solid – solution systems studied in this work is presented in Table 5.1.

Table 5.1 Physical parameters of the three goethite samples used in model simulations

Parameter	Goethite Sample		
	VIL70 [a]	BAR76 [b]	BON15 [c]
Specific surface area (m^2/g)	70	76	15
Solid's Concentration (g/L)	13.8[d] and 9.4[e]	4.02 – 4.51	10
pH_{pzc}	8.9	7.7	7.85
Proton reactive site density (sites/nm^2)	6.97	6.81	8.51

[a] Villalobos and Leckie [74, 75]
[b] Barrow and Cox [69]
[c] Bonnissel-Gissinger et al. [83]
[d] Solids concentration employed for potentiometric titrations
[e] Solids concentration employed for carbonate adsorption experiments
For the three goethite systems studied, all adsorption experiments were conducted at 25°C. Proton reactive site density is calculated using Equation 5.3 and discussed in detail below.

Potentiometric titration data obtained at varying ionic strengths yields a surface charge profile similar to the one shown in Figure 5.2. The point at which these different data sets intersect is an estimate of the point of zero charge (pH_{pzc}) and is labeled as the point of zero salt effect [175]. While some research has suggested that the pH_{pzc} value varies for a given mineral depending on the background electrolytes employed and the method by which the mineral was synthesized in the laboratory [176], multiple experimental studies have revealed goethite's pH_{pzc} value remains fairly constant (around pH 9), regardless of the background electrolytes employed [74, 111, 177-179]. In the case of goethite, pH_{pzc} values below 9 are regularly accredited to carbonate's presence in the solid – solution system [73, 74, 99, 111, 179-181]. Hence, the low pH_{pzc} estimates reported by Barrow and Cox [69] and Bonnissel-Gissinger et al. [83] ($pH_{pzc} \approx 7.7$ and

7.85, respectively) are thought to be the result of carbonate contamination in their experimental systems.

5.2.2. Modeling approach (CD-MUSIC Model)

In solid – solution systems, ion adsorption behavior is greatly influenced by the crystal morphology of the mineral surface [24, 25, 82, 84, 85]. The crystal faces that make up the mineral surface possess reactive surface oxygens, herein referred to as surface sites, which can vary in type and density (sites/nm^2) from one crystal face to another. There are four principal crystal faces found on goethite: the (101), (001), (210), and (010), using the Pnma space group [23, 26, 85, 97, 99, 114, 127, 129]. The surface site types present on these four crystal faces are presented in Table 5.2 along with their reactive site densities (N_S). Each surface site type is thought to possess its own unique reactivity to adsorbing ions, including protons [26, 27, 29, 97]. Doubly coordinated sites located on the (101) and (001) crystal faces of goethite are considered to be non-reactive [26, 27, 85, 97, 99], and only one third of the triply coordinated sites present on the (101) and (001) crystal faces are regarded as reactive [23, 27, 28, 30, 31, 85].

Table 5.2 Reactive site densities of singly, doubly, and triply coordinated sites on the predominant crystal faces of goethite

	Crystal Face N_s (sites/nm^2)			
Site Type	(101) [a]	(001) [b]	(210) [a]	(010) [c]
≡FeOH	3.03	3.34	7.5	9.1
≡Fe_2OH	0	0	7.5	9.1
≡Fe_3O	3.03	3.34	0	0
N_H	6.06	6.68	7.5	9.1

Site densities are taken from:
[a] Venema et al. [29]
[b] Gaboriaud and Ehrhardt [99]
[c] Lutzenkirchen et al. [129]
Doubly coordinated sites located on the (101) and (001) crystal faces of goethite are considered to be non-reactive [26, 27, 85, 97, 99]. Only one third of the triply coordinated sites present on the (101) and (001) crystal faces are considered reactive (3.03 and 3.34 Fe_3O_I sites/nm^2, respectively) [23, 27, 28, 30, 31, 85]. Proton reactive site density (N_H) is the sum of reactive singly and triply coordinated surface sites [26, 27, 29, 82, 85, 97, 131].

The CD-MUSIC model developed by Hiemstra et al. [24-26] and Hiemstra and Van Riemsdijk [23] describes surface acidity using a 1-p*K* assumption for singly (≡FeOH) and triply (≡Fe_3O) coordinated surface sites on goethite (Equations 5.1 and 5.2).

$$\equiv FeOH^{-0.5} + H^+ \leftrightarrow \equiv FeOH_2^{+0.5} \quad (5.1)$$

$$\equiv Fe_3O^{-0.5} + H^+ \leftrightarrow \equiv Fe_3OH^{+0.5} \quad (5.2)$$

Doubly coordinated surface sites present on goethite are considered to be non-reactive to protons within the normal pH range tested [26, 27, 29, 85, 97]. This assumption is based on the findings of Hiemstra et al. [26] who predicted the log K_H values (i.e., protonation constants) for goethite's different surface sites via a linear relationship the authors discovered between a specie's log K_H value and its oxygen atom's formal charge. Using the bond valence approach presented in Brown and Altermatt [150], Hiemstra et al. [23] was able to calculate the formal charge of the $\equiv Fe_2OH$ surface oxygen and subsequently predict the surface site's log K_H value to be 0.4, too low for $\equiv Fe_2OH$ to react with protons in the normal pH range considered. Detailed descriptions of the CD-MUSIC model, in particular its depiction of the mineral – water interface, as well as further explanation of site reactivity and the charge distribution factor, can be found elsewhere (e.g., [23, 26, 29, 93, 182]).

Hg(II) adsorption onto goethite was simulated using the CD-MUSIC model and the computer software FITEQL 4.0 [21] and FITEQLC [22]. The modeling approach employed in this modeling study consisted of five different steps: (1) fitting of the potentiometric titration data collected for VIL70 to determine the intrinsic surface protonation and ion pair formation equilibrium constants; (2) fitting of carbonate adsorption data collected on VIL70 utilizing surface species proposed by Hiemstra et al. [32] and Rahnemaie et al. [35]; (3) simulation of the potentiometric titration data obtained from Barrow and Cox [69] assuming a fixed total carbonate concentration ($[CO_3^{2-}]_{TOT}$) and using the affinity constants and parameters previously determined in steps 1 and 2; (4) fitting of Hg(II) adsorption data collected on BAR76 using the data

published by Barrow and Cox [69] while accounting for carbonate's presence in the experimental system and utilizing the same surface species and equilibrium constants previously determined in steps 1 - 3; and (5) prediction of Hg(II) adsorption data collected on the BON15 goethite sample using the data published by Bonnissel-Gissinger et al. [83] for model verification. The model's performance in predicting adsorption edge data was assessed by determining the weighted sum of squares divided by degrees of freedom (WSOS/DF) for each data set, where values between 0.1 and 20 reflect acceptable model fits of the experimental data [21]. The relative and absolute error estimates utilized in CD-MUSIC were taken from previous modeling studies for ion adsorption onto iron hydroxide minerals [2] (see Chapter 3).

5.2.3. Estimation of model parameters

5.2.3.1 Capacitance values

Model fitting of the titration data taken from VIL70 was used to determine the log K_{in} values for goethite's surface protonation reactions (Equations 5.1 and 5.2) and ion pair formation reactions (cf. Table 5.3). The capacitance values (C_1 and C_2) for each system (VIL70, BAR76, and BON15) were determined through fitting each goethite sample's titration data with the CD-MUSIC model. In this study $C_1 \equiv C_2$ based upon the work of Hiemstra and Van Riemsdijk [93], who after re-evaluating the work of Rahnemaie et al. [86] in which the position of specific electrolyte ions at the interface was investigated, suggested that the value of C_2 is very similar to C_1. Sverjensky [101] arrived at a similar conclusion in deciding that the outer layer capacitance used in the

triple layer model (TLM) should be changed from 0.2 F/m^2, as previously defined for the TLM, and set equal to C_1. Additionally, recent modeling studies with CD-MUSIC have followed this same suggestion of setting C_2 equal to C_1 [34, 35, 38, 98].

Table 5.3 Summary of reactions used in CD-MUSIC for the segregate and composite approaches to characterizing goethite's surface

Adsorbate	Approach [a]	Crystal Face [b]	Surface Complexation Reaction	Δz_0	Δz_1	Log K_{in}	
						Segregate	Composite
H^+	Segregate; Composite	(101), (010)	$\equiv FeOH + H^+ \leftrightarrow \equiv FeOH_2$	1	0	8.6	8.6
			$\equiv FeOH + H^+ + NO_3^- \leftrightarrow \equiv FeOH_2\_NO_3$	1	-1	7.7	7.7
			$\equiv FeOH + H^+ + Cl^- \leftrightarrow \equiv FeOH_2\_Cl$	1	-1	7.7	7.7
			$\equiv FeOH + Na^+ \leftrightarrow \equiv FeOH\_Na$	0	1	-0.45	-0.45
	Segregate; Composite	(101)	$\equiv Fe_3O + H^+ \leftrightarrow \equiv Fe_3OH$	1	0	10.6	10.6
			$\equiv Fe_3O + H^+ + NO_3^- \leftrightarrow \equiv Fe_3OH\_NO_3$	1	-1	10.0	10.0
			$\equiv Fe_3O + H^+ + Cl^- \leftrightarrow \equiv Fe_3OH\_Cl$	1	-1	10.0	10.0
			$\equiv Fe_3O + Na^+ \leftrightarrow \equiv Fe_3O\_Na$	0	1	-0.45	-0.45
CO_3^{2-}	Composite	–	$2(\equiv FeOH) + CO_3^{2-} + 2H^+ \leftrightarrow (\equiv FeO)_2\text{-}CO + 2H_2O$	0.62	-0.62	–	19.20
	Segregate	(010)	$(\equiv FeOH^{-1/2}) + (\equiv Fe_2OH^{-1/2}) + 2H^+ + CO_3^{2-} \leftrightarrow (\equiv FeO)\text{-}CO\text{-}(\equiv Fe_2O) + 2H_2O$	0.62	-0.62	21.27	–
Hg^{2+}	Composite	–	$2(\equiv FeOH) + Hg^{2+} \leftrightarrow (\equiv FeO)_2H\text{-}Hg + H^+$	0.8	0.2	–	3.57
			$2(\equiv FeOH) + Hg^{2+} \leftrightarrow (\equiv FeO)_2Hg + 2H^+$	-0.03	0.03	–	-5.03
	Segregate	(010)	$(\equiv FeOH^{-1/2}) + (\equiv Fe_2OH^{-1/2}) + Hg^{2+} \leftrightarrow (\equiv FeO)\text{-}Hg\text{-}(\equiv Fe_2O) + 2H^+$	-0.12	0.12	-2.44	–
Hg^{2+} and Cl^-	Segregate; Composite	(010)	$\equiv FeOH + Hg^{2+} + Cl^- \leftrightarrow \equiv FeO\text{-}HgCl + H^+$	-0.02	0.02	7.34	7.17

[a] Column labeled "Approach" specifies which surface characterization approach (i.e., segregate or composite) the reactions listed in the corresponding row are applicable for.

[b] Column labeled "Crystal Face" denotes which crystal face or faces are involved in a particular reaction when using the segregate approach to characterize the mineral's surface. In the segregate approach, the surface is pictured as being composed of different crystal faces that each possess a particular number of singly, doubly, and triply coordinated sites. The composite approach assumes all sites of a given type are identical and the mineral surface is pictured as being composed of only singly, doubly, and triply coordinated sites with no further differentiation; hence the "Crystal Face" column is not applicable for the CD-MUSIC model utilizing this approach.

Charge for surface species is based on the Pauling bond valence approach used by Hiemstra et al. [26]. Using this approach, the charge on $\equiv FeOH$ and $\equiv Fe_3O$ is -0.5, while the charge for $\equiv FeOH_2$ and $\equiv Fe_3OH$ is +0.5. Δz_0 and Δz_1 are the charge distribution coefficients that represent the change in charge on the 0 and 1 electrostatic planes that occurs as a result of the surface reaction. Capacitance values were determined through model fitting of potentiometric titration data for VIL70 and BAR76 and of Hg(II) adsorption data for BON15 since no potentiometric titration data was available. For both segregate and composite approaches $C_1 = C_2 = 1.1$ F/m^2 for VIL70 and $C_1 = C_2 = 1.0$ F/m^2 for BON15. For BAR76, $C_1 = C_2 = 1.65$ and 1.70 F/m^2 using the segregate and composite approaches, respectively.

In a study conducted by Evans et al. [183], the authors found that goethite suspensions purged with N_2 gas between 1 and 2 months time achieved a measured pH_{PZC} of 9.2; whereas goethite samples purged with nitrogen for only 1 - 2 days possessed a

lower pH_{PZC} value due to carbonate's continued presence in the system. A similar investigation by Zeltner and Anderson [179] found that increased purging of goethite suspensions by N_2 gas for periods of up to 2 months could increase the measured pH_{PZC} value of the sample from 8.1 to 9.0. With these findings in mind, Lumsdon and Evans [111] conducted a literature review of pH_{PZC} values previously reported for goethite in "carbonate free" systems. The pH_{PZC} values were found to range from 7.5 to 9.38; demonstrating the variability in purging time employed by researchers on their goethite suspensions prior to conducting adsorption experiments. These studies by Evans et al. [183], Zeltner and Anderson [179], and Lumsdon and Evans [111], illustrate the difficulty in removing all traces of carbonate from a solid – solution system, suggest that carbonate's presence in "carbonate free" systems is a fairly common occurrence, and highlight the need for an approach to quantify the amount of residual carbonate present in a system. Therefore, given carbonate's ubiquity and persistence in solid – solution systems, we contend that experimental data possessing carbonate contamination is commonly used in modeling studies, oftentimes without carbonate's presence being taken into account. In this work, adsorption data taken from Barrow and Cox [69] and Bonnissel-Gissinger et al. [83] will be used to develop a CD-MUSIC model capable of predicting mercury uptake onto goethite. The presence of carbonate in both experimental systems will be considered in the model and quantified (i.e., $[CO_3^{2-}]_{TOT}$) using an approach developed herein by the authors.

As stated previously, ion adsorption behavior in solid – solution systems is greatly influenced by the mineral surface's crystal morphology [24, 25, 82, 84, 85]. One of the

primary reasons for selecting CD-MUSIC to use in this study is that the model takes into account the mineral surface's heterogeneity. Therefore, in order to properly apply this adsorption model, the crystal face composition (CFC) of the mineral sample in question must first be determined. Unfortunately, neither of the mercury adsorption studies (Barrow and Cox [69] and Bonnissel-Gissinger et al.[83]) employed in this work supplied a CFC for their particular goethite sample, BAR76 and BON15, respectively. Furthermore, determination of BAR76's and BON15's CFC through traditional means such as microscopic image analysis [23, 29, 99, 114, 127] or consideration of surface saturation data [85] was unattainable given the information provided by the authors. Although surface charging data for BAR76 and BON15 was presented in their respective studies, estimation of each sample's CFC using the titration congruency method of Salazar-Camacho and Villalobos [84] could not be accomplished due to carbonate's presence in the experimental systems of Barrow and Cox [69] and Bonnissel-Gissinger et al. [83]. Since it was not possible to determine BAR76's and BON15's CFC using any of the methods previously established (i.e. microscopic image analysis, surface saturation data, or titration congruency), a new approach for estimating a sample's CFC was needed.

5.2.3.2 New approach to estimating CFC

Through examining goethite adsorption data found in the literature [23, 24, 82, 99, 118, 127-130], Villalobos and co-workers [82, 85, 130] observed that, when normalized by surface area, goethite's surface reactivity toward ions varies between

samples. In particular, goethite samples with a SSA below ≈ 60 m^2/g were found to have an appreciably higher reactivity [85, 130]. To explain these findings, Villalobos and co-workers [82, 85] hypothesized that as the mineral sample's SSA decreases, the contribution from the (210) and (010) capping faces towards the sample's CFC increases since these two crystal faces possess higher reactive site densities than the (101) and (001) faces (Table 5.2). This idea is supported by the findings of Weidler et al. [114] who in studying goethite's surface morphology via atomic force microscopy (AFM), observed (210) step faces present on the (001) crystal face at such a high frequency that the (001) face was practically transformed into a (210) vicinal face. In other words, the (001) crystal face was blanketed by these (210) step faces to such a degree that the (001) face all but disappeared from goethite's surface and was replaced by the (210) crystal face [85, 114]. The goethite crystals examined by Weidler et al. [114] had a measured SSA of 7.9 m^2/g. In contrast to these findings by Weidler et al. [114], goethite preparations with SSAs ranging from 94 to 105 m^2/g presented in the literature are found to have surfaces comprised primarily of the (101) and (001) crystal faces (Table 5.4). From this evidence, Villalobos et al. [85] contended that as goethite crystals get larger and SSA decreases, the occurrence of these (210) step faces forming on the (001) crystal face increases, thereby elevating (210)'s contribution to the mineral surface. Furthermore, Villalobos et al. [85] postulated that the step faces observed by Weidler et al. [114] to be forming on the (001) face could be either the (210) or (010) crystal face. In fact, Villalobos et al. [85] used the (010) face in lieu of the (210) in characterizing goethite samples with SSAs of 70 and 50 m^2/g.

Table 5.4 CFCs for goethite samples with SSAs between 94 and 105 m^2/g

SSA	CFC (%)		
(m^2/g)	(101)	(001)	(210)
105 [a]	90	–	10
96.4 [b]	90	–	10
95 [c]	90	–	10
95 [d]	70	30	–
94 [e]	70	30	–

[a – d] CFCs determined using microscopic image analysis
[a] Hiemstra and Van Riemsdijk [23]
[b] Rietra et al. [30]
[c] Venema et al. [27]
[d] Gaboriaud and Ehrhardt [99]
[e] CFC determined using chromate surface saturation data. Villalobos et al. [85]

In their 2010 work, Salazar-Camacho and Villalobos [84] modeled arsenate adsorption onto goethite using previously published experimental data from several different studies. The authors estimated the CFC for a number of goethite samples, with SSAs ranging from 2 – 98 m^2/g, via the titration congruency method, described in detail elsewhere (Salazar-Camacho and Villalobos [84]). None of the previously published adsorption studies that Salazar-Camacho and Villalobos [84] used in their work provided surface saturation data. Furthermore, in nearly all of these studies, the sample goethite's surface charging data was not presented. To circumvent this problem, Salazar-Camacho and Villalobos [84] utilized titration data from goethite samples possessing similar characteristics (i.e. SSA) and in similar environments (i.e. background electrolytes and ionic strength) as a surrogate for those samples that were missing surface charge data; thereby allowing for the CFC of each goethite sample to be ascertained via the titration

congruency method. In a few cases, no reference goethite system with available titration data could be found to act as a reasonable substitute for the samples being studied. For these samples, their CFC was determined through modeling arsenate adsorption in a trial and error fashion.

Using the CFCs determined by Salazar-Camacho and Villalobos [84], the proton reactive site density (N_H), defined as the sum of reactive singly and triply coordinated surface sites per nm^2 [26, 27, 29, 82, 85, 97, 131], was calculated for each goethite sample and then plotted versus SSA revealing a fairly linear relationship (Equation 5.3, $R^2 = 0.8633$) between the two variables and demonstrating that as SSA decreases, N_H increases (Figure 5.1). As seen in the data of Salazar-Camacho and Villalobos [84] and presented in Figure 5.1 of this study, samples with a SSA $\leq$ 71 m^2/g were found to possess a $N_H \geq 6.9$ sites/nm^2. Of the crystal faces considered to be prevalent on goethite's surface [23, 26, 85, 97, 99, 114, 127, 129], only the (210) and (010) crystal faces possess a N_H greater than 6.9 sites/nm^2 (Table 5.2). Given this information in conjunction with Figure 5.1 and Equation 5.3, it is evident that the contribution from the (210) and/or (010) crystal faces to the mineral's CFC must increase as SSA decreases; a conclusion which further substantiates Villalobos' and co-workers' [82, 85] hypothesis regarding increased reactivity for larger goethite crystals (lower SSA).

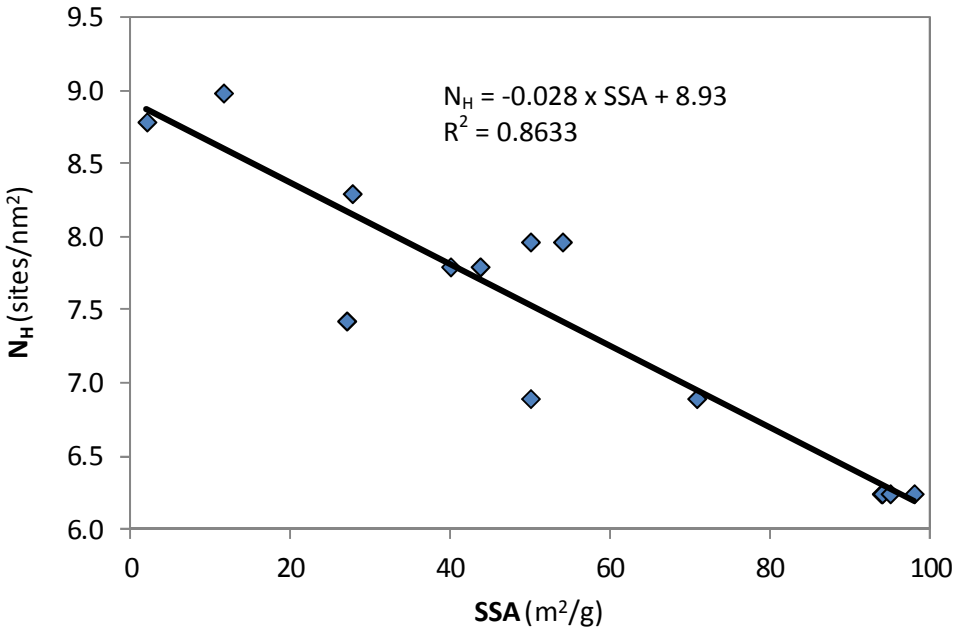

Figure 5.1 Relationship between SSA (m^2/g) and proton-reactive site N_s (sites/nm^2) for the different goethite systems. Symbols denote data taken from Salazar-Camacho and Villalobos [84]. Solid line denotes a linear trend line of the data points.

$$N_H = -0.028*(SSA) + 8.93 \quad (5.3)$$

The proton reactive site density for each goethite sample considered in this current modeling study was calculated using Equation 5.3 along with the samples' reported SSA (Table 5.1). Once a sample's N_H is determined, the CFC of the mineral can be calculated using the N_H values of each crystal face, presented in Table 5.2, and assuming that the mineral surface is comprised of only two crystal faces. In this work the two crystal faces considered to be present on goethite's surface were the (101) main face and the (010) capping face. The (101) crystal face was selected because of the amount of evidence supporting it as the dominant crystal face on goethite's surface [113, 114, 129,

144, 145]. The (010) capping face was selected over the (210) because only it possessed a high enough proton reactive site density to accommodate the N_H calculated for BON15 (N_H = 8.51 sites/nm^2) using Equation 5.3.

The ability of Equation 5.3 to predict a goethite sample's N_H and in turn, that sample's CFC, was checked against previously published studies where the sample's CFC had been determined via microscopic image analysis or surface saturation data. Through examination of electron micrographs, Venema et al. (1998) [29] estimated the CFC of a goethite sample, SSA 95 m^2/g, to be composed of approximately 90% (101) main face and 10% (210) capping face. Applying Equation 5.3 to this goethite sample results in a N_H value of 6.28 sites/nm^2. Using this N_H and assuming that only the (101) and (210) crystal faces are present on the mineral surface, a CFC of 85% (101) and 15% (210) results. In this case the (210) crystal face is considered rather than the (010) to stay consistent with Venema et al.'s [29] work. A 2009 study conducted by Villalobos et al. [85] estimated the CFC of a goethite sample with a SSA of 50 m^2/g using chromate surface saturation data. The resulting CFC determined by Villalobos et al. for this goethite sample yielded a N_H value of 6.73 sites/nm^2. In the same study, the CFC of a second goethite sample, also with SSA 50 m^2/g, was established using chromate surface saturation data as well. For this case however, a different CFC was arrived at and the resulting N_H was found to be 7.98 sites/nm^2. When Equation 5.3 is applied to goethite samples with a SSA of 50 m^2/g, a N_H of 7.53 sites/nm^2 is calculated. The above examples are given to illustrate Equation 5.3's usefulness in estimating the CFC of a goethite sample when information regarding the mineral surface is lacking; thereby

reducing the number of adjustable parameters needed for the CD-MUSIC model to fit experimental data. Using Equation 5.3 along with each sample's SSA, and considering only the (101) and (010) crystal faces to be present on mineral's surface, the CFCs for VIL70, BAR76, and BON15 were determined (Table 5.5).

Table 5.5 Properties of the three goethite samples considered in this study

Goethite Sample	SSA (m^2/g)	N_H (sites/nm^2)	CFC (%)	
			(101)	(010)
VIL70	70	7.0	70	30
BAR76	76	6.8	75	25
BON15	15	8.5	19	81

It has been reasoned that the amorphous iron oxide ferrihydrite can be described using the crystal faces of goethite as a proxy. Given ferrihydrite's morphology, the (210) and (010) crystal faces are considered to be the dominant faces present on the mineral's surface in these proxy models [97]. Given this information, the predicted CFC for the BON15 goethite sample can be considered similar to that of ferrihydrite. Good agreement between the predicted tritium exchange value (N_{TRIT}) for BON15 of 24.9 surface protons/nm^2 (calculated using the N_{TRIT} values presented in Table 3.3) and the experimentally observed value for ferrihydrite of 25.6 surface protons/nm^2 [136], shows that the CFC obtained using Equation 3 aligns with the unifying theory presented in Chapter 3.

5.2.3.2 Model description of the mineral surface's heterogeneity

Once the CFC for a goethite sample is known, the mineral surface's heterogeneity can be quantitatively expressed in CD-MUSIC using one of two methods, the segregate approach or the composite approach (Table 5.6). In the segregate approach, each surface site type on the (101) and (010) crystal faces is input into CD-MUSIC as its own entity. There are a total of four site types considered using the segregate approach: 1) singly coordinated sites on the (101) face; 2) singly coordinated sites on the (010) face; 3) doubly coordinated sites on the (010) face; and 4) triply coordinated sites on the (101) face (Table 5.6). In the composite approach, all sites of a given type are considered to be identical to each other, regardless of which crystal face they are located on. Using the composite approach, there are three site types to take into account when modeling: 1) singly coordinated sites from the (101) and (010) crystal faces, 2) doubly coordinated sites from the (010) face, and 3) triply coordinated sites present on the (101) face (Table 5.6). Surface site types and densities determined using the segregate and composite approaches were employed separately in CD-MUSIC to ascertain the impact that each surface characterization method had on the model's predictive capabilities. Therefore, two unique adsorption models were developed in this study: (1) the segregate CD-MUSIC model; and (2) the composite CD-MUSIC model.

Table 5.6 N_S employed in CD-MUSIC using the segregate and composite approaches to describing the mineral's surface

Goethite Sample	Site Type	Crystal Face	N_S (sites/nm^2)	
			Segregate [a]	Composite [b]
VIL70	≡FeOH	(101)	2.12	4.85
		(010)	2.74	
	≡Fe_2OH	(101)	0.00	2.74
		(010)	2.74	
	≡Fe_3O	(101)	2.12	2.12
		(010)	0.00	
BAR76	≡FeOH	(101)	2.29	4.52
		(010)	2.23	
	≡Fe_2OH	(101)	0.00	2.23
		(010)	2.23	
	≡Fe_3O	(101)	2.29	2.29
		(010)	0.00	
BON15	≡FeOH	(101)	0.59	7.92
		(010)	7.33	
	≡Fe_2OH	(101)	0.00	7.33
		(010)	7.33	
	≡Fe_3O	(101)	0.59	0.59
		(010)	0.00	

[a] For each goethite sample, values under the column labeled "segregate" were calculated by multiplying the CFC percentage, presented in Table 5.5, for the crystal face being considered by that crystal face's reactive site density (cf. Table 5.2) for the site type of interest (i.e. singly, doubly, or triply coordinated surface sites).

[b] Values under the column labeled "composite" are determined for a given site type by summing the N_S values presented in that site type's row, under the "segregate" column for the (101) and (010) crystal faces.

For example consider the VIL70 goethite sample. In the "segregate" approach, the N_S of singly coordinated sites from the (101) and (010) crystal faces is calculated by multiplying the CFC percentage for each face (70% and 30%, respectively), by the reactive N_S of singly coordinated sites present on the (101) and (010) faces (3.03 and 9.1 sites/nm^2, respectively). The resulting N_S values of 2.12 and 2.74 sites/nm^2, presented in the "segregate" column of Table 5.6, are summed together to give the N_S of singly coordinated sites (4.85 sites/nm^2) used in the composite approach and presented in the "composite" column.

5.2.3.3 Charge Distribution (CD) values

Charge distribution (CD) coefficients, Δz_0 and Δz_1, for inner-sphere complexes modeled in this work, were taken from the literature when available; however, for the adsorbates of concern in this study, the only CD values previously published were for carbonate surface species [32, 35]. For mercury adsorption onto goethite, the CD coefficients for each complex considered were determined using a similar method to the one discussed by Hiemstra et al. [32]. In this approach, bond valence analysis of a number of mercury surface complexes, predicted by Kim et al. [71, 72] through the use of EXAFS spectroscopy and molecular modeling, were performed to ascertain which configurations of the mercury surface complex are stable from a bond valence perspective and what CD values are necessary to ensure the complex's stability. As described in detail by Hiemstra and Van Riemsdijk [93], for specifically adsorbed ions, the change of charge (Δz) on the 0- and 1-planes can be obtained using Equations 5.4 and 5.5, respectively:

$$\Delta z_0 = n_0 + n_{H0} - \phi(n_0 + n_{H0} + \Sigma n_{ref} z_{ref}) \quad (5.4)$$

$$\Delta z_1 = n_1 + n_{H1} + \phi(n_0 + n_{H0} + \Sigma n_{ref} z_{ref}) \quad (5.5)$$

where n_0 and n_1 represent the portion of the adsorbate's charge ascribed to the 0- and 1-planes, respectively. The n_{H0} and n_{H1} values represent the charge of additional protons positioned in the 0- and 1-planes, respectively. The symbol ϕ is a proportionality factor

($\phi \approx 0.17$). The term n_{ref} represents the number and z_{ref} the charge of the reference surface group(s) involved in the surface complexation reaction [93].

5.3. Results and Discussion

5.3.1. Dissolved mercury speciation

Aqueous Hg(II) speciation was determined using the equilibrium constants provided in MINEQL+ 4.5 [146, 147] at 25°C and presented in Table 5.7. When chloride is not present in the system, $Hg(H_2O)_6^{2+}$ is the dominant mercury species at pH values below 3. The $HgOH^+$ and $Hg(OH)_2$ aqueous complexes become more prevalent as pH rises. As Kim et al. [71] and others [166, 171, 174, 184] have observed in systems free of complexing ligands and competing adsorbates, Hg(II) uptake onto goethite and other adsorbents peaks around pH 3 ± 1 and tapers off slightly as pH increases past this point. This low pH range at which the zenith of Hg(II) adsorption is attained coincides with $Hg(OH)_2$ becoming the dominant mercury species in solution (Figure 5.5b). As pH increases above the adsorption edge (pH > 4), the amount of Hg(II) adsorbed decreases marginally as a result of desorption to form the $Hg(OH)_2$ aqueous complex [184] and an increase in weakly sorbing aqueous species such as $Hg(OH)_3^-$ [71]. In the presence of chloride, $HgCl_2$ and HgOHCl can become dominant in the low to mid pH range thereby shifting the region of $Hg(OH)_2$ dominance to higher pH values (Figure 5.5d).

Table 5.7 The equilibrium constants of various Hg(II) aqueous species used in the CD-MUSIC model

Reactions	log *K*
$Hg^{2+} + H_2O \leftrightarrow HgOH^+ + H^+$	-3.40 ± 0.08
$Hg^{2+} + 2H_2O \leftrightarrow Hg(OH)_2 + 2H^+$	-6.17
$Hg^{2+} + 3H_2O \leftrightarrow Hg(OH)_3^- + 3H^+$	-21.1
$Hg^{2+} + Cl^- \leftrightarrow HgCl^+$	6.72
$Hg^{2+} + 2Cl^- \leftrightarrow HgCl_2$	13.23
$Hg^{2+} + 3Cl^- \leftrightarrow HgCl_3^-$	14.2
$Hg^{2+} + 4Cl^- \leftrightarrow HgCl_4^{2-}$	15.3
$Hg^{2+} + H^+ + CO_3^{2-} \leftrightarrow HgHCO_3^+$	16.372
$Hg^{2+} + CO_3^{2-} \leftrightarrow HgCO_{3(aq)}$	12.102
$Hg^{2+} + H_2O + Cl^- \leftrightarrow HgOHCl + H^+$	4.27 ± 0.35

5.3.2. Surface Protonation and Ion Pair Formation

The equilibrium constants for goethite's surface protonation reactions and ion pair formation reactions were determined through model fitting of the potentiometric titration data collected for VIL70 [74, 75] (Figure 5.2).

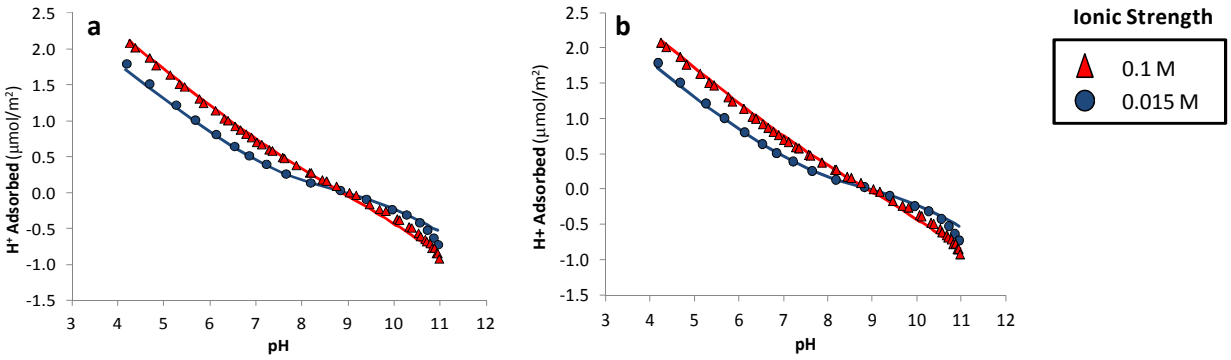

Figure 5.2 Potentiometric titration data for goethite sample VIL70 at two different ionic strengths using $NaNO_3$ as the background electrolyte. Symbols denote experimental data taken from Villalobos and Leckie [74, 75] and lines denote CD-MUSIC model simulations using the **(a)** segregate and **(b)** composite approaches to describing the mineral's surface (see text for more details). Reactions listed in Table 5.3 were used in performing model simulations.

5.3.3. Carbonate species on goethite

A number of studies investigating carbonate adsorption onto goethite using IR spectoscopy [54, 75, 76] have previously concluded that carbonate binds to the mineral's surface as an inner-sphere monodentate complex. More recently however, Hiemstra et al.[32] re-examined these spectroscopic results and argued in favor of carbonate forming a bidentate inner-sphere complex with goethite's surface based on the magnitude of carbonate's $\Delta\nu_3$ band splitting, the charge distribution values determined for carbonate via surface complexation modeling, and comparison of proton co-adsorption data between carbonate and other oxyanions such as selenite. Further evidence in support of the bidentate structure proposed by Hiemstra et al. [32] was provided by Bargar et al. [73], who found carbonate to form a binuclear bidentate complex on hematite through the use of attenuated total reflectance Fourier transform infrared (ATR-FTIR) spectroscopy and quantum chemical calculations. In addition to the bidentate inner-sphere surface

species, Bargar et al [73] also observed a C – O stretching band around 1460 cm^{-1} in D_2O that was attributed to the formation of an outer-sphere carbonate complex on hematite and confirmed with molecular orbital calculations using density functional theory (MO/DFT). Wijnja and Schulthess [76] observed a similar C – O stretching band (1462 cm^{-1} in D_2O) when investigating carbonate adsorption onto goethite using ATR-FTIR spectroscopy. Given this similarity between the C – O stretching bands, Rahnemaie et al. [35] proposes that the same outer-sphere complex Bargar et al. [73] found to form on hematite also forms on goethite. The carbonate surface species employed by Rahnemaie et al. [35], which are supported by spectroscopic evidence and MO/DFT calculations, were considered in developing the CD-MUSIC model used in our work.

To account for the presence of carbonate in the solid – solution systems of Barrow and Cox [69] and Bonnissel-Gissinger et al. [83], carbonate adsorption was incorporated into our CD-MUSIC model and calibrated using experimental data provided in Villalobos and Leckie [75]. Using CD-MUSIC to model this data in conjunction with the carbonate surface complexes employed by Rahnemaie et al. [35] allowed for identification of the relevant carbonate surface species and their intrinsic formation constants. The best fits of Villalobos' and Leckie's [75] experimental data were obtained when only the inner-sphere bidentate complex was utilized in our model (Table 5.3); a result that is in agreement with Hiemstra et al. [32] who successfully modeled the same experimental data using only the inner-sphere bidentate complex as well.

When employing the segregate approach to characterizing goethite's surface (Table 5.6), the CD-MUSIC model worked best when the carbonate surface complex only formed on the (010) crystal face (Table 5.3). At higher surface loadings, adsorption of carbonate onto the (101) crystal face is expected to occur; however, for the experimental data modeled from Villalobos and Leckie [75], the formation of an inner-sphere bidentate complex on the (101) crystal face was not necessary since there were sufficient sites present on the (010) face to accommodate all carbonate adsorbed and these sites possess a higher reactivity than those on the (101) face [39, 78]. It is important to note that carbonate's inner-sphere bidentate complex is thought to be a double-corner bidentate complex, binding to two singly coordinated surface sites present on the corners of adjacent octahedra [32, 35, 73]. While this configuration is possible on the (101), (001), and (210) crystal faces, it is not attainable on the (010) face because singly coordinated sites are present as pairs on the edges of the same octahedra rather than corners on adjacent octahedra [97]. As illustrated by Salazar-Camacho and Villalobos [84], on the (010) face, the corners of adjacent octahedra are comprised of one singly coordinated site and one doubly coordinated site. Hence, in order to model a double corner bidentate complex on the (010) crystal face, carbonate must bind to one singly and one doubly coordinated site. Therefore, in the segregate CD-MUSIC model employed in this work, carbonate was modeled as complexing with one singly and one doubly coordinated site on the (010) crystal face of goethite; thereby allowing for the model to agree with spectroscopy and molecular modeling simulations.

With the relevant carbonate surface species known and the intrinsic log K values for surface protonation, ion pair formation, and carbonate surface complexation reactions determined from modeling the data provided in Villalobos and Leckie [75], the CD-MUSIC model could now predict the carbonate contaminated potentiometric titration data of Barrow and Cox [5]. Since the extent of carbonate contamination was not known, the value of $[CO_3^{2-}]_{TOT}$ present in the solid – solution system was optimized using FITEQLC to achieve the best model fits of the titration data. In performing this modeling procedure it was discovered that the optimal $[CO_3^{2-}]_{TOT}$ value varied with the ionic strength of the system and that one $[CO_3^{2-}]_{TOT}$ value could not satisfactorily describe all three potentiometric titration data sets (ionic strengths of 0.001, 0.01, and 0.1 M $NaNO_3$) presented in Barrow and Cox [5]. Given that the Hg(II) adsorption experiments of Barrow and Cox [5] were all conducted at an ionic strength of 0.1 M $NaNO_3$, the optimized $[CO_3^{2-}]_{TOT}$ value obtained for the titration data set possessing that same ionic strength was utilized in all CD-MUSIC simulations of Hg(II) adsorption onto BAR76 (Table 5.3).

For the BAR76 solid – solution system at 0.1 M $NaNO_3$, the optimized $[CO_3^{2-}]_{TOT}$ values were determined to be 1.79 x 10^{-4} M and 2.52 x 10^{-4} M for the segregate and composite CD-MUSIC models, respectively. Model calculations using the conditions described by Barrow and Cox [69] (i.e., $[Hg(II)]_{TOT}$ = 0 - 50 μM, $[Cl^-]_{TOT}$ = 0 – 5,000 μM, [goethite] = 4.02 – 4.51 g/L, ionic strength of 0.1 M $NaNO_3$) reveal that both of these optimized $[CO_3^{2-}]_{TOT}$ values are in agreement with the experimental system being in equilibrium with the atmosphere (P_{CO2} = 0.38 matm) at pH values around 7. In other

words, the optimized $[CO_3^{2-}]_{TOT}$ values for the BAR76 solid-solution system, obtained using the procedure outlined above, are equivalent to the $[CO_3^{2-}]_{TOT}$ concentrations predicted for the experimental system when constrained by equilibrium with the atmosphere.

It is important to clarify that in Bonnissel-Gissinger et al.'s [83] study, no potentiometric titration data was presented; rather, the reported pH_{PZC} of the BON15 goethite sample was based on a previous study conducted by Mueller and Sigg [185] who utilized the same goethite preparation, Bayferrox 910 (standard 86), from Bayer. With no potentiometric titration data available for the goethite sample actually used in Bonnissel-Gissinger et al.'s [83] work, it is difficult to ascertain the existence and extent of carbonate contamination present in the solid – solution systems they studied based solely on another study's (Mueller and Sigg [185]) titration data. Fortunately, Bonnissel-Gissinger et al. [83] utilized x-ray photoelectron spectroscopy (XPS) to determine the cleanliness of their mineral sample's surface and upon analyzing BON15's XPS spectrum, observed carbon to be present on the mineral's surface; thereby providing direct evidence of carbonate contamination on BON15. It should be noted that Bonnissel-Gissinger et al. [83] stipulate that prior to experimentation, their goethite preparation was washed with degassed Milli-Q water and dried in a dessicator to prevent carbonate formation on the mineral surface. Given all this information, specifically the pH_{PZC} referenced by the authors, the XPS results, and the statement by the authors regarding the steps taken to ensure experiments were conducted in a carbon free environment, it is unclear whether or not carbonate was present in the system. To be

thorough in our investigation, both scenarios (i.e. with and without carbonate present in the system) were considered separately when modeling the Hg(II) adsorption data presented in Bonnissel-Gissinger et al. [83]. For the scenario where carbonate is present, $[CO_3^{2-}]_{TOT}$ was optimized using FITEQLC to achieve the best model fits of the Hg(II) adsorption data (Table 5.8).

Table 5.8 Summary of CD-MUSIC model fits to Hg(II) adsorption data for BAR76 and BON15

Goethite Sample	Electrolyte	Surface Loading		Model Fit	
		Hg(II)	Cl^-	Segregate	Composite
BAR76	$NaNO_3$	0.01	–	19.4	19.6
		0.03	–	3.6	4.2
		0.07	–	3.3	3.1
		0.15	–	4.3	5.9
	$NaNO_3$ and NaCl	0.03	0.016	3.7	3.3
		0.03	0.164	7.2	7.8
		0.03	1.64	7.9	8.2
		0.03	16.4	3.0	4.4
BON15	$NaNO_3$ and NaCl	0.08	0.13	6.7	6.3
		0.08	0.13	7.2 *	6.2 *
		0.08	667	1.8	2.4
		0.08	667	2.5 *	2.4 *

"Segregate" and "Composite" headings denote which surface characterization method was employed in the CD-MUSIC model (see text for more details). Surface loadings are in units of μmol/m^2. Model fits were calculated with the WSOS/DF parameter. Using the segregate method for BAR76 and BON15, $[CO_3^{2-}]_{TOT} = 1.79 \times 10^{-4}$ M and 3.05×10^{-4} M, respectively. Using the composite method for BAR76 and BON15, $[CO_3^{2-}]_{TOT} = 2.52 \times 10^{-4}$ M and 2.52×10^{-8} M, respectively. The * symbol denotes model simulations performed assuming no carbonate was present in the system. All experiments were conducted in a background electrolyte solution of 0.1 M ionic strength.

5.3.4. Hg(II) adsorption on goethite

CD-MUSIC modeling for Hg(II) adsorption onto BAR76 accounted for carbonate's presence in the solid – solution system since, as stated previously, it was reasoned that the experimental systems of Barrow and Cox [69] were contaminated with carbonate. The CD-MUSIC model was first calibrated using Hg(II) adsorption data collected in the absence of chloride. The model was then calibrated using Hg(II) adsorption data in the presence of chloride to determine the intrinsic equilibrium constant for the Hg–Cl ternary surface complex. Model parameters and constants determined from CD-MUSIC simulations of the potentiometric titration data and carbonate adsorption data were employed when modeling the Hg(II) adsorption data. Furthermore, it should be noted that the same log K_{in} values were used in every model simulation to describe Hg(II) adsorption onto goethite in the presence and absence of chloride. In other words, for all model simulations presented in this work using either the segregate or composite CD-MUSIC model, all equilibrium constants were fixed. A total of eight Hg(II) pH adsorption edges, four with and four without chloride present in solution, were successfully predicted on BAR76 using the 1-p*K* CD-MUSIC model (Figures 3 and 4).

Using EXAFS analysis in conjunction with molecular modeling simulations to investigate Hg(II) adsorption onto goethite, both Kim et al. [71] and Collins et al. [70] found strong evidence suggesting that Hg(II) binds to the mineral surface as an inner-sphere binuclear bidentate corner sharing complex via two deprotonated singly coordinated surface oxygens. Utilizing bond valence analysis as a complement to their EXAFS and molecular modeling work, Kim et al. [71] found that Hg(II) bound to either

singly protonated or deprotonated singly coordinated surface oxygens (≡FeOH and ≡FeO, respectively) resulted in a saturated oxygen coordinative state signifying a stable surface species. In other words, bond valence calculations indicate that the two singly coordinated surface sites that bind with Hg(II) to form the binuclear bidentate surface complex can be singly protonated or deprotonated. This result contradicts molecular modeling simulations that found only deprotonated singly coordinated sites complexing with Hg(II) are capable of achieving the Hg – O interatomic distance observed using EXAFS spectroscopy [70, 71]. Given that bond valence analysis has been employed in a number of studies to help guide selection of surface species based on EXAFS data [49, 50, 54], the bond valence findings of Kim et al. [71] should not be immediately dismissed despite the disagreement with molecular modeling results; therefore, three different Hg(II) bidentate surface complexes were considered in developing the composite CD-MUSIC model: $(\equiv FeOH)_2$–Hg, $(\equiv FeO)_2H$–Hg, and $(\equiv FeO)_2$–Hg. Upon modeling the experimental data of Barrow and Cox [69] with the composite CD-MUSIC model, it was found that both the $(\equiv FeO)_2H$–Hg and $(\equiv FeO)_2$–Hg complexes were needed to describe Hg(II)'s adsorption behavior onto goethite (cf. Table 5.3).

In the case of the segregate CD-MUSIC model, Hg(II) was only considered to complex with the (010) crystal face. The reason for this is that surface sites present on the (010) face are thought to be more reactive than those on the (101) face [39, 78], and, for the experimental conditions tested by Barrow and Cox [69] and Bonnissel-Gissinger et al. [83], all adsorbed Hg(II) can be accommodated on the (010) crystal face. Therefore, it stands to reason that, whenever possible, all Hg(II) would preferentially

adsorb to the (010) face; similar to Cd(II)'s, Pb(II)'s, and Se(IV)'s adsorption behavior with the (210) face of GOE63 (discussed in Chapters 3 and 4). To be sure, Hg(II) is expected to complex with the (101) face at higher surface loadings; however, under the conditions considered in this work, that is not believed to occur. In the segregate CD-MUSIC model, Hg(II) complexes with the (010) face as a double corner bidentate complex to one singly and one doubly coordinated surface site (i.e., (≡FeO)-Hg-($\equiv Fe_2O$)). This double corner bidentate complex was chosen because it provided the best agreement with the spectroscopic observations, molecular modeling simulations, and bond valence analysis of Kim et al. [71].

In the presence of chloride, Barrow and Cox [69] and Gunneriusson and Sjoeberg [184] both observed enhanced Hg(II) uptake onto goethite that could not be explained without the addition of a Hg-Cl ternary surface complex. To confirm the formation of this proposed surface species, Kim et al. [72] conducted a series of Hg(II) uptake measurements onto goethite with varying levels of chloride present in solution and examined the resulting sorption products using EXAFS spectroscopy. Through interpretation of their spectroscopic data and confirmation via molecular modeling simulations, the authors concluded that a Type A (surface–metal–ligand) Hg–Cl ternary surface complex forms on goethite in a monodentate fashion; in agreement with the findings of Bargar et al. [186]. The Hg–Cl surface species complexed to a deprotonated singly coordinated surface oxygen provided the best agreement between EXAFS data and molecular modeling results [72], and was therefore employed in the current modeling study (Table 5.3).

CD-MUSIC was able to provide satisfactory model fits (0.1 < WSOS/DF < 20) of all mercury pH adsorption edge experiments conducted on BAR76 using either surface characterization method, segregate or composite, employed in this study (Figure 5.3 and Figure 5.4).

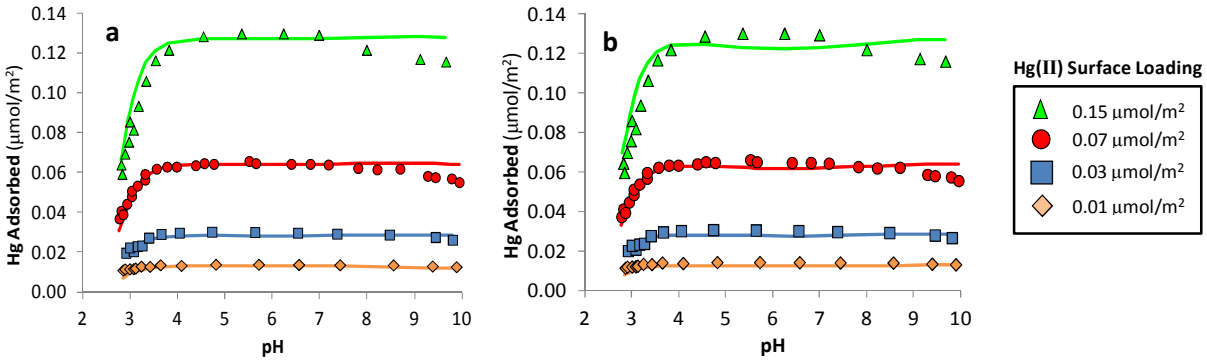

Figure 5.3 Mercury pH adsorption edge data for goethite sample BAR76 at four different total Hg(II) surface loadings in the absence of chloride. Symbols denote experimental data taken from Barrow and Cox [69] and lines denote CD-MUSIC model simulations using the **(a)** segregate and **(b)** composite approaches to describing the mineral's surface (see text for more details). Reactions listed in Table 5.3 and $[CO_3^{2-}]_{TOT}$ values found in Table 5.8 were used in performing model simulations.

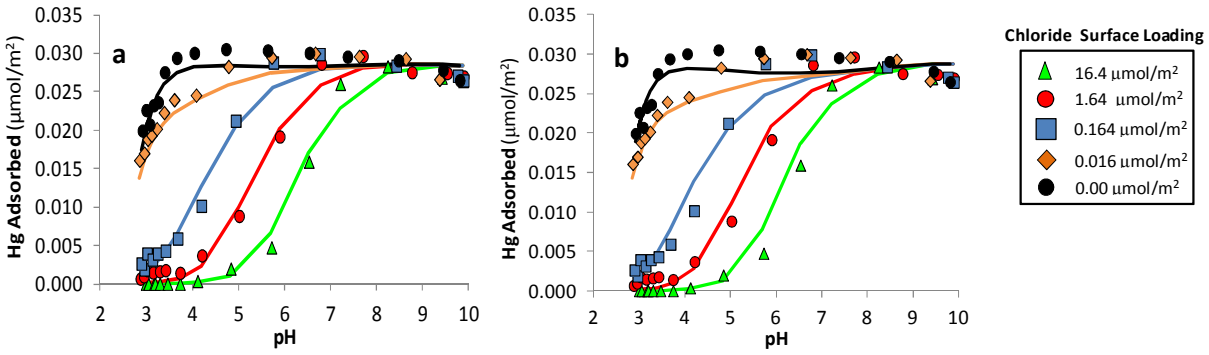

Figure 5.4 Mercury pH adsorption edge data for goethite sample BAR76 at a Hg(II) surface loading of 0.03 µmol/m^2 and five different total chloride surface loadings. Symbols denote experimental data taken from Barrow and Cox [69] and lines denote CD-MUSIC model simulations using the **(a)** segregate and **(b)** composite approaches to describing the mineral's surface (see text for more details). Reactions listed in Table 5.3 and $[CO_3^{2-}]_{TOT}$ values found in Table 5.8 were used in performing model simulations.

Whether in the absence or presence of chloride, Hg(II) adsorption was found to peak around the same pH that $Hg(OH)_2$ became the dominant mercury species in solution (Figure 5.5). In the presence of chloride, the adsorption edge shifted to a higher pH because of the dominance of the non-sorbing aqueous species $HgCl_2$ in the lower pH range. From the model results seen in Figure 5.5, the HgOHCl aqueous complex appears to be the sorbing species responsible for the formation of the ≡FeOHgCl surface complex given how the concentrations of the aqueous and surface species coincide well with each other. As pH increases in systems containing chloride, $Hg(OH)_2$ eventually becomes the dominant mercury species in solution; the rise of this aqueous complex (Figure 5.5d) corresponds fittingly with the rise in concentration of the (≡FeO)-Hg-(≡Fe_2O) surface complex (Figure 5.5c).

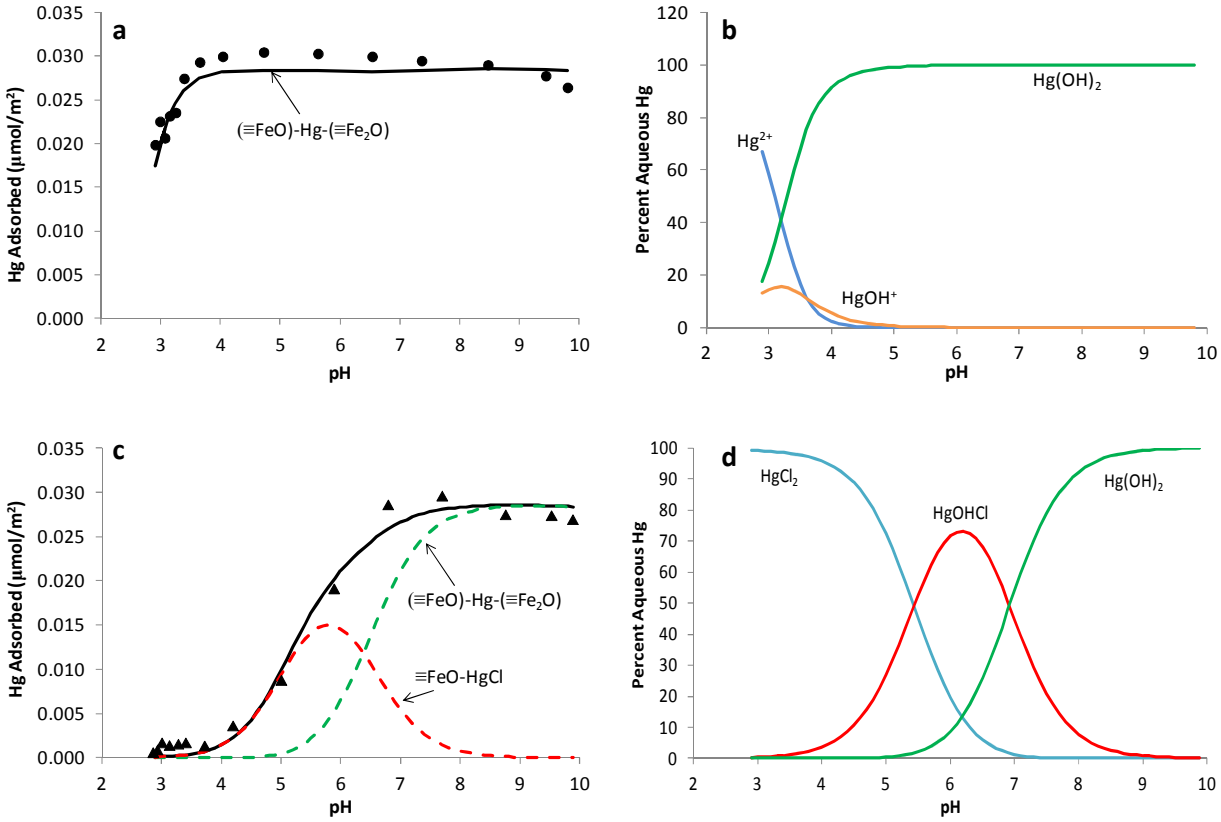

Figure 5.5 **(a)** Surface speciation of mercury on BAR76 for a pH adsorption edge experiment in the absence of chloride (Hg(II) surface loading of 0.03 µmol/m^2). The symbols represent experimental data points for total Hg(II) adsorbed. The solid line is taken from the model simulation and denotes the total Hg(II) adsorbed. In the absence of chloride, all mercury adsorbs to goethite as (≡FeO)-Hg-(≡Fe_2O). The segregate method of characterizing the mineral's surface was used in CD-MUSIC for this model simulation. **(b)** Aqueous speciation of Hg(II) in solution during the pH adsorption edge experiment presented in plot a. **(c)** Surface speciation of Hg(II) on BAR76 in a model simulation of a pH adsorption edge in the presence of chloride (Hg(II) and Cl^- surface loadings of 0.03 and 16.4 µmol/m^2). The symbols represent experimental data points for total Hg(II) adsorbed. The lines are taken from the model simulation with the solid line denoting the total Hg(II) adsorbed and the dashed lines representing the surface species used in the CD-MUSIC model. The segregate method of characterizing the mineral's surface was used in CD-MUSIC for this model simulation. **(d)** Aqueous speciation of Hg(II) in solution during the pH adsorption edge experiment presented in plot c.

Using the optimized $[CO_3^{2-}]_{TOT}$ values determined for the BAR76 solid – solution system ($[CO_3^{2-}]_{TOT}$ = 1.79 x 10^{-4} M and 2.52 x 10^{-4} M for the segregate and composite CD-MUSIC models, respectively), both models predicted carbonate to have minimal influence on Hg(II)'s adsorption to goethite (Figure 5.6). To ascertain what impact, if any, carbonate has on mercury uptake *in the absence of chloride*, model simulations employing higher $[CO_3^{2-}]_{TOT}$ values were conducted for the BAR76 system using a Hg(II) surface loading of 0.07 μmol/m^2.

At elevated $[CO_3^{2-}]_{TOT}$ concentrations, both the segregate and composite CD-MUSIC models predict the mercury adsorption edge to not only elongate, but also become increasingly sinusoidal in appearance as $[CO_3^{2-}]_{TOT}$ rises (Figure 5.6a and 5.6b). In both models, Hg(II) and carbonate compete for the same reactive surface sites (Table 5.3); therefore, as $[CO_3^{2-}]_{TOT}$ increases, more carbonate will bind to the goethite sample thereby reducing the number of surface sites available for Hg(II) adsorption (Figure 5.6e and 5.6f). Comparison of Figure 5.6a with Figure 5.6e, and Figure 5.6b with Figure 5.6f, reveal that the pH around which the Hg(II) adsorption edge experiences a minimum (i.e., the trough of the wave) corresponds well with the pH at which maximum carbonate adsorption occurs. In addition to competition with carbonate for surface sites, Hg(II)'s uptake onto BAR76 may also be affected by its aqueous speciation with carbonate (Figure 5.6c and Figure 5.6d). As the $[CO_3^{2-}]_{TOT}$ value rises, Hg(II) becomes increasingly complexed with carbonate in solution (i.e., $HgHCO_3^+$ and $HgCO_3$ aqueous complexes) (Figure 5.6c and Figure 5.6d). As stated previously, evidence suggest that mercury's bidentate complex forms on goethite's surface primarily by means of the

$Hg(OH)_2$ aqueous complex (Figure 5.5a and Figure 5.5b); therefore, it is reasoned that these mercury carbonate aqueous complexes are effectively trapping Hg(II) in solution and preventing its adsorption to goethite.

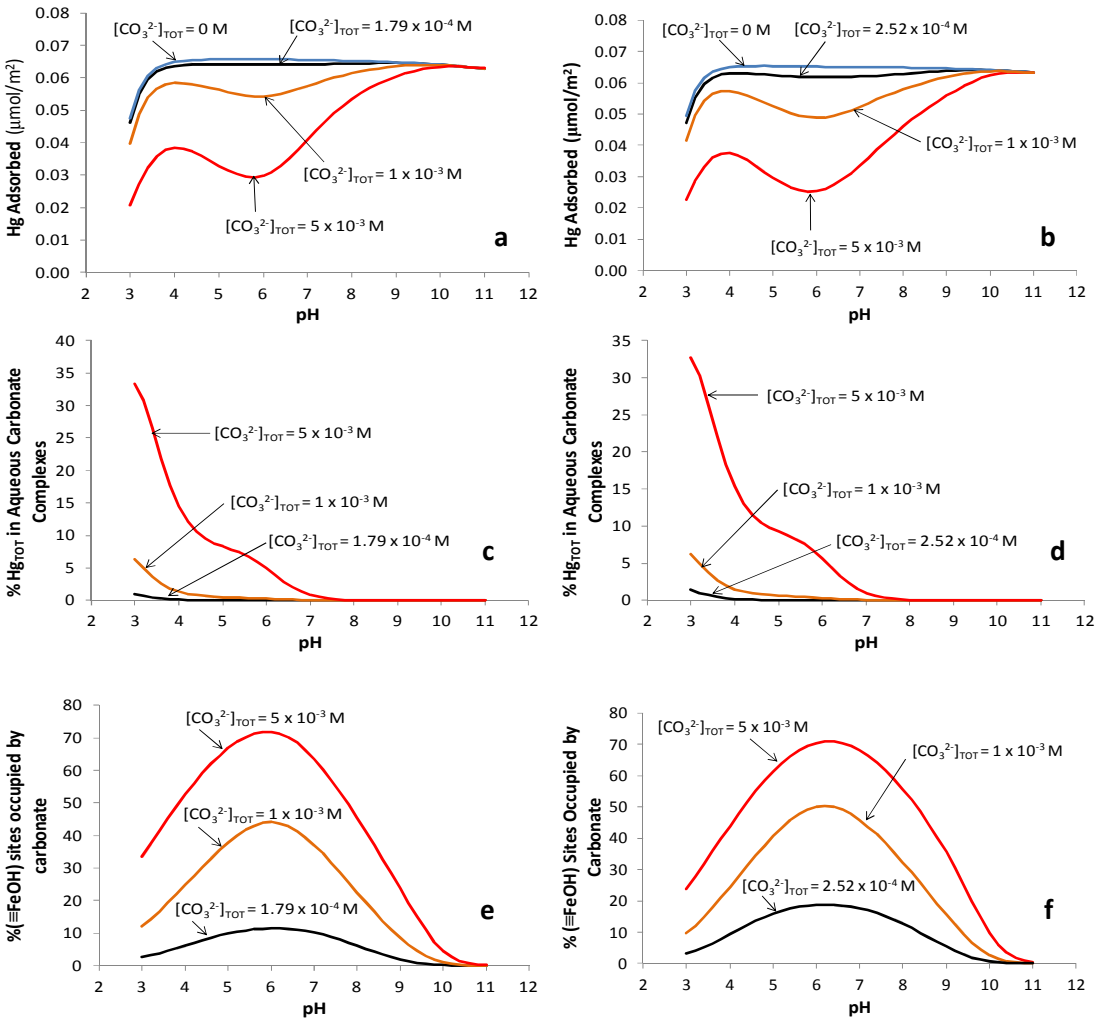

Figure 5.6 **(a) and (b)** Affect of $[CO_3^{2-}]_{TOT}$ on predicted mercury adsorption to BAR76 in the absence of chloride using the CD-MUSIC model with the **(a)** segregate and **(b)** composite approaches, respectively, for describing the mineral's surface (see text for more details). Simulations were conducted using a Hg(II) surface loading of 0.07 µmol/m^2. No precipitates were predicted to form under the conditions tested in these simulations. **(c) and (d)** Percent of $Hg(II)_{TOT}$ present in the system as an aqueous carbonate complex (i.e., $HgCO_3$ and $HgHCO_3^+$) for CD-MUSIC simulations presented in plot a using the segregate approach and plot b using the composite approach, respectively. **(e) and (f)** Percent of Hg(II) reactive surface sites occupied by carbonate for CD-MUSIC simulations presented in plot a using the segregate approach and plot b using the composite approach, respectively. The labels and corresponding arrows used in all plots are to denote the carbonate conditions used in each model simulation.

5.3.5 Model verification

Mercury adsorption data taken from Bonnissel-Gissinger et al. [83] was used to verify the predictive capability of the CD-MUSIC model developed in this study. Model simulations were conducted using the reactions and affinity constants reported in Table 5.3. For both segregate and composite surface characterizations of BON15, the CD-MUSIC model was able to satisfactorily simulate Hg(II) uptake onto the goethite sample for the experimental conditions tested by Bonnissel-Gissinger et al. [83] (Figure 5.7). In contrast to the modeling results of BAR76, the CD-MUSIC model utilizing the composite method produced the best model fits for Hg(II) adsorption onto BON15.

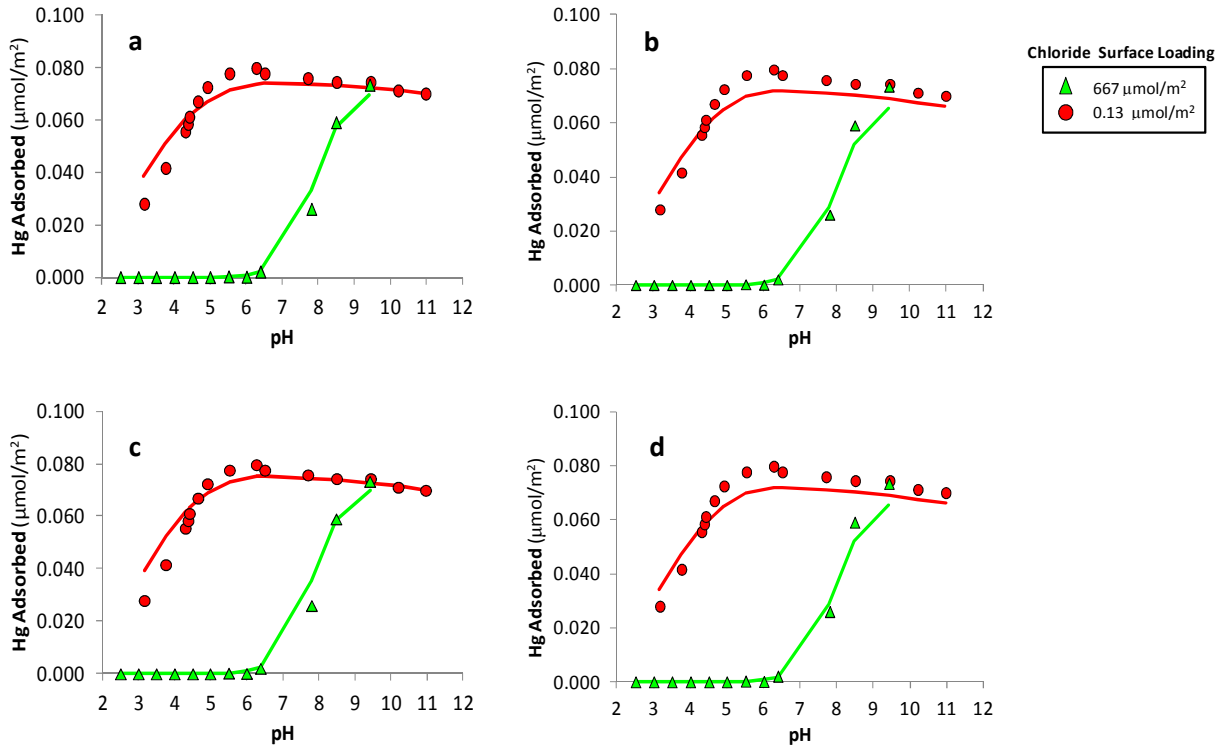

Figure 5.7 Mercury pH adsorption edge data for goethite sample BON15 at a Hg(II) surface loading of 0.08 µmol/m^2 and two different total chloride surface loadings. Symbols denote experimental data taken from Bonnissel-Gissinger et al. [83] and lines denote CD-MUSIC model simulations using the [**(a) and (c)**] segregate and [**(b and d)**] composite approaches to describing the mineral's surface (see text for more details). Reactions listed in Table 5.3 $[CO_3^{2-}]_{TOT}$ values of $3.05x10^{-4}$ M for plot a and $2.52x10^{-8}$ M for plot b, found in Table 5.8, were used in performing the model simulations. Model simulations for plots **(c)** and **(d)** were conducted assuming no carbonate was present in the system.

As discussed previously, two scenarios, one with and one without carbonate present in the BON15 solid-solution system, were considered when modeling the Hg(II) adsorption data of Bonnissel-Gissinger et al. [83]. Examination of Figure 5.7 and Table 5.8 reveals that the difference in model fit between the two scenarios tested was minimal; suggesting that, under the conditions tested ($[CO_3^{2-}]_{TOT}$ = $3.05x10^{-4}$ M and $2.52x10^{-8}$ M for the segregate and composite CD-MUSIC models, respectively), carbonate's presence in the system has little to no impact on Hg(II)'s adsorption behavior onto goethite.

Similar to the analysis performed on the BAR76 system, model simulations were carried out for the BON15 solid – solution system at elevated $[CO_3^{2-}]_{TOT}$ values to ascertain what impact, if any, carbonate has on mercury adsorption *in the presence of chloride* (Figure 5.8a and Figure 5.8b). Simulations were performed using Hg(II) and chloride surface loadings of 0.08 and 0.13 μmol/m^2, respectively.

As $[CO_3^{2-}]_{TOT}$ increases, both the segregate and composite CD-MUSIC models predict the mercury adsorption edge to elongate and shift to higher pH values; however, one discernible difference between the two models' simulations is the degree of elongation. In particular, whereas the adsorption edge predicted by the composite CD-MUSIC model becomes increasingly elongated as $[CO_3^{2-}]_{TOT}$ rises, the segregate version of the model predicts mercury's adsorption edge to shift to higher pH values while maintaining a similar, albeit slightly elongated, shape when compared with the adsorption edge simulated under experimental conditions (Figure 5.7a and Figure 5.8a, segregate CD-MUSIC model, $[CO_3^{2-}]_{TOT} = 3.05 \times 10^{-4}$ M; Figure 5.7b and Figure 5.8b, composite CD-MUSIC model, $[CO_3^{2-}]_{TOT} = 2.52 \times 10^{-8}$ M). For both models, the reason mercury's adsorption edge is predicted to shift towards higher pH values and elongate with higher $[CO_3^{2-}]_{TOT}$ values is due to increased competition between Hg(II) and carbonate for the same surface sites (Table 5.3). For the segregate and composite CD-MUSIC models, carbonate competes with mercury surface species for reactive sites present on BON15's surface, resulting in decreased amounts of each Hg(II) surface complex formed (Figure 5.8c - Figure 5.8f).

In contrast to the model results found for the BAR76 system, mercury adsorption to BON15 is not heavily influenced by complexation to carbonate for either the segregate or composite CD-MUSIC models due to the presence of chloride in the system which acts as a much stronger ligand to Hg(II) than carbonate. At the highest $[CO_3^{2-}]_{TOT}$ value tested ($5x10^{-3}$ M) for the BON15 system, the maximum percentage of $Hg(II)_{TOT}$ complexed with carbonate in solution (max $Hg(II)_{TOT,CO3}$) was found to be 2% for the segregate model and 4% for the composite model. Using that same $[CO_3^{2-}]_{TOT}$ value ($5x10^{-3}$ M) for the BAR76 system, in the absence of chloride, the max $Hg(II)_{TOT,CO3}$ value was predicted to be 33% in the segregate and composite models.

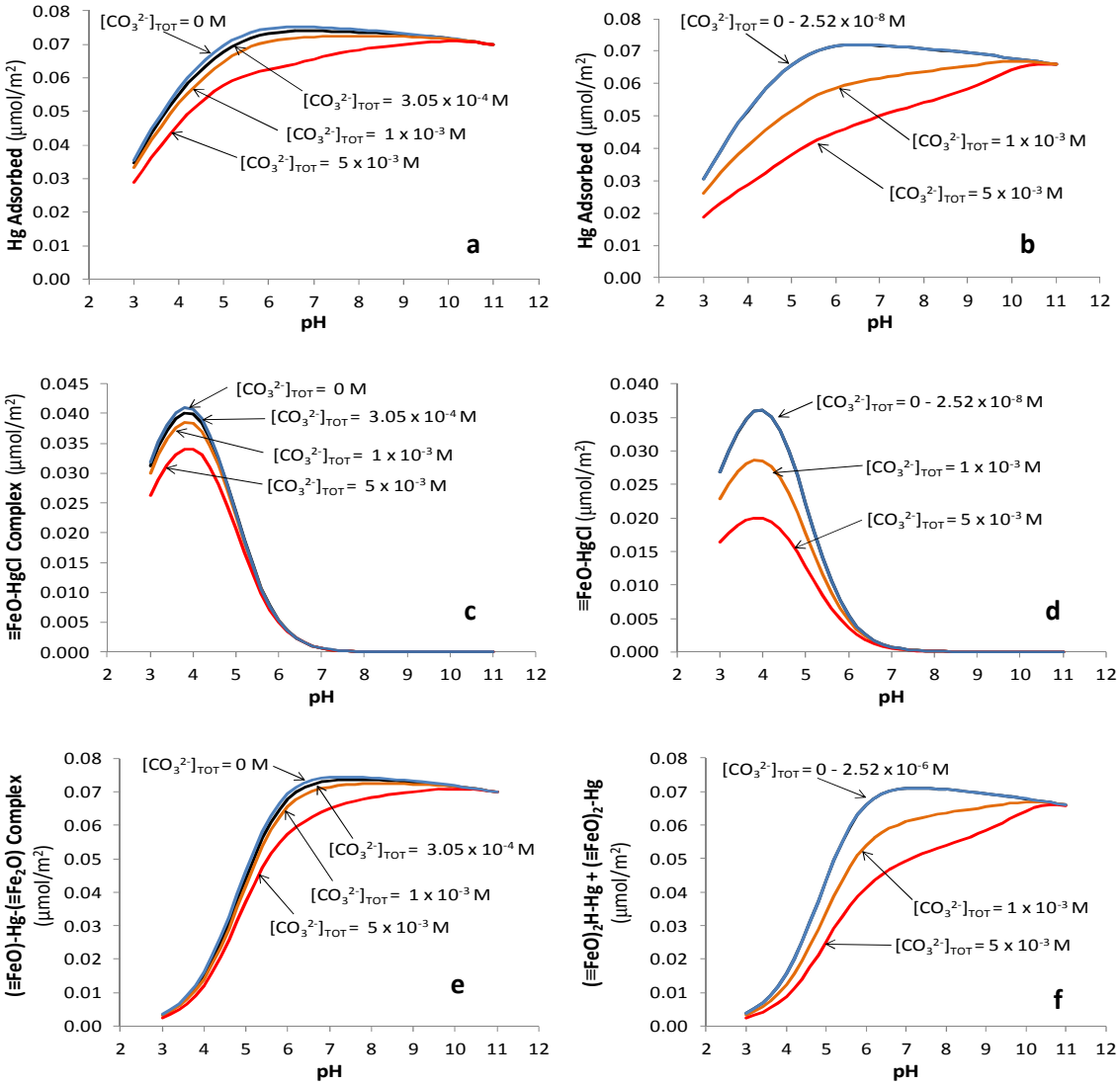

Figure 5.8 **(a) and (b)** Affect of $[CO_3]_{TOT}$ on predicted mercury adsorption to BON15 in the presence of chloride using the CD-MUSIC model with the **(a)** segregate and **(b)** composite approaches to describing the mineral's surface (see text for more details). Simulations were conducted using Hg(II) and chloride surface loadings of 0.08 and 0.13 µmol/m^2, respectively. No precipitates were predicted to form under the conditions tested in these simulations. **(c) and (d)** Predicted concentrations of the HgCl ternary surface complex (≡FeO-HgCl), in units of µmol/m^2, for the CD-MUSIC model simulations presented in plots a and b, respectively. **(e) and (f)** Predicted concentrations of (≡FeO)-Hg-(≡Fe_2O) for the segregate CD-MUSIC model and (≡FeO)$_2$H-Hg and (≡FeO)$_2$-Hg for the composite CD-MUSIC model, in units of µmol/m^2, for the model simulations presented in plots a and b, respectively. The labels and corresponding arrows used in all plots are to denote the carbonate conditions used in each model simulation.

For the BON15 system, optimized $[CO_3^{2-}]_{TOT}$ concentrations were calculated using the mineral sample's mercury adsorption data. Hg(II) uptake onto BON15 was predicted using the segregate and composite CD-MUSIC models along with the surface complexes and equilibrium constants previously determined from fitting the adsorption data of VIL70 and BAR76 (Table 5.3). Since the amount of carbonate present in the BON15 solid – solution system was unknown, the value of $[CO_3^{2-}]_{TOT}$ was optimized using FITEQLC to achieve the best model fits of the mercury adsorption data. The difference between the two CD-MUSIC models optimized $[CO_3^{2-}]_{TOT}$ concentrations for the BON15 system ($[CO_3^{2-}]_{TOT}$ = $3.05x10^{-4}$ M and $2.52x10^{-8}$ M for the segregate and composite CD-MUSIC models, respectively), stems from the fact that the segregate CD-MUSIC model possesses a larger log K value than the composite CD-MUSIC model for the ≡FeO-HgCl ternary surface complex (Table 5.3).

As a result of this larger log K value, the segregate CD-MUSIC model predicts more mercury to bind to BON15 (chloride surface loading, Γ_{Cl}, of 0.13 μmol/m^2) at the lower end of the pH adsorption edge than the composite CD-MUSIC model (Figure 5.7, Figure 5.8c and 5.8d). In fact, in the absence of carbonate, the segregate CD-MUSIC model slightly over predicts mercury adsorption at pH values below 4.5; while, within that same pH range, the composite CD-MUSIC model's prediction of Hg(II) uptake is closer in line with the observed experimental values (Figure 5.7c and 5.7d). As previously discussed, when carbonate is present in the segregate CD-MUSIC model, it competes with Hg(II) for reactive surface sites present on the (010) crystal face. For the BON15 system (Γ_{Cl} = 0.13 μmol/m^2), increasing $[CO_3^{2-}]_{TOT}$ concentrations in the

segregate CD-MUSIC model will reduce the amount of mercury predicted to adsorb to the mineral surface (Figure 5.8a). In a similar way, carbonate's presence in the composite CD-MUSIC model results in a predicted decrease in mercury adsorption (Figure 5.8b).

Given carbonate's influence on mercury's predicted adsorption behavior for both CD-MUSIC models considered, and in light of the model predictions for Hg(II) adsorption onto BON15 (Γ_{Cl} = 0.13 μmol/m^2) in the absence of carbonate (Figure 5.7c and Figure 5.7d); the optimized $[CO_3^{2-}]_{TOT}$ values can be better understood. Recall that in a carbonate free simulation of BON15 (Γ_{Cl} = 0.13 μmol/m^2), the segregate CD-MUSIC model was found to over predict mercury adsorption below pH 4.5. Introducing carbonate into the segregate CD-MUSIC model at a concentration of $[CO_3^{2-}]_{TOT}$ = 3.05x10^{-4} M, causes the predicted mercury adsorption edge to shift downward, thereby allowing for the model to better align with the experimental data, specifically at the lower end of the pH adsorption edge. (It should be noted that the optimized $[CO_3^{2-}]_{TOT}$ value of 3.05x10^{-4} M is in agreement with the BON15 solid – solution system being constrained by equilibrium with the atmosphere, P_{CO2} = 0.38 matm, around pH 7.) For the composite CD-MUSIC model, the carbonate free simulation of the BON15 (Γ_{Cl} = 0.13 μmol/m^2) system (above pH 4) appears to predict mercury adsorption just at or below the experimentally observed values of Bonnissel-Gissinger et al. [83] (Figure 5.7d). Since, in the case of the composite CD-MUSIC model, carbonate shifts the mercury adsorption edge downward (Figure 5.8b); the optimized $[CO_3^{2-}]_{TOT}$ value needs to be very small, relative to the segregate model's optimized $[CO_3^{2-}]_{TOT}$ concentration, to avoid

diminishing the model's accuracy by causing further under predictions of Hg(II) adsorption onto BON15. For this reason, the optimized $[CO_3^{2-}]_{TOT}$ value for the composite CD-MUSIC model was found to be $2.52x10^{-8}$ M, resulting in no discernible difference in the model's predicted mercury adsorption edge for the carbonate free simulation and the optimized $[CO_3^{2-}]_{TOT}$ simulation (Figure 5.8b).

5.4. Conclusions

The adsorption behavior of Hg(II) on two different goethite samples in the presence of chloride and carbonate was accurately predicted using the CD-MUSIC model. Not only was the model's predicted removal of Hg(II) consistent with the experimental data tested, but the speciation of mercury in the aqueous phase helped to explain the impacts of pH, chloride, and carbonate on Hg(II) uptake. Model simulations conducted at elevated $[CO_3^{2-}]_{TOT}$ values reveal that carbonate does indeed influence mercury adsorption onto goethite. In particular, competition between carbonate and Hg(II) for the same reactive sites on the mineral surface results in mercury's adsorption edge elongating and shifting to higher pH values as the concentration of $[CO_3^{2-}]_{TOT}$ increases.

The CD-MUSIC model developed in this work is entirely self-consistent. In all model simulations performed, the same affinity constants for surface protonation, ion pair formation, carbonate adsorption, and mercury surface complexation reactions were utilized. Spectroscopic evidence and molecular modeling studies found in the literature were used to guide the selection of surface species incorporated into the adsorption

model. The crystal face composition (CFC) of each goethite sample studied was estimated using a new approach based off the work of Salazar-Camacho and Villalobos [84] that only requires knowledge of the mineral sample's SSA. In successfully simulating Hg(II) adsorption onto BAR76 and BON15, the CD-MUSIC model developed here has proven capable of describing Hg(II) adsorption onto goethite samples with varying surface reactivity in relatively complex, multi-solute systems. Furthermore, the success of the CD-MUSIC model demonstrates the applicability of the CFC estimation technique proposed in this study and its utility when there is limited information available concerning the adsorbent.

With the composite CD-MUSIC model's success in satisfactorily fitting all experimental data tested in this study, it is tempting to suggest that the composite surface characterization method should be employed more often in CD-MUSIC models; given that it is more simplistic than the segregate approach and easier to model. However, it is important to recall that while some of the more simplistic surface complexation models (SCMs) such as the diffuse layer model (DLM) have proven capable of correctly predicting metal ion adsorption behavior in certain instances, their deficiencies have also been demonstrated for increasingly complex systems [187]. Of the two surface characterization methods considered in this study, the segregate approach provides a more detailed description of the mineral surface's heterogeneity and permits greater specificity within the CD-MUSIC model regarding each surface complex's bonding environment; thereby allowing for the modeled surface species to be in closer agreement with molecular scale analyses (i.e. spectroscopy, molecular modeling). As stated

previously, ion adsorption behavior in solid – solution systems is greatly influenced by the mineral surface's crystal morphology [24, 25, 82, 84, 85]; hence, it would be expected that the more accurately a model can describe a mineral surface, the better its predictive capability becomes. Therefore, while both CD-MUSIC models were successful in simulating Hg(II) adsorption onto BAR76 and BON15, and are suitable for use within the experimental conditions tested here; we speculate that the segregate version of the CD-MUSIC model is better suited for predicting Hg(II) adsorption in more complex systems with variable environmental conditions.

Chapter 6 : CONCLUSIONS AND RECOMMENDATIONS

In natural aqueous systems, adsorption processes occurring at the mineral – water interface can play a pivotal role in determining the fate and transport and bioavailability of metal ions, oxyanions and other trace elements and contaminants. Surface complexation models (SCMs) developed over the last 40 years to describe adsorption processes occurring at the mineral – water interface represent the state-of-the-art for predicting adsorption behavior in both natural and engineered systems. While such models have proven capable of describing ion adsorption in single solute systems, their predictive capability in these systems is highly dependent on the ability of the model parameters to represent the characteristics of each mineral surface and the accuracy of the surface complexation reactions to describe the adsorption of each minera.

Microscopic imaging studies have shown mineral surfaces to not be homogenous but rather the conglomeration of several different crystal faces. On the iron hydroxide mineral goethite, these crystal faces have been found to possess unique surface site types and site densities that vary from one crystal face to the next. Spectroscopic investigations, molecular modeling simulations, and bond valence analysis have revealed that surface complex formation occurs on specific surface site types with particular coordination environments. Moreover, the site types involved and the coordination environment required for surface complex formation can vary between adsorbates. As a result, the predictive capabilities of surface complexation models has been hampered by the challenge of incorporating this heterogeneity into modeling efforts.

6.1. Surface site density estimation

Crystallography, tritium exchange, and surface saturation data have all been previously used to estimate the site density of goethite, and produced N_S values ranging from 0.5 to 20 sites/nm^2. A simplified view of the mineral surface (e.g., homogenous, single site type) cannot be reconciled with these predicted site density values. Furthermore, more rigorous characterizations of the mineral surface have also failed to explain all the N_S values predicted from these different techniques.

In this work, a methodology was developed for describing mineral surface heterogeneity in terms of a crystal face composition (CFC) that unifies the seemingly different N_S values predicted from crystallography, microscopic image analysis, tritium exchange, surface saturation, and surface charging data. This new methodology was applied to the goethite sample GOE63 and resulted in a CFC capable of harmonizing the different N_S values determined from various estimation techniques.

Utilizing the site types and site densities predicted from GOE63's CFC, along with surface complexes predicted from molecular scale analyses, the CD-MUSIC model was able to accurately simulate Cd(II), Pb(II), and Se(IV) adsorption in single and multi-solute systems over all experimental conditions tested. Furthermore, the conditions under which certain surface complexes formed in the model were in good agreement with spectroscopic observations. For example, CD-MUSIC predicts the monodentate Cd(II) surface complex to only form at high surface coverages and more alkaline pH values; consistent with spectroscopic evidence. For the first time, Pb(II) adsorption to goethite

could be simulated across the range of pH and surface coverages expected in the field while staying in agreement with spectroscopic results.

For the bi-solute systems investigated, the model proved successful in predicting ion adsorption in cation-cation and cation-oxyanion systems; however only the Cd(II)/Pb(II) system could be accurately modeled without the use of an additional surface complex. In the Cd(II)/Se(IV) and Pb(II)/Se(IV) bi-solute systems, the addition of a $CdSeO_3$ and $PbSeO_3$ ternary surface complex, respectively, was required for the model to successfully predict ion adsorption onto goethite. While no spectroscopic studies have been conducted to investigate the formation of these proposed ternary surface complexes, $CdSeO_3^0$, $Cd(SeO_3)_2^{2-}$, and $PbSeO_3^0$ aqueous complexes have all been observed to form in solution. Furthermore, spectroscopic investigations have revealed that both Cd(II) and Pb(II) form ternary surface complexes with sulfate. Given that selenite is a much stronger ligand than sulfate in aqueous complexation reactions with Cd(II) and Pb(II), we contend that the same is true for surface complexation reactions.

The CD-MUSIC model developed in this work for GOE63 demonstrates that a more rigorous characterization of the mineral surface and utilization of surface complexes based on molecular scale analyses results in a model capable of predicting ion adsorption in single and bi-solute systems.

6.2. Hg(II) adsorption modeling

Experimental data from batch adsorption studies is commonly used by researchers in developing and calibrating SCMs. Despite the meticulous care taken in these

experiments to ensure a CO_2 free environment for the solid – solution system under investigation, carbonate is often found to be present. Previous research has illustrated the difficulty in removing all traces of carbonate from a solid – solution system, and suggest that carbonate's presence in "carbonate free" systems is a fairly common occurrence. These studies have highlighted the need for an approach to quantify the amount of carbonate present in solid – solution systems.

Utilizing carbonate adsorption data collected presented in the literature and carbonate surface complexes based on spectroscopic evidence and molecular modeling simulations, a CD-MUSIC model was developed to predict carbonate adsorption onto goethite. Employing this model to potentiometric titration data collected possessing undocumented carbonate present in the solid – solution system, a value of $[CO_3^{2-}]_{TOT}$ was determined. The concentration of $[CO_3^{2-}]_{TOT}$ calculated was in agreement with the system being constrained by equilibrium with the atmosphere. Utilizing this $[CO_3^{2-}]_{TOT}$ value, Hg(II) adsorption onto BAR76 in the presence and absence of chloride was accurately predicted using the CD-MUSIC model. In contrast to previous Hg(II) adsorption models developed, all surface species employed in the model were in agreement with spectroscopic data, molecular modeling simulations, and bond valence analysis. Model validation was performed on a second, separate goethite sample where Hg(II) adsorption data had been collected in the presence and absence of chloride. In this instance as well, the CD-MUSIC model was able to accurately predict Hg(II) adsorption onto goethite.

Through this Hg(II) adsorption modeling work, a methodology has been developed for determining the concentration of $[CO_3^{2-}]_{TOT}$ present in a solid – solution system. Employing this method for solid – solution systems where carbonate is present has resulted in realistic $[CO_3^{2-}]_{TOT}$ concentrations being predicted. Utilizing these predicted $[CO_3^{2-}]_{TOT}$ values in CD-MUSIC model simulations of Hg(II) adsorption onto goethite has resulted in one of the first models capable of predicting Hg(II) uptake onto goethite utilizing only surface complexes consistent with molecular scale analyses.

In addition, this modeling effort utilized a linear relationship between goethite's SSA and proton reactive site density (N_H) to determine the CFC of each goethite sample considered. The relationship was developed using N_H values predicted from the titration congruency method for different goethite samples and plotting these values against their respective SSA. For the BON15 goethite sample, good agreement between the predicted tritium exchange value and the experimental value obtained for ferrihydrite, an iron oxide mineral with a comparable CFC, provides further confirmation that the methodology developed in this research can be extended to a wider range of systems. Indeed, the CD-MUSIC model's success in predicting Hg(II) adsorption under all experimental conditions studied provides support for using more simplistic versions of the methodology as a viable option for estimating CFC in the absence of other data (e.g., microscopic images, surface saturation data, tritium exchange data).

6.3. Engineering Implications

From an engineering perspective, the goal of surface complexation modeling is to develop a tool capable of accurately predicting ion adsorption behavior in natural and engineered systems. While SCMs have proven capable of simulating ion adsorption in relatively simple, single solute systems, their inability to consistently predict ion adsorption in more complex systems presents an obstacle to their acceptance and implementation in field studies. The CD-MUSIC model results presented in this work illustrate the robustness of the model and its potential in predicting adsorption in complex, multi-solute systems when the mineral's surface heterogeneity is properly accounted for.

The methodology developed in this work for ascertaining the CFC of a goethite sample utilizing multiple surface characterization techniques proved useful for the GOE63 goethite sample in helping to explain the different N_S values that have been obtained for goethite. Application of this methodology to the GOE63 goethite sample yielded a crystal face composition (CFC) that allowed for CD-MUSIC to describe ion adsorption in single and bi-solute systems accurately and in better agreement with spectroscopic observations than models previously developed. Hence, the methodology developed here holds great promise for better characterizing mineral surfaces and helping facilitate the development of SCMs capable of consistently predicting ion adsorption in more complex systems. Furthermore, utilization of this approach should allow for surface complex formation constants determined on one goethite sample to be applicable on all other goethite samples; something that is currently very difficult to achieve without

the use of additional surface species or parameter adjustment. Application of the methodology developed in this work to additional adsorption data sets collected on goethite and other oxide minerals will allow for a database to be constructed consisting of spectroscopically observed surface species and their equilibrium constants.

In order to employ CD-MUSIC at the field scale, a method for estimating the average surface heterogeneity (i.e., CFC) of each mineral present in the sediment has been needed. For goethite, the linear relationship between proton reactive site density and specific surface area (presented in Chapter 5) provides a good starting point for estimating the average CFC of goethite present in the sediment. In this instance, only the SSA of the mineral sample would be needed to determine the average CFC of goethite.

Application of SCMs at field-scale also requires methodologies for estimating the impacts of competition with carbonate species. The methodology presented in this research for incorporating carbonate adsorption into CD-MUSIC or other SCMs provides a relatively simplistic tool for predicting the oxyanion's presence and its impact in solid – solution systems. Finally, while many modelers have shied away from the application of CD-MUSIC due to the large number of model parameters, this research has demonstrated that many of these parameters can be resolved through careful consideration of the experimental data available. By determining model parameters in this way, the CD-MUSIC model becomes more manageable and its application much more consistent.

6.4. Recommendations

While this research has made great progress toward developing approaches to make the CD-MUSIC model more predictive and extensible, further advancements in CD-MUSIC modeling and SCM modeling should be considered. Certainly, this work only considered one mineral surface and a few contaminants. Extension of this approach to other minerals and, other solutes is a natural next step to demonstrate the validity of the methodology developed for site density estimation and incorporation of carbonate.

With respect to the specific research examining the Pb(II), Cd(II) and Se(VI) systems, further confirmation of the surface complexes proposed in this research is warranted. The tridentate Pb(II) surface complex proposed in this work, consisting of one edge and two corner linkages, allowed for good agreement between the CD-MUSIC model and spectroscopic observations. Computational molecular modeling simulations are needed to confirm that this surface species is possible and that its bond lengths for the edge and corner linkages correspond well with the Pb – O and Pb – Fe distances obtained from previous EXAFS studies. In addition, EXAFS investigations for Cd(II)/Se(IV) and Pb(II)/Se(IV) bi-solute systems are needed to determine if any ternary surface complexes form on goethite, and if so, what their coordination environment is.

Finally, the methodology developed in this work for CD-MUSIC could be applied to more simplistic models such as the triple layer surface complexation model and the diffuse layer model. While such models would not provide the accuracy that CD-MUSIC does, the methodology could be employed to determine the N_S parameter used in these

models; thereby reducing the number of adjustable parameters required to run these SCMs.

APPENDIX

One of the primary limitations of the titration congruency method is that the goethite of interest's proton reactive site coverage can depart from that of the ideal goethite sample as the proportion of crystal faces contributing to the surface changes. To illustrate this point, consider the titration of a solid – solution system where goethite is the solid, and the solution consists of water with a 1:1 background electrolyte dissolved in it (Table A.1).

Table A.1 Tableau for a solid – solution system being titrated using the CD-MUSIC model

		Components				
		H^+	$\equiv FeOH_{3/2}$	$\equiv Fe_3OH_{1/2}$	Cation	Anion
Species	H+	1				
	OH-	-1				
	Cation				1	
	Anion					1
	$\equiv FeOH^{-0.5}$	-0.5	1			
	$\equiv FeOH_2^{+0.5}$	0.5	1			
	≡FeOH_Cat	-0.5	1		1	
	$\equiv FeOH_2$_An	0.5	1			1
	$\equiv Fe_3O^{-0.5}$	-0.5		1		
	$\equiv Fe_3OH^{+0.5}$	0.5		1		
	$\equiv Fe_3O$_Cat	-0.5		1	1	
	$\equiv Fe_3OH$_An	0.5		1		1
Added To Solution	Strong Acid	1				1
	Strong Base	-1			1	
	Salt				1	1
	$\equiv FeOH_{3/2}$		1			
	$\equiv Fe_3OH_{1/2}$			1		

The solid in this case is goethite and the solution is water containing a 1:1 background electrolyte. All surface species have a ≡ symbol preceding the species chemical formula. ≡FeOH_Cat and ≡FeOH_An represent outer-sphere surface complexes formed between a singly coordinated surface site and the background electrolyte's cation and anion, respectively. $\equiv Fe_3O$_Cat and $\equiv Fe_3OH$_An represent the same thing except the outer-sphere complex is forming at triply coordinated surface sites rather than singly coordinated ones. The two surface components used in this Tableau approach are $\equiv FeOH_{3/2}$ and $\equiv Fe_3OH_{1/2}$. These two surface components are both hypothetical but necessary, because of their charge neutrality, when looking at surface charge through the lens of the MUSIC model. Before the mineral solid is added to the solution, it is neutral (assuming no isomorphic substitution has taken place); therefore the surface components selected must result in a net charge of zero being added to solution. This is analogous to the salt (e.g. $NaNO_3$, NaCl) that is added to the system to provide a background electrolyte. The salt cannot be charged; it is a neutral compound prior to entering the solution. This must also be true in the case of goethite being added to solution.

Table A.1 is an example of the tableau method that can be used for describing chemical reactions in aquatic systems by means of a tabular format [188]. The components listed under the row labeled "Components" are independent of each other and are used to define the reference state of the system. All chemical species present in or added to the system (labeled "species" or "added to solution", respectively) are formed using a combination of the components listed at the top of the table. For example, the species $\equiv Fe_3OH\_An$ is formed using the following combination of components: $\equiv Fe_3OH_{1/2} + ½\ H^+ + An^-$. From the tableau method/table, a proton balance equation termed TOTH can be created that calculates the number of protons present in the system relative to the reference components used in describing the system. Using Table A.1, TOTH can be expressed as Equation A.1:

$$\begin{aligned} TOTH = C_A - C_B = [H^+] - [OH^-] + ½\ [(\equiv FeOH_2^{+1/2}) - (\equiv FeOH^{-1/2}) + (\equiv FeOH_2\_An) - (\equiv FeOH\_Cat) \\ + (\equiv Fe_3OH^{+1/2}) - (\equiv Fe_3O^{-1/2}) + (\equiv Fe_3OH\_An) - (\equiv Fe_3O\_Cat)] \end{aligned} \quad (A.1)$$

where C_A and C_B are the concentrations of acid and base added to the system, respectively (mol/L), and . When Equation A.1, is rearranged it yields the net protons adsorbed (NPA), in units of mol/L, written here as Equations A.2 and A.3

$$NPA = C_A - C_B - [H^+] + [OH^-] \quad (A.2)$$

$$\text{NPA} = \tfrac{1}{2}\left[(\equiv FeOH_2^{+1/2}) - (\equiv FeOH^{-1/2}) + (\equiv FeOH_2\_An) - (\equiv FeOH\_Cat) + (\equiv Fe_3OH^{+1/2}) - (\equiv Fe_3O^{-1/2}) + (\equiv Fe_3OH\_An) - (\equiv Fe_3O\_Cat)\right] \quad \text{(A.3)}$$

For simplicity, interactions between background electrolytes and surface sites will not be considered in this example. Hence, Equation A.3 reduces down to Equation A.4.

$$\text{NPA} = \tfrac{1}{2}\left[(\equiv FeOH_2^{+1/2}) - (\equiv FeOH^{-1/2}) + (\equiv Fe_3OH^{+1/2}) - (\equiv Fe_3O^{-1/2})\right] \quad \text{(A.4)}$$

Under the simplifying assumption that interactions between electrolytes and surface sites can be ignored, there are only two surface complexation reactions that need to be considered at a given pH. These two reactions and their respective mass law expressions are presented in Equations A.5 - A.8:

$$\equiv FeOH^{-0.5} + H^+ \leftrightarrow \equiv FeOH_2^{+0.5} \quad \text{(A.5)}$$

$$K_1 = \frac{X_{\equiv FeOH2}}{X_{\equiv FeOH}\{H^+\}} \quad \text{(A.6)}$$

$$\equiv Fe_3O^{-0.5} + H^+ \leftrightarrow \equiv Fe_3OH^{+0.5} \quad \text{(A.7)}$$

$$K_2 = \frac{X_{\equiv Fe_3OH}}{X_{\equiv Fe_3O}\{H^+\}} \quad \text{(A.8)}$$

where ≡FeOH and $\equiv Fe_3O$ represent singly and triply coordinated surface functional groups present on goethite, respectively, K_1 and K_2 are equilibrium constants that take into account both the chemical and electrical energy of the protonation reaction on a singly and triply coordinated site, respectively. It is important to note that in this

example, the K_1 equilibrium constant for singly coordinated sites is assumed to be the same value for all singly coordinated sites, regardless of which crystal face the sites are located on. This same assumption is also applied to K_2 and all triply coordinated sites.

At a given pH value, the activity of H^+ is constant, so Equation A.6 can be simplified to Equation A.9.

$$K_1\{H^+\} = K_1^{'} = \frac{X_{\equiv FeOH_2^+}}{X_{\equiv FeOH}} \tag{A.9}$$

Performing a site balance and rearranging terms

$$X_{\equiv FeOH,TOT} = 1 = X_{\equiv FeOH} + X_{\equiv FeOH_2^+} \tag{A.10}$$

$$X_{\equiv FeOH} = 1 - X_{\equiv FeOH_2^+} \tag{A.11}$$

Inserting Equation A.11 into Equation A.9 and rearranging terms results in Equation A.12.

$$X_{\equiv FeOH_2^+} = \frac{K_1^{'}}{1 + K_1^{'}} \tag{A.12}$$

Converting $X_{\equiv FeOH2+}$ from a mole fraction to concentration units of mol/L, yields Equation A.13:

$$X_{\equiv FeOH_2^+} = \frac{\left[\equiv FeOH_2^{+0.5}\right]}{[\equiv FeOH]_{TOT}} \tag{A.13}$$

where $[FeOH_2^{+0.5}]$ is the concentration of protonated singly coordinated surface sites and $[FeOH]_{TOT}$ is the concentration of all singly coordinated sites, both expressed in units of mol/L. Applying Equation A.13 to Equation A.12and rearranging yields Equation A.14.

$$\left[\equiv FeOH_2^{+0.5}\right] = \left(\frac{K_1^{'}}{1 + K_1^{'}}\right)[\equiv FeOH]_{TOT} \tag{A.14}$$

Revisiting Equation A.9 and solving for $X_{\equiv FeOH}$ results in Equation A.15.

$$X_{\equiv FeOH} = \frac{X_{\equiv FeOH_2^+}}{K_1^{'}} \tag{A.15}$$

Converting $X_{\equiv FeOH}$ from a mole fraction to concentration units of mol/L

$$X_{\equiv FeOH} = \frac{[\equiv FeOH^{-0.5}]}{[\equiv FeOH]_{TOT}} \tag{A.16}$$

Substituting Equation A.13and Equation A.16 into Equation A.15 results in Equation A.17.

$$[\equiv FeOH^{-0.5}] = \frac{\left[\equiv FeOH_2^{+0.5}\right]}{K_1^{'}} \tag{A.17}$$

Inserting Equation A.14 into Equation A.17

$$[\equiv FeOH^{-0.5}] = \left(\frac{1}{1 + K_1^{'}}\right)[\equiv FeOH]_{TOT} \tag{A.18}$$

Applying the same approach to goethite's triply coordinated sites, described by Equation A.7 and Equation A.8, will yield Equation A.19 and A.20.

$$[\equiv Fe_3OH^{+0.5}] = \left(\frac{K_2^{'}}{1 + K_2^{'}}\right)[\equiv Fe_3O]_{TOT} \tag{A.19}$$

$$[\equiv Fe_3O^{-0.5}] = \left(\frac{1}{1 + K_2^{'}}\right)[\equiv Fe_3O]_{TOT} \tag{A.20}$$

Applying Equation A.14, Equation A.18, Equation A.19, and Equation A.20 to Equation A.4 and recalling that the titration congruency method measures net protons adsorbed (NPA) divided by the total number of proton reactive sites (PRS) results in Equation A.21 and A.22:

$$\frac{NPA}{PRS} = \left(\frac{1}{2}\right)\left(\frac{\left[\equiv FeOH_2^{+0.5}\right] - \left[\equiv FeOH^{-0.5}\right] + \left[\equiv Fe_3OH^{+0.5}\right] - \left[\equiv Fe_3O^{-0.5}\right]}{[\equiv FeOH]_{TOT} + [\equiv Fe_3O]_{TOT}}\right) \quad \text{(A.21)}$$

$$\frac{NPA}{PRS} = \left(\frac{1}{2}\right)\left[\frac{\left(\frac{[\equiv FeOH]_{TOT}}{1+K_1'}\right)(K_1' - 1) + \left(\frac{[\equiv Fe_3O]_{TOT}}{1+K_2'}\right)(K_2' - 1)}{[\equiv FeOH]_{TOT} + [\equiv Fe_3O]_{TOT}}\right] \quad \text{(A.22)}$$

where both NPA and PRS are expressed in units of mol/L.

In the titration congruency method, the NPA/PRS ratio is plotted against pH. First, using the titration data from an ideal goethite sample (i.e. GOE94 or HVR94) with a known CFC, the NPA/PRS ratio vs. pH can be plotted for the ideal goethite preparation. Next, the titration data for a second goethite sample, a sample with an unknown CFC, is plotted in the same manner as the ideal goethite sample. The N_H for this second goethite sample is then adjusted until the two plots align. The N_H value that results in these two plots aligning is deemed the true N_H value for the goethite of interest and can be used to calculate the sample's CFC.

Expanding out the $[\equiv FeOH]_{TOT}$ and $[\equiv Fe_3O]_{TOT}$ terms yields Equations A.23 and A.24:

$$[\equiv FeOH]_{TOT} = \frac{\left(N_{s,\equiv FeOH}\right)(10^{18})(SSA)(C_s)}{N_A} \quad \text{(A.23)}$$

$$[\equiv Fe_3O]_{TOT} = \frac{(N_{s,\equiv Fe_3O})(10^{18})(SSA)(C_s)}{N_A} \quad \text{(A.24)}$$

where $N_{s,\equiv FeOH}$ and $N_{s,\equiv Fe3O}$ are the site densities of singly and triply coordinated sites, respectively, in units of sites·nm^{-2}, 10^{18} is the conversion factor from nm^2 to m^2, SSA is in units of m^2·g^{-1}, Cs is the solid's concentration in units of g·L^{-1}, and N_A is Avogadro's number ($6.023 \cdot 10^{23}$).

Consolidating the constants from Equation A.22

$$K_1'' = \left(\frac{K_1' - 1}{1 + K_1'}\right) \quad \text{(A.25)}$$

$$K_2'' = \left(\frac{K_2' - 1}{1 + K_2'}\right) \quad \text{(A.26)}$$

Substituting Equation A.23 - A.26 into Equation A.22 will result in Equation A.27.

$$\frac{NPA}{PRS} = \left(\frac{1}{2}\right)\left[\frac{(K_1'')(N_{s,\equiv FeOH}) + (K_2'')(N_{s,\equiv Fe_3O})}{N_{s,\equiv FeOH} + N_{s,\equiv Fe_3O}}\right] \quad \text{(A.27)}$$

To better understand the limitations of the titration congruency method, consider the ratio between $N_{s,\equiv FeOH}$ and $N_{s,\equiv Fe3O}$.

$$R_{N_s} = \frac{N_{s,\equiv FeOH}}{N_{s,\equiv Fe_3O}} \tag{A.28}$$

When the ratio from Equation A.28is substituted into Equation A.27, Equation A.29 will result.

$$\frac{NPA}{PRS} = \left(\frac{1}{2}\right)\left[\frac{\left(K_1''\right)R_{N_s} + \left(K_2''\right)}{R_{N_s} + 1}\right] \tag{A.29}$$

The titration congruency method is based on the idea that at a given pH, the NPA/PRS ratio has the same value regardless of the goethite sample under consideration. Equation A.29 however, illustrates the problem with this idea. Assuming that for a given pH and ionic strength the values of K_1'' and K_2'' are the same for all goethite samples, Equation A.29 demonstrates that at a given pH, the NPA/PRS ratio will change as the ratio between $N_{s,\equiv FeOH}$ and $N_{s,\equiv Fe3O}$ varies between the ideal goethite and the goethite of interest. In other words, if the goethite of interest's R_{Ns} varies from that of the ideal goethite sample, then at a given pH, the NPA/PRS ratio will not be equivalent between the two samples and hence their plots of NPA/PRS vs. pH will diverge to some degree.

REFERENCES

1. Barron, V., et al., Epitaxial overgrowth of goethite on hematite synthesized in phosphate media: a scanning force and transmission electron microscopy study. Am. Mineral., 1997. **82**, p. 1091-1100.

2. Dzombak, D.A. and F.M.M. Morel, Surface complexation modeling : hydrous ferric oxide. 1990, New York: Wiley. xvii, 393 p.

3. Hochella, M.F., Jr., Mineral–water interface geochemistry. Reviews in Mineralogy, 1990. **23**: p. 1 - 15.

4. Stumm, W. and J.J. Morgan, Aquatic Chemistry : Chemical Equilibria and Rates in Natural Waters. 3rd ed. 1996, New York: Wiley. xvi, 1022 p.

5. Honeyman, B.D. and J.O. Leckie, Macroscopic partitioning coefficients for metal ion adsorption. Proton stoichiometry at variable pH and adsorption density. ACS Symp. Ser., 1986. **323**, p. 162-90.

6. Davis, J.A. and D.B. Kent, Surface complexation modeling in aqueous geochemistry. Rev. Mineral., 1990. **23**, p. 176-260.

7. Davis, J.A., et al. Influence of redox environment and aqueous speciation on metal transport in groundwater: preliminary results of trace injection studies. Lewis, 1993.

8. Honeyman, B.D. and P.H. Santschi, Metals in aquatic systems. Environ. Sci. Technol., 1988. **22**, p. 862-71.

9. Kent, D.B., et al., Surface-complexation modeling of radionuclide adsorption in subsurface environments, 1988, 128 p.

10. Dugger, D.L., et al., The exchange of twenty metal ions with the weakly acidic silanol group of silica gel 1,2. The Journal of Physical Chemistry, 1964. **68**, p. 757-760.

11. Schindler, P.W., et al., Ligand properties of surface silanol groups. I. Surface complex formation with iron(3+), copper(2+), cadmium(2+), and lead(2+). J. Colloid Interface Sci., 1976. **55**, p. 469-75.

12. Stumm, W., R. Kummert, and L. Sigg, A ligand exchange model for the adsorption of inorganic and organic ligands at hydrous oxide interfaces. Croat. Chem. Acta, 1980. **53**, p. 291-312.

13. Sposito, G., The Surface Chemistry of Soils. 1984, Oxford Univ. Press, 304 p.

14. Sposito, G., The Chemistry of Soils. 2nd ed. 2008, Oxford University Press, 344 p.

15. James, R.O. and G.A. Parks, Characterization of aqueous colloids by their electrical double layer and intrinsic surface chemical properties. Surf. Colloid Sci., 1982. **12**, p. 119-216.

16. Chapman, D.L., A contribution to the theory of electrocapillarity. Philosophical Magazine Series 6, 1913. **25**, p. 475-481.

17. Gouy, L.G., Constitution of the electric charge at the surface of an electrolyte. J. physique, 1910. **9**, p. 457-467.

18. Guggenheim, E.A., Conceptions of electric potential differences between two phases and the individual activities of ions. J. Phys. Chem., 1929. **33**, p. 842-849.

19. Guggenheim, E.A., The conception of electrical potential difference between two phases. II. J. Phys. Chem., 1930. **34**, p. 1540-1543.

20. Chan, D., et al., Regulation of surface potential at amphoteric surfaces during particle-particle interaction. J. Chem. Soc., Faraday Trans. 1, 1975. **71**, p. 1046-57.

21. Herbelin, A.L. and J.C. Westall, FITEQL 4.0: A computer program for determination of chemical equilibrium constants from experimental data; Report 99-01, 1999, Department of Chemistry, Oregon State University, Corvalis

22. Gustafsson, J.P. Implementation of CD-MUSIC in FITEQL 4.0 2003 September 2, 2003. Available from: http://www2.lwr.kth.se/forskningsprojekt/mow/fiteql.htm.

23. Hiemstra, T. and W.H. Van Riemsdijk, A surface structural approach to ion adsorption: the charge distribution (CD) model. J. Colloid Interface Sci., 1996. **179**, p. 488-508.

24. Hiemstra, T., W.J.C.M. De, and W.H. Van Riemsdijk, Multisite proton adsorption modeling at the solid/solution interface of (hydr)oxides: a new approach. II. Application to various important (hydr)oxides. J. Colloid Interface Sci., 1989. **133**, p. 105-117.

25. Hiemstra, T., W.H. Van Riemsdijk, and G.H. Bolt, Multisite proton adsorption modeling at the solid/solution interface of (hydr)oxides: a new approach. I. Model description and evaluation of intrinsic reaction constants. J. Colloid Interface Sci., 1989. **133**, p. 91-104.

26. Hiemstra, T., P. Venema, and W.H. Van Riemsdijk, Intrinsic proton affinity of reactive surface groups of metal (hydr)oxides: the bond valence principle. J. Colloid Interface Sci., 1996. **184**, p. 680-692.

27. Venema, P., T. Hiemstra, and W.H. Van Riemsdijk, Multisite adsorption of cadmium on goethite. J. Colloid Interface Sci., 1996. **183**, p. 515-527.

28. Venema, P., T. Hiemstra, and W.H. Van Riemsdijk, Interaction of Cadmium with Phosphate on Goethite. Journal of Colloid and Interface Science, 1997. **192**, p. 94-103.

29. Venema, P., et al., Intrinsic proton affinity of reactive surface groups of metal (hydr)oxides: application to iron (hydr)oxides. J. Colloid Interface Sci., 1998. **198**, p. 282-295.

30. Rietra, R.P.J.J., T. Hiemstra, and W.H. Van Riemsdijk, Sulfate adsorption on goethite. J. Colloid Interface Sci., 1999. **218**, p. 511-521.

31. Rietra, R.P.J.J., T. Hiemstra, and W.H. Van Riemsdijk, Interaction between Calcium and Phosphate Adsorption on Goethite. Environ. Sci. Technol., 2001. **35**, p. 3369-3374.

32. Hiemstra, T., R. Rahnemaie, and W.H. Van Riemsdijk, Surface complexation of carbonate on goethite: IR spectroscopy, structure and charge distribution. J. Colloid Interface Sci., 2004. **278**, p. 282-290.

33. Ponthieu, M., et al., Metal ion binding to iron oxides. Geochim. Cosmochim. Acta, 2006. **70**, p. 2679-2698.

34. Hiemstra, T., R.P.J.J. Rietra, and W.H. Van Riemsdijk, Surface complexation of selenite on goethite: MO/DFT geometry and charge distribution. Croat. Chem. Acta, 2007. **80**, p. 313-324.

35. Rahnemaie, R., T. Hiemstra, and W.H. Van Riemsdijk, Carbonate adsorption on goethite in competition with phosphate. J. Colloid Interface Sci., 2007. **315**, p. 415-425.

36. Hiemstra, T., et al., A surface structural model for ferrihydrite II: Adsorption of uranyl and carbonate. Geochim. Cosmochim. Acta, 2009. **73**, p. 4437-4451.

37. Rahnemaie, R., T. Hiemstra, and W.H. Van Riemsdijk, Inner- and outer-sphere complexation of ions at the goethite-solution interface. J Colloid Interface Sci, 2006. **297**, p. 379-388.

38. Hiemstra, T., M.O. Barnett, and W.H. Van Riemsdijk, Interaction of silicic acid with goethite. J. Colloid Interface Sci., 2007. **310**, p. 8-17.

39. Spadini, L., et al., Structure and stability of Cd2+ surface complexes on ferric oxides. 1. Results from EXAFS spectroscopy. J. Colloid Interface Sci., 1994. **168**, p. 73-86.

40. Randall, S.R., et al., The mechanism of cadmium surface complexation on iron oxyhydroxide minerals. Geochim. Cosmochim. Acta, 1999. **63**, p. 2971-2987.

41. Waychunas, G.A., et al., Surface chemistry of ferrihydrite: Part 1. EXAFS studies of the geometry of coprecipitated and adsorbed arsenate. Geochimica Et Cosmochimica Acta, 1993. **57**, p. 2251-2269.

42. Fendorf, S., et al., Arsenate and Chromate Retention Mechanisms on Goethite. 1. Surface Structure. Environ. Sci. Technol., 1997. **31**, p. 315-320.

43. Manning, B.A., S.E. Fendorf, and S. Goldberg, Surface Structures and Stability of Arsenic(III) on Goethite: Spectroscopic Evidence for Inner-Sphere Complexes. Environmental Science & Technology, 1998. **32**, p. 2383-2388.

44. Ona-Nguema, G., et al., EXAFS analysis of arsenite adsorption onto two-line ferrihydrite, hematite, goethite, and lepidocrocite. Environmental Science & Technology, 2005. **39**, p. 9147-9155.

45. Hayes, K.F., et al., In situ x-ray absorption study of surface complexes: selenium oxyanions on goethite (α-FeOOH). Science, 1987. **238**, p. 783-786.

46. Manceau, A. and L. Charlet, The mechanism of selenate adsorption on goethite and hydrous ferric oxide. J. Colloid Interface Sci., 1994. **168**, p. 87-93.

47. Su, C. and D.L. Suarez, Selenate and selenite sorption on iron oxides: an infrared and electrophoretic study. Soil Sci. Soc. Am. J., 2000. **64**, p. 101-111.

48. Bargar, J.R., et al., Outer-sphere Pb(II) adsorbed at specific surface sites on single crystal α-alumina. Geochim. Cosmochim. Acta, 1996. **60**, p. 3541-3547.

49. Bargar, J.R., G.E. Brown, Jr., and G.A. Parks, Surface complexation of Pb(II) at oxide-water interfaces: II. XAFS and bond-valence determination of mononuclear Pb(II) sorption products and surface functional groups on iron oxides. Geochim. Cosmochim. Acta, 1997. **61**, p. 2639-2652.

50. Bargar, J.R., G.E. Brown, Jr., and G.A. Parks, Surface complexation of Pb(II) at oxide-water interfaces: I. XAFS and bond-valence determination of mononuclear and polynuclear Pb(II) sorption products on aluminum oxides. Geochim. Cosmochim. Acta, 1997. **61**, p. 2617-2637.

51. Bargar, J.R., et al., XAFS and bond-valence determination of the structures and compositions of surface functional groups and Pb(II) and Co(II) sorption products on single-crystal α-Al2O3. J. Colloid Interface Sci., 1997. **185**, p. 473-492.

52. Bargar, J.R., G.E. Brown, Jr., and G.A. Parks, Surface complexation of Pb(II) at oxide-water interfaces: III. XAFS determination of Pb(II) and Pb(II)-chloro adsorption complexes on goethite and alumina. Geochim. Cosmochim. Acta, 1998. **62**, p. 193-207.

53. Ostergren, J.D., et al., Inorganic Ligand Effects on Pb(II) Sorption to Goethite (α-FeOOH): II. Sulfate. Journal of Colloid and Interface Science, 2000. **225**, p. 483-493.

54. Ostergren, J.D., et al., Inorganic ligand effects on Pb(II) sorption to goethite (α-FeOOH) I. Carbonate. J. Colloid Interface Sci., 2000. **225**, p. 466-482.

55. Trivedi, P., J.A. Dyer, and D.L. Sparks, Lead sorption onto ferrihydrite. 1. A macroscopic and spectroscopic assessment. Environ. Sci. Technol., 2003. **37**, p. 908-914.

56. Huang, C.-P. and W. Stumm, Specific adsorption of cations on hydrous γ-aluminum oxide. J. Colloid Interface Sci., 1973. **43**, p. 409-20.

57. Stumm, W., C.P. Huang, and S.R. Jenkins, Specific chemical interaction affecting the stability of dispersed systems. Croat. Chem. Acta, 1970. **42**, p. 223-45.

58. Hohl, H. and W. Stumm, Interaction of lead(2+) with hydrous γ-alumina. J. Colloid Interface Sci., 1976. **55**, p. 281-288.

59. Schindler, P. and H.R. Kamber, Acidity of silanol groups. Helv. Chim. Acta, 1968. **51**, p. 1781-1786.

60. Schindler, P.W. and H. Gamsjaeger, Acid-base reactions of the titanium dioxide (anatase)-water interface and the point of zero charge of titanium dioxide suspensions. Kolloid-Z. Z. Polym., 1972. **250**, p. 759-63.

61. Stumm, W., H. Hohl, and F. Dalang, Interaction of metal ions with hydrous oxide surfaces. Croat. Chem. Acta, 1976. **48**, p. 491-504.

62. Davis, J.A., R.O. James, and J.O. Leckie, Surface ionization and complexation at the oxide/water interface. I. Computation of electrical double layer properties in simple electrolytes. J. Colloid Interface Sci., 1978. **63**, p. 480-499.

63. Davis, J.A. and J.O. Leckie, Surface ionization and complexation at the oxide/water interface. 2. Surface properties of amorphous iron oxyhydroxide and adsorption of metal ions. J. Colloid Interface Sci., 1978. **67**, p. 90-107.

64. Davis, J.A. and J.O. Leckie, Surface ionization and complexation at the oxide/water interface. 3. Adsorption of anions. J. Colloid Interface Sci., 1980. **74**, p. 32-43.

65. Blesa, M.A., A.J.G. Maroto, and A.E. Regazzoni, Boric acid adsorption on magnetite and zirconium dioxide. J. Colloid Interface Sci., 1984. **99**, p. 32-40.

66. Hayes, K.F. and J.O. Leckie, Mechanism of lead ion adsorption at the goethite-water interface. ACS Symp. Ser., 1986. **323**, p. 114-141.

67. Hayes, K.F. and J.O. Leckie, Modeling ionic strength effects on cation adsorption at hydrous oxide/solution interfaces. J. Colloid Interface Sci., 1987. **115**, p. 564-572.

68. Hayes, K.F., C. Papelis, and J.O. Leckie, Modeling ionic strength effects on anion adsorption at hydrous oxide/solution interfaces. J. Colloid Interface Sci., 1988. **125**, p. 717-726.

69. Barrow, N.J. and V.C. Cox, The effects of pH and chloride concentration on mercury sorption. I. By goethite. J. Soil Sci., 1992. **43**, p. 295-304.

70. Collins, C.R., D.M. Sherman, and K.V. Ragnarsdottir, Surface complexation of Hg2+ on goethite: mechanism from EXAFS spectroscopy and density functional calculations. J. Colloid Interface Sci., 1999. **219**, p. 345-350.

71. Kim, C.S., J.J. Rytuba, and G.E. Brown, EXAFS study of mercury(II) sorption to Fe- and Al-(hydr)oxides I. Effects of pH. J. Colloid Interface Sci., 2004. **271**, p. 1-15.

72. Kim, C.S., J.J. Rytuba, and G.E. Brown, EXAFS study of mercury(II) sorption to Fe- and Al-(hydr)oxides II. Effects of chloride and sulfate. J. Colloid Interface Sci., 2004. **270**, p. 9-20.

73. Bargar, J.R., et al., ATR-FTIR spectroscopic characterization of coexisting carbonate surface complexes on hematite. Geochimica Et Cosmochimica Acta, 2005. **69**, p. 1527-1542.

74. Villalobos, M. and J.O. Leckie, Carbonate adsorption on goethite under closed and open CO2 conditions. Geochimica Et Cosmochimica Acta, 2000. **64**,: p. 3787-3802.

75. Villalobos, M. and J.O. Leckie, Surface complexation modeling and FTIR study of carbonate adsorption to goethite. J. Colloid Interface Sci., 2001. **235**, p. 15-32.

76. Wijnja, H. and C.P. Schulthess, Carbonate adsorption mechanism on goethite studied with ATR-FTIR, DRIFT, and proton coadsorption measurements. Soil Sci. Soc. Am. J., 2001. **65**, p. 324-330.

77. Chen, C.-C., Characterization of surface hydroxyl and fixed-charge surface sites for trace metal sorption in mineral systems. 2000. University of Michigan at Ann Arbor.

78. Manceau, A., et al., Influence of anionic layer structure of Fe-oxyhydroxides on the structure of Cd surface complexes. J. Colloid Interface Sci., 2000. **228**, p. 306-316.

79. Anderson, M.A. and A.J. Rubin, Adsorption of Inorganics at Solid-Liquid Interfaces. 1981: Ann Arbor Science, 357 p.

80. Hingston, F.J., A.M. Posner, and J.P. Quirk, Anion adsorption by goethite and gibbsite. I. Role of the proton in determining adsorption envelopes. J. Soil Sci., 1972. **23**, p. 177-192.

81. Parfitt, R.L. and J.D. Russell, Adsorption on hydrous oxides. IV. Mechanisms of adsorption of various ions on goethite. J. Soil Sci., 1977. **28**, p. 297-305.

82. Villalobos, M. and A. Perez-Gallegos, Goethite surface reactivity: A macroscopic investigation unifying proton, chromate, carbonate, and lead(II) adsorption. J. Colloid Interface Sci., 2008. **326**, p. 307-323.

83. Bonnissel-Gissinger, P., et al., Modeling the adsorption of mercury(II) on (Hydr)oxides II. α-FeOOH (goethite) and amorphous silica. J. Colloid Interface Sci., 1999. **215**, p. 313-322.

84. Salazar-Camacho, C. and M. Villalobos, Goethite surface reactivity: III. Unifying arsenate adsorption behavior through a variable crystal face - site density model. Geochim. Cosmochim. Acta, 2010. **74**, p. 2257-2280.

85. Villalobos, M., M.A. Cheney, and J. Alcaraz-Cienfuegos, Goethite surface reactivity: II. A microscopic site-density model that describes its surface area-normalized variability. J. Colloid Interface Sci., 2009. **336**, p. 412-422.

86. Rahnemaie, R., T. Hiemstra, and W.H. Van Riemsdijk, A new surface structural approach to ion adsorption: tracing the location of electrolyte ions. J Colloid Interface Sci, 2006. **293,** p. 312-321.

87. Kanematsu, M., et al., Arsenic(III, V) adsorption on a goethite-based adsorbent in the presence of major co-existing ions: Modeling competitive adsorption consistent with spectroscopic and molecular evidence. Geochim. Cosmochim. Acta, 2013. **106**, p. 404-428.

88. Ridley, M.K., et al., Calcium adsorption at the rutile-water interface: a potentiometric study in NaCl media to 250°C. Geochim. Cosmochim. Acta, 1999. **63**, p. 3087-3096.

89. Ali, M.A. and D.A. Dzombak, Competitive sorption of simple organic acids and sulfate on goethite. Environ. Sci. Technol., 1996. **30**, p. 1061-1071.

90. Sverjensky, D.A., Prediction of the speciation of alkaline earths adsorbed on mineral surfaces in salt solutions. Geochim. Cosmochim. Acta, 2006. **70**, p. 2427-2453.

91. Sverjensky, D.A. and K. Fukushi, Anion adsorption on oxide surfaces: Inclusion of the water dipole in modeling the electrostatics of ligand exchange. Environ. Sci. Technol., 2006. **40**, p. 263-271.

92. Vieira, A.R., Surface complexation modeling of Pb(II), Cd(II) and Se(IV) onto iron hydroxides in single and bisolute systems. 2006. The University of Texas at Austin.

93. Hiemstra, T. and W.H. Van Riemsdijk, On the relationship between charge distribution, surface hydration, and the structure of the interface of metal hydroxides. J Colloid Interface Sci, 2006. **301**, p. 1-18.

94. Sprycha, R., Surface charge and adsorption of background electrolyte ions at anatase/electrolyte interface. J. Colloid Interface Sci., 1984. **102**, p. 173-185.

95. Sprycha, R., Electrical double layer at alumina/electrolyte interface. II. Adsorption of supporting electrolyte ions. J. Colloid Interface Sci., 1989. **127**, p. 12-25.

96. Yates, D.E., S. Levine, and T.W. Healy, Site-binding model of the electrical double layer at the oxide/water interface. Journal of the Chemical Society, Faraday Transactions 1: Physical Chemistry in Condensed Phases, 1974. **70**, p. 1807-1818.

97. Hiemstra, T. and W.H. Van Riemsdijk, A surface structural model for ferrihydrite I: Sites related to primary charge, molar mass, and mass density. Geochim. Cosmochim. Acta, 2009. **73**, p. 4423-4436.

98. Rahnemaie, R., T. Hiemstra, and W.H. Van Riemsdijk, Geometry, charge distribution, and surface speciation of phosphate on goethite. Langmuir, 2007. **23**, p. 3680-3689.

99. Gaboriaud, F. and J.-J. Ehrhardt, Effects of different crystal faces on the surface charge of colloidal goethite ([alpha]-FeOOH) particles: an experimental and modeling study. Geochimica Et Cosmochimica Acta, 2003. **67,** p. 967-983.

100. Pauling, L., The principles determining the structure of complex ionic crystals. J. Am. Chem. Soc., 1929. **51**, p. 1010-1026.

101. Sverjensky, D.A., Prediction of surface charge on oxides in salt solutions: Revisions for 1:1 (M+L-) electrolytes. Geochimica Et Cosmochimica Acta, 2005. **69**, p. 225-257.

102. Hiemstra, T. and W.H. Van Riemsdijk, Surface structural ion adsorption modeling of competitive binding of oxyanions by metal (hydr)oxides. J. Colloid Interface Sci., 1999. **210**, p. 182-193.

103. Stachowicz, M., T. Hiemstra, and W.H. Van Riemsdijk, Multi-competitive interaction of As(III) and As(V) oxyanions with Ca2+, Mg2+, PO3-4, and CO2-3 ions on goethite. J. Colloid Interface Sci., 2008. **320**, p. 400-414.

104. Swedlund, P.J., J.G. Webster, and G.M. Miskelly, Goethite adsorption of Cu(II), Pb(II), Cd(II), and Zn(II) in the presence of sulfate: Properties of the ternary complex. Geochim. Cosmochim. Acta, 2009. **73**, p. 1548-1562.

105. Villalobos, M., M.A. Trotz, and J.O. Leckie, Surface complexation modeling of carbonate effects on the adsorption of Cr(VI), Pb(II), and U(VI) on goethite. Environ. Sci. Technol., 2001. **35**, p. 3849-3856.

106. Christl, I. and R. Kretzschmar, Competitive sorption of copper and lead at the oxide-water interface: Implications for surface site density. Geochimica Et Cosmochimica Acta, 1999. **63**, p. 2929-2938.

107. Criscenti, L.J. and D.A. Sverjensky, A single-site model for divalent transition and heavy metal adsorption over a range of metal concentrations. Journal of Colloid and Interface Science, 2002. **253**, p. 329-352.

108. Criscenti, L.J. and D.A. Sverjensky, The role of electrolyte anions (ClO4-, NO3-, and Cl-) in divalent metal (M2+) adsorption on oxide and hydroxide surfaces in salt solutions. Am. J. Sci., 1999. **299**, p. 828-899.

109. Swedlund, P.J. and J.G. Webster, Cu and Zn ternary surface complex formation with SO4 on ferrihydrite and schwertmannite. Applied Geochemistry, 2001. **16**, p. 503-511.

110. Robertson, A.P. and J.O. Leckie, Acid/base, copper binding, and Cu2+/H+ exchange properties of goethite, an experimental and modeling study. Environ. Sci. Technol., 1998. **32**, p. 2519-2530.

111. Lumsdon, D.G. and L.J. Evans, Surface complexation model parameters for Goethite (α-FeOOH). J. Colloid Interface Sci., 1994. **164**, p. 119-125.

112. Cornell, R.M. and R. Giovanoli, Factors that govern the formation of multi-domainic goethites. Clays Clay Miner., 1986. **34**, p. 557-564.

113. Cornell, R.M., U. Schwertmann, and Editors, The Iron Oxides: Structure, Properties, Reactions, Occurrence and Uses. 1996, VCH. 573 p.

114. Weidler, P.G., T. Schwinn, and H.E. Gaub, Vicinal faces on synthetic goethite observed by atomic force microscopy. Clays Clay Miner., 1996. **44**, p. 437-442.

115. Yates, D.E., The structure of the oxide/aqueous electrolyte Interface. 1975.

116. Sahai, N. and D.A. Sverjensky, Solvation and electrostatic model for specific electrolyte adsorption. Geochimica Et Cosmochimica Acta, 1997. **61**, p. 2827-2848.

117. Hawke, D., P.D. Carpenter, and K.A. Hunter, Competitive adsorption of phosphate on goethite in marine electrolytes. Environ. Sci. Technol., 1989. **23**, p. 187-191.

118. Lutzenkirchen, J., et al., Protonation of different goethite surfaces--Unified models for NaNO3 and NaCl media. J Colloid Interface Sci, 2008. **317**, p. 155-165.

119. Sahai, N. and D.A. Sverjensky, Evaluation of internally consistent parameters for the triple-layer model by the systematic analysis of oxide surface titration data. Geochimica Et Cosmochimica Acta, 1997. **61**, p. 2801-2826.

120. Weng, L.P., et al., Interactions of calcium and fulvic acid at the goethite-water interface. Geochimica Et Cosmochimica Acta, 2005. **69**, p. 325-339.

121. Hayes, K.F., et al., Surface complexation models: an evaluation of model parameter estimation using FITEQL and oxide mineral titration data. J. Colloid Interface Sci., 1991. **142**, p. 448-469.

122. Dixit, S. and J.G. Hering, Comparison of arsenic(V) and arsenic(III) sorption onto iron oxide minerals: implications for arsenic mobility. Environmental Science & Technology, 2003. **37**, p. 4182-4189.

123. Chen, H.-w., C.C. Davis, and M. Edwards, Using surface complexation modeling to assess the role of silica in arsenate adsorption onto metal oxides. J. Water Supply: Res. Technol.--AQUA, 2005. **54**, p. 339-348.

124. Morrison, S.J., R.R. Spangler, and V.S. Tripathi, Adsorption of uranium(VI) on amorphous ferric oxyhydroxide at high concentrations of dissolved carbon(IV) and sulfur(VI). J. Contam. Hydrol., 1995. **17**, p. 333-346.

125. Pierce, M.L. and C.B. Moore, Adsorption of arsenite on amorphous iron hydroxide from dilute aqueous solution. Environ. Sci. Technol., 1980. **14**, p. 214-16.

126. Pierce, M.L. and C.B. Moore, Adsorption of arsenite and arsenate on amorphous iron hydroxide. Water Res., 1982. **16**, p. 1247-53.

127. Boily, J.F., et al., Modeling proton binding at the goethite (α-FeOOH)-water interface. Colloids Surf., A, 2001. **179**, p. 11-27.

128. Hiemstra, T. and W.H. Van Riemsdijk, Fluoride adsorption on goethite in relation to different types of surface sites. J. Colloid Interface Sci., 2000. **225**, p. 94-104.

129. Lützenkirchen, J., et al., Limitations of the potentiometric titration technique in determining the proton active site density of goethite surfaces. Geochimica Et Cosmochimica Acta, 2002. **66**, p. 3389-3396.

130. Villalobos, M., M.A. Trotz, and J.O. Leckie, Variability in goethite surface site density: evidence from proton and carbonate sorption. J Colloid Interface Sci, 2003. **268,** p. 273-87.

131. Hiemstra, T. and W.H. Van Riemsdijk, Effect of different crystal faces on experimental interaction force and aggregation of hematite. Langmuir, 1999. **15**, p. 8045-8051.

132. Stachowicz, M., T. Hiemstra, and R.W.H. van, Surface speciation of As(III) and As(V) in relation to charge distribution. J. Colloid Interface Sci., 2006. **302**, p. 62-75.

133. Benjamin, M.M. and J.O. Leckie, Multiple-site adsorption of Cd, Cu, Zn, and Pb on amorphous iron oxyhydroxide. Journal of Colloid and Interface Science, 1981. **79**, p. 209-221.

134. Kuo, S. and B.L. McNeal, Effects of pH and phosphate on cadmium sorption by a hydrous ferric oxide 1. Soil Sci. Soc. Am. J., 1984. **48**, p. 1040-1044.

135. Cowan, C.E., J.M. Zachara, and C.T. Resch, Cadmium adsorption on iron oxides in the presence of alkaline-earth elements. Environmental Science & Technology, 1991. **25**, p. 437-446.

136. Yates, D.E., et al., Tritium exchange studies on metal oxide colloidal dispersions. Aust. J. Chem., 1977. **30**, p. 1655-1660.

137. Koretsky, C.M., D.A. Sverjensky, and N. Sahai, A model of surface site types on oxide and silicate minerals based on crystal chemistry. Implications for site types and densities, multisite adsorption, surface infrared spectroscopy, and dissolution kinetics. Am. J. Sci., 1998. **298**, p. 349-438.

138. Brown, G.E., Jr., et al., Metal Oxide Surfaces and Their Interactions with Aqueous Solutions and Microbial Organisms. Chem. Rev., 1999. **99**, p. 77-174.

139. Berube, Y.G., G.Y. Onoda, Jr., and B.P.L. De, Proton adsorption at the ferric oxide-aqueous solution interface. II. Analysis of kinetic data. Surface Sci., 1967. **7**, p. 448-461.

140. Rustad, J.R., A.R. Felmy, and B.P. Hay, Molecular statics calculations of proton binding to goethite surfaces: A new approach to estimation of stability constants for multisite surface complexation models. Geochimica Et Cosmochimica Acta, 1996. **60**, p. 1563-1576.

141. Eggleston, C.M. and M.F. Hochella, Jr., The structure of hematite {001} surfaces by scanning tunneling microscopy: image interpretation, surface relaxation, and step structure. Am. Mineral., 1992. **77**, p. 911-922.

142. Loring, J.S., et al., Rethinking arsenate coordination at the surface of goethite. Chem.--Eur. J., 2009. **15**, p. 5063-5072.

143. Barron, V. and J. Torrent, Surface hydroxyl configuration of various crystal faces of hematite and goethite. J. Colloid Interface Sci., 1996. **177**, p. 407-410.

144. Schwertmann, U. and R.M. Cornell, Iron Oxides in the Laboratory: Preparation and Characterization. 1991, VCH. 137 pp.

145. Schwertmann, U., The influence of aluminum on iron oxides: IX. Dissolution of Al-goethites in 6 M HCl. Clay Mineral., 1984. **19**.

146. Schecher, W.D.M., D.C. , MINEQL+ 4.5, in MINEQL+2003, Environmental Research Software: Hallowell, ME.

147. Schecher, W., MINEQL, 2001, Environmental Research Software: Hallowell, ME.

148. Parfitt, R.L., R.J. Atkinson, and R.S.C. Smart, Mechanism of phosphate fixation by iron oxides. Soil Sci. Soc. Am., Proc., 1975. **39**, p. 837-841.

149. Parkman, R.H., et al., Reactions of copper and cadmium ions in aqueous solution with goethite, lepidocrocite, mackinawite, and pyrite. Am. Mineral., 1999. **84,** p. 407-419.

150. Brown, I.D. and D. Altermatt, Bond-valence parameters obtained from a systematic analysis of the inorganic crystal structure database. Acta Crystallogr., Sect. B: Struct. Sci., 1985. **B41**, p. 244-247.

151. Pauling, L., The Nature of the Chemical Bond and the Structure of Molecules and Crystals: An Introduction to Modern Structural Chemistry. 1960. Cornell University Press. 644 p.

152. Brown, I.D. and R.D. Shannon, Empirical bond-strength-bond-length curves for oxides. Acta Crystallographica Section A, 1973. **29**, p. 266-282.

153. Farges, F., C.W. Ponader, and G.E. Brown Jr, Structural environments of incompatible elements in silicate glass/melt systems: I. Zirconium at trace levels. Geochimica Et Cosmochimica Acta, 1991. **55**, p. 1563-1574.

154. Schuster, P., G. Zundel, and C. Sandorfy, The Hydrogen Bond: Structure and spectroscopy. 1976: North-Holland Pub. Co. 1549 p.

155. Szytuła, A., et al., Neutron Diffraction Studies of α-FeOOH. physica status solidi (b), 1968. **26**, p. 429-434.

156. Feroci, G., R. Badiello, and A. Fini, Interactions between different selenium compounds and zinc, cadmium and mercury. Journal of Trace Elements in Medicine and Biology, 2005. **18**, p. 227-234.

157. Toropova, V.F., Stability of the complex compounds with ligands containing selenium. Zh. Neorg. Khim., 1957. **2**, p. 515-522.

158. Feroci, G., et al., Interaction between selenium derivatives and heavy metal ions: Cu2+and Pb2+. Microchemical Journal, 1997. **57**, p. 379-388.

159. Manceau, A., et al., Sorption and speciation of heavy metals on hydrous iron and manganese oxides. From microscopic to macroscopic. Appl. Clay Sci., 1992. **7**, p. 201-23.

160. Weesner, F.J. and W.F. Bleam, Binding characteristics of Pb2+ on anion-modified and pristine hydrous oxide surfaces studied by electrophoretic mobility and X-ray absorption spectroscopy. J. Colloid Interface Sci., 1998. **205**, p. 380-389.

161. Zhang, P. and D.L. Sparks, Kinetics of selenate and selenite adsorption/desorption at the goethite/water interface. Environmental Science & Technology, 1990. **24**, p. 1848-1856.

162. Elzinga, E.J., D. Peak, and D.L. Sparks, Spectroscopic studies of Pb(II)-sulfate interactions at the goethite-water interface. Geochim. Cosmochim. Acta, 2001. **65**, p. 2219-2230.

163. Zhang, G.Y. and D. Peak, Studies of Cd(II)–sulfate interactions at the goethite–water interface by ATR-FTIR spectroscopy. Geochimica Et Cosmochimica Acta, 2007. **71**, p. 2158-2169.

164. EPA, EPA's Roadmap for Mercury, 2006.

165. Schindler, P., Heterogeneous equilibria involving oxides, hydroxides, carbonates, and hydroxide carbonates. Adv. Chem. Ser., 1967. **67**, p. 196-122.

166. Sarkar, D., M.E. Essington, and K.C. Misra, Adsorption of mercury(II) by variable charge surfaces of quartz and gibbsite. Soil Sci. Soc. Am. J., 1999. **63**, p. 1626-1636.

167. Farrah, H. and W.F. Pickering, The sorption of mercury species by clay minerals. Water, Air, Soil Pollut., 1978. **9**, p. 23-31.

168. Forbes, E.A., A.M. Posner, and J.P. Quirk, Specific adsorption of inorganic mercury(II) species and cobalt(III) complex ions on goethite. J. Colloid Interface Sci., 1974. **49**, p. 403-409.

169. Jean, G.E. and G.M. Bancroft, Heavy metal adsorption by sulfide mineral surfaces. Geochim. Cosmochim. Acta, 1986. **50**, p. 1455-1463.

170. Kinniburgh, D.G. and M.L. Jackson, Adsorption of mercury(II) by iron hydrous oxide gel. Soil Sci. Soc. Am. J., 1978. **42**, p. 45-47.

171. MacNaughton, M.G. and R.O. James, Adsorption of aqueous mercury(II) complexes at the oxide/water interface. J. Colloid Interface Sci., 1974. **47**, p. 431-40.

172. Newton, D.W., R. Ellis, Jr., and G.M. Paulsen, Effect of pH and complex formation on mercury (II) adsorption by bentonite. J. Environ. Qual., 1976. **5**, p. 251-254.

173. Tiffreau, C., J. Luetzenkirchen, and P. Behra, Modeling the adsorption of mercury(II) on (hydr)oxides I. Amorphous iron oxide and α-quartz. J. Colloid Interface Sci., 1995. **172**, p. 82-93.

174. Lockwood, R.A. and K.Y. Chen, Adsorption of Hg (II) by ferric hydroxide. Environ. Lett., 1974. **6**, p. 151-166.

175. Sposito, G., On points of zero charge. Environ. Sci. Technol., 1998. **32**, p. 2815-2819.

176. Weerasooriya, R., B. Dharmasena, and D. Aluthpatabendi, Copper-gibbsite interactions: an application of 1-pK surface complexation model. Colloids Surf., A, 2000. **170**, p. 65-77.

177. Filius, J.D., T. Hiemstra, and R.W.H. Van, Adsorption of small weak organic acids on goethite: modeling of mechanisms. J. Colloid Interface Sci., 1997. **195**, p. 368-380.

178. van, G.A., A.P. Robertson, and J.O. Leckie, Complexation of carbonate species at the goethite surface: implications for adsorption of metal ions in natural waters. Geochim. Cosmochim. Acta, 1994. **58**, p. 2073-2086.

179. Zeltner, W.A. and M.A. Anderson, Surface charge development at the goethite/aqueous solution interface: effects of CO2 adsorption. Langmuir, 1988. **4**, p. 469-474.

180. Naveau, A., et al., Sorption of europium on a goethite surface: influence of background electrolyte. J. Contam. Hydrol., 2005. **77**, p. 1-16.

181. van, R.W.H. and T. Hiemstra. Adsorption to heterogeneous surfaces. Lewis, 1993.

182. Tadanier, C.J. and M.J. Eick, Formulating the charge-distribution multisite surface complexation model using FITEQL. Soil Sci. Soc. Am. J., 2002. **66**, p. 1505-1517.

183. Evans, T.D., J.R. Leal, and P.W. Arnold, The interfacial electrochemistry of goethite (α-FeOOH) especially the effect of carbon dioxide contamination. J. Electroanal. Chem. Interfacial Electrochem., 1979. **105**, p. 161-167.

184. Gunneriusson, L. and S. Sjoeberg, Surface complexation in the hydrogen ion-goethite (α-FeOOH)-mercury(II)-chloride system. J. Colloid Interface Sci., 1993. **156**, p. 121-128.

185. Mueller, B. and L. Sigg, Adsorption of lead(II) on the goethite surface: voltammetric evaluation of surface complexation parameters. J. Colloid Interface Sci., 1992. **148**, p. 517-532.

186. Bargar, J.R., P. Persson, and G.E. Brown, Jr., XAFS studies of Pb(II)-chloro and Hg(II)-chloro ternary complexes on goethite. J. Phys. IV, 1997. **7**, p. 825-826.

187. Stokes, S.N., Diffuse Layer Modeling on Iron Oxides – Single and Multi-solute Systems on Ferrihydrite and Granular Ferric Hydroxide. 2009. The University of Texas at Austin.

188. Benjamin, M., Water chemistry. 2001. McGraw-Hill Book Company, 688 p.